# 3D-PRINTED IN VITRO ANALYTICAL DEVICES FOR DIABETES THERAPEUTICS AND BLOOD BANKING STUDIES

Ву

Chengpeng Chen

# A DISSERTATION

Submitted to
Michigan State University
in partial fulfillment of the requirements
for the degree of

Chemistry - Doctor of Philosophy

2015

#### **ABSTRACT**

# 3D-PRINTED IN VITRO ANALYTICAL DEVICES FOR DIABETES THERAPEUTICS AND BLOOD BANKING STUDIES

By

## Chengpeng Chen

Erythrocytes (ERYs) play an important role in regulating blood flow via a pathway involving ERY-derived adenosine triphosphate (ATP) and endothelium-derived nitric oxide (NO). Impaired ATP release from ERYs of diabetic patients is potentially responsible for diabetic complications, thereby therapies involving stimulation of ERYderived ATP release might limit such complications. This work explores 3D-printing to fabricate a novel microfluidic device to mimic the physiology of ERYs. 3D-printing enables fabrication of the device following a standard 96-well plate geometry for efficient and high throughput readout with a plate reader. This 3D-printed rugged device was reusable after simple rinsing, which enables the detection of a batch of samples on the same device during a long-term experiment. This 3D-printed fluidic device facilitated the investigation of the efficacy of C-peptide on stimulating ERYderived ATP. Without albumin, C-peptide and Zn<sup>2+</sup> cannot increase ERY-derived ATP, suggesting the indispensable role of albumin in the process. The glutamic acid at the 27 position of C-peptide participated in the binding to albumin. Collectively, the ensemble of albumin, C-peptide, and Zn<sup>2+</sup> enhances ERY-derived ATP, which may reduce diabetes complications. To make the results more physiologically conclusive, an Organs-on-a-Chip platform that combined pancreatic β-cells, ERYs and endothelial cells as a blood barrier mimic was developed. The secretion profiles of the  $\beta$ -cells on the device simulate the physiological secreting process well. Subsequent cell-cell communication investigations showed that  $\beta$ -cell secretions do not affect the endothelial cells but increase ATP release from ERYs, which in turn, exerts a downstream effect on endothelial cells by stimulating NO production.

Currently approved hyperglycemic ERY storage solutions impair ATP release from ERYs. This work continues to investigate the reversibility of ATP release from stored ERYs and shows that 15 days of storage is a turning point, after which the ATP release is no longer reversible. This result is consistent with the clinical reports that blood stored longer than 2 weeks is more likely to result in transfusion complications. The mechanism by which hyperglycemia impairs ATP release was also explored by studying ERY deformability using a 3D-printed demand-based cell filter, finding that hyperglycemia permanently alters the deformability of ERYs after 5 days of storage. A 3D-printed intravenous device was developed to mimic a transfusion process *in vitro*. Addition of  $\beta$ -cells on the platform showed that hyperglycemia-stored ERYs failed to respond to the endocrine cells.

Summarily, 3D-printing yields reusable, robust and reproducible microfluidic devices, and demand-based devices. The ensemble of albumin, C-peptide and Zn<sup>2+</sup> can be a potential therapy for diabetes complications, and the current ERY storage protocol adversely alter the physiology of stored ERYs. A normoglycemic alternative may avoid this problem.

#### **ACKNOWLEDGEMENTS**

First, I would like to thank the organizations responsible for funding this research work, including Michigan State University for travel funding supports, and National Institute of Health (NIH) for research funding. I greatly appreciate the investments made by the organizations in my development as a scientist.

My undergraduate education at Ocean University of China (OUC) laid a solid foundation for my scientific career. With the abundant research funding provided by OUC, I was able to start real scientific research when I was a sophomore, and I gradually recognized my interest and potential in research, which served as the initial motivation to continue my education in a graduate school. The knowledge, skills and scientific habits I acquired from these research experiences also facilitate my graduate study.

After I joined Michigan State University (MSU), the faculty of the department of chemistry has provided me with a great graduate education that has enabled me to think critically and independently. Importantly, I would like to thank Dr. Dana M. Spence, my advisor, for his guidance in the past three and a half years. He does not push his students too much, but let them develop independently. He will check your progress to make sure you are on the correct track. This "free" atmosphere made me feel comfortable, but also trained me to conduct research in a more independent manner. I believe the training I have received from him is invaluable, which will undoubtedly benefit me throughout life. I would also like to thank Dr. L. Karl Olson

from the department of physiology at MSU, who trained me how to culture INS-1 cells in his laboratory, without which, this research work cannot be completed. I also appreciated the help provided by Dr. Merlin Bruening and Dr. David P. Weliky in the past a few years.

I sincerely thank the past and current group members in the Spence group. When I first joined the group, Yueli Liu, Paul Vogel, Adam Giebink and Steve Halpin provided their help and encouragement generously, which helped me get through the transition pain in a very short time. I would also like to thank the other members in this group: Yimeng Wang, Kari Brook-Anderson Engelkemier, Suzanne Summers, Jayday Meisel, Sarah O'Brien, Bethany Gross, Kristen Entwistle, Ruipeng Mu, Tiffany Bell, Hamideh Keshavarz, Cody Pinger and Andrew Heller.

I would like to thank my family and friends for their generous support and help. My parents have been working hard for tens of years, which set an excellent example for me in my life. I am also grateful that I always have kind and supportive friends around me. Some activities such as cards, mahjong, BBQ and hot pots with these friends also left a joyful memory in the chapter of my graduate school life.

# TABLE OF CONTENTS

LIST OF TABLES.	x
LIST OF FIGURES	xi
KEY TO ABBREVIATIONS	xvi
Chapter 1 – Introduction	
1.1 Erythrocytes Regulated Vasodilation	
1.2 Microfluidics	
1.2.1 Concept and Development	
1.2.2 On-chip Fluidic Component Integration	
1.2.3 Applications of Microfluidics	
1.2.3 Advantages and Disadvantages of PDMS Based Microfluidics	
1.3 Three Dimensional (3D)-printing and Microfluidics	
1.3.1 3D-printing	
1.3.2 3D-printing Methods	
1.3.3 3D-printed Microfluidics	
1.3.2 Current Challenges and Future Directions	
1.4 Dissertation Motivation and Overview	
REFERENCES	36
Chapter 2 – Study of C-peptide Stimulated ATP Release from Erythrocytes on	2 SD−
printed Circulation-mimic Fluidic Device	47
2.1 Background	
2.1.1 Diabetes Complications	
2.1.2 C-peptide and Vasodilation	48
2.1.3 Chapter Motivation and Overview	
2.2 Methods	
2.2.1 The Design and Fabrication of the Fluidic Device	53
2.2.2 ATP Measurement Optimization	
2.2.3 Evaluation of Analytical Features of the Device	
2.2.4 ERY Sample Preparation	
2.2.5 ERY Derived ATP Determination	
2.3 Results	
2.3.1 Device Design and Fabrication	
2.3.2 ATP Measurement Optimization	
2.3.3 Evaluation of Analytical Features of the Device	
2.3.4 Investigation of ERY Derived ATP Release stimulated by C-peptide	
2.4 Discussion	
2.5 Conclusion	
REFERENCES	
TEL ENERGES	01
Chapter 3 – An Organs-on-a-Chip platform to Study the Interactions between	
Pancreatic β-cells and Blood Vessels	86
3.1 Background	
3.1.1 Organs-on-a-Chip	86
3.1.2 Cell Selection for Organs-on-a-Chip	
3.1.3 Reconstruction of <i>in vivo</i> Microenvironments	

3.1.4 Current development of Organs-on-a-Chip	93
3.1.5 Challenges and Future Directions	95
3.1.6 Chapter Overview	96
3.2 Methods	98
3.2.1 Culture of INS-1 Cells in Membrane Inserts	98
3.2.2 Culture of Endothelial Cells in Membrane Inserts	99
3.2.3 Integration of Cells onto the Fluidic Device	99
3.2.4 INS-1 Cell Secretion Profile Measurement	102
3.2.5 ATP Quantification	102
3.2.6 NO Quantification	103
3.3 Results	104
3.3.1 Cell culture in Membrane Inserts	104
3.3.2 INS-1 cell Secretion Profile	
3.3.3 Cell-cell Interaction Studies	
3.4 Discussion	114
3.5 Conclusion	119
REFERENCES	
Chapter 4 - Evaluating Stored Erythrocytes Used in Transfusion Medicine using	
Printed Analytical Devices	
4.1 Blood Barking	
4.1.1 Blood Banking	
4.1.2 Transfusion Related Complications	
4.1.3 Chapter Motivation and Overview	
4.2 Methods	
4.2.1 ERY Collection and Storage	
4.2.2 Sample Preparation	
4.2.3 Determination of ATP Release Reversibility	
4.2.4 Study of Reversibility of ERY Deformability by a 3D-printed Cell Filter	
4.2.5 Design and Fabrication of an i.v. Injection Device	
4.2.6 Characterization of the i.v. Injection Device	
4.2.6 Study of Responsiveness of Stored ERYs to Pancreatic β-cells	
4.3 Results	
4.3.1 ERY Collection and Storage, Sample Preparation	
4.3.2 Study of Reversibility of ATP Release on the 3D-Printed Fluidic Device	
4.3.3 Study of Reversibility of ERY Deformability	
4.3.4 Characterization of the i.v. Injection Device	
4.3.5 Study of Responsiveness of Stored ERYs to Pancreatic β-cells	
4.4 Discussion	
4.5 Conclusion	
REFERENCES	166
Chanter E - Conclusions and Euture Directions	170
Chapter 5 – Conclusions and Future Directions	
5.1.1. C-peptide Stimulated ATP Release from Erythrocytes on a 3D-printed	
Circulation-mimic Fluidic Device	170
5.1.2 An Organs-on-a-Chip platform to Study the Interactions between	0
Pancreatic β-cells and Blood Components	172
5.1.3 Evaluating Stored Erythrocytes used in Transfusion Medicine by 3D-Pi	inted
Analytical Devices	173
5.1.4 Summarized Conclusion	175

5.2 Future Directions	.175
5.2.1 C-peptide Stimulated ATP Release from Erythrocytes on a 3D-printed Circulation-mimic Fluidic Device	. 175
5.2.2 An Organs-on-a-Chip platform to Study the Interactions between Pancreatic β-cells and Blood Components	. 177
5.2.3 Evaluating Stored Erythrocytes used in Transfusion Medicine by 3D-Pring Analytical Devices	
REFERENCES	

# LIST OF TABLES

Table 2.1. Remaining Volumes of Water in Inserts68
Table 2.2. Optimization of ATP Collection Time70
Table 2.3. Optimization of Luciferin/luciferase Assay Volume71
Table 2.4. Observed quantitative detection of 150 nM and 250 nM ATP from channel 1, channel 3 and channel 573
Table 3.1. Summary of currently developed Organs-on-a-Chip models94
Table 4.1. Constituents of CPD and AS Used for Blood Banking130
Table 4.2. The concentration of fluorescein in each loop after an injection154
Table 4.3. The concentrations of fluorescein in each part of a loop154
Table 4.4. The hematocrit of ERYs in each loop after an injection155
Table 4.5. The hematocrit of ERYs in each part of a loop155

# LIST OF FIGURES

Figure 1.1. The process by which ERYs help regulate blood flow. ERYs-released ATF binds to the P2y receptor on endothelial cells and evokes NO synthesis and release NO diffuses to smooth muscle layers, the main structural component of a vessel wall resulting in relaxation of these cells, and subsequent vasodilation
Figure 1.2. A scheme for rapid prototyping and replica molding of microfluidic devices in PMDS. (A), a photomask with desired transparent features (white parts) is placed on a photoresist layer coated on a silicon wafer, which is exposed to UV light. (B), after the photoresist under the transparent feature areas is cured and the rest photoresist removed (called a master), PDMS prepolymer (the yellow part) is poured onto the master. After curing, the PDMS layer is peeled off the master, with negative replication of the features.
Figure 1.3. (A), a scheme for an on-chip pneumatic pump. A top channel in a thin PDMS layer is placed across a bottom channel in another PDMS layer. When proper pressure is applied in the top channel, it inflates and deflects down to occlude the bottom channel. (B), in Lander's device, an array of pneumatic pumps are integrated to create peristaltic force that drives sample forward into the separation channel. (C), in Martin's device, the pneumatic pump enables accurate injection of a sample plug into the electrophoresis channel from a continuous sample stream. The design of a pushback channel prevents stagnant samples from entering the channel in the next injection
Figure 1.4. Electrokinetic injection of a sample on an electrophoresis microfluidic platform. The sample channel crosses the electrophoresis channels where a potential will applied across. After the sample channel is filled, the plug at the crossing area will be driven into the electrophoresis channel when the potential is applied across the electrophoresis channel
Figure 1.5. A microfluidic electrophoresis device that contains valves to manipulate sample injection. When Valve 1 is closed and Valve 2 open, a sample is injected to the electrophoresis channel. By applying the two valves, accurate sample introduction car be achieved
Figure 1.6. A sandwich PDMS microfluidic device for blood analysis. A), device design Porous membrane was placed between two layers of PDMS, the bottom channel layer of channels and the top layer of wells. B), the schematic side view of a channel. While RBCs were flowing through the channel, produced molecules such as NO will diffuse through the membrane and be collected in the above well, where fluorescence detection can be performed to quantify NO

Figure 1.7. Current 3D-printing methods. A), stereolithography; B), inkjet printing; C), selective laser sintering; D), fused deposition modeling; E), laminated object manufacturing; F) continuous printing model
Figure 2.1. Proinsulin. Each sphere represent an amino acid. The labeled amino acids represent C-peptide. Upon cleavage, the two chains connected with disulfide bond forms insulin, while the connecting segment forms C-peptide51
Figure 2.2. The engineering sketch of the fluidic device with detailed dimensions54
Figure 2.3. ERY sample preparation and measurement. A), four ERY samples were prepared with different treatments: without C-peptide or $Zn^{2+}$ ; only with C-peptide; only with $Zn^{2+}$ ; and with both C-peptide and $Zn^{2+}$ , the concentrations of C-peptide and $Zn^{2+}$ were both 10 nM. B), the four samples were introduced into four channels of the fluidic device. After the samples circulated for 1.5 hours in the fluidic device that was placed in a 37 °C incubator, aliquots of 50 $\mu$ L of PSS were loaded in the wells in row E to collect ATP from the flowing via diffusion, which was then quantified with the luciferin/luciferase assay by a plate reader
Figure 2.4. (A): The 3D-printed fluidic device (bottom) used in this study is modeled after the dimensions of a 96-well plate (top). Column and row markers make it convenient to localize wells. Six channels were printed on the odd number columns, with three wells corresponding to each channel. Static wells, printed on the even number columns allow for internal standards or calibration. (B): Membrane inserts (top), which have a semi-permeable polyester membrane, are inserted into wells (bottom) of the 3-D printed device. (C): Threads, printed at both ends of the channel, connect external tubing through a finger tight adaptor. (D): A schematic cross section of a channel and the membrane inserts. (E): The device locks into the sample holder of the commercial plate reader
Figure 2.5. Validation of the alignment of the device and printed wells in the plate reader. Six fluorescein solutions (concentrations ranging from 0 to 20 $\mu$ M) were prepared and were loaded into the six inserts in wells B above each channel, respectively. Fluorescence intensity above these inserts was detected by plate reader and was plotted versus fluorescein concentration. The good linearity ( $r^2 = 0.99$ ) shows that the device and wells are aligned well with the plate reader. $n = 3$ , Error = stdev66
Figure 2.6. A fluorescence image of a channel after flowing fluorescein. The dotted circles indicate the well areas. The image implies that leakage of liquid from channel across the membranes did not occur. Due to the limited scope view, images on separate parts of the channel were obtained and integrated into a single image69

Figure 2.7. ATP release from circulating ERYs with different treatments. The data summarized in black bars were collected from ERYs flowing in PSS, which suggest that

Zn <sup>2+</sup> alone did not show this effect. Without albumin in the ERY streams, however, C peptide and Zn <sup>2+</sup> fail to stimulate ATP release (grey bars), which confirmed the role o albumin in the ATP stimulation process. In this experiment, 10 nM C-peptide and Zn <sup>2</sup> were used to treat ERY samples. (N=5, error=S.E.M)
Figure 2.8. ATP release from ERYs treated with C-peptide/Zn <sup>2+</sup> and E27A/Zn <sup>2+</sup> . Unlike C-peptide/Zn <sup>2+</sup> , E27A/Zn <sup>2+</sup> cannot stimulate ATP release from ERYs77
Figure 3.1. The concept of Human-on-a-Chip and its potential applications in fundamental physiological studies and in pharmaceutical research87
Figure 3.2. The setup of the Organs-on-a-Chip device. This study used four channels above which, inserts cultured with INS-1 cells (β-cells) and bPAECs (endothelial cells were integrated. The static wells in columns 8 and 10 contained ATP and NO standards for on-chip simultaneous calibration
Figure 3.3. (A), microscope images cells cultured in a membrane insert. (A) INS-1 cells (B) bPAECs105
Figure 3.4. (A), INS-1 cell secretion profile in albumin-containing stimulation buffer (B), INS-1 cell secretion profile in albumin-free stimulation solution. (C), the amount of C-peptide diffused to the following solution underneath flowing on the device, with albumin presented in the system. (D), without albumin in the system, the amount of C-peptide diffused to flowing
Figure 3.5. (A), the top view of the four channels with different treatments. Channel 2 contains INS-1 cells, bPAECs cultured in the membrane inserts, and ERYs flowing in PSS; channel 2 contains all three cells, but all buffers are albumin-free; channel 3 does not contain INS-1 cells, with the rest identical as channel 1; channel 4 is almost identical to channel 1, except the endothelial cells were pretreated with PPADS, a P2 receptor inhibitor. B), a side schematic view of channel 1
Figure 3.6. The amount of ATP collected in the insert above each channel, which is proportional to the ATP amount in corresponding flowing. Comparing channels 1 and 3, INS-1 cell stimulated ATP release from ERYs, as is shown by increased ATP amount in the collecting well. Without albumin (channel 2), however, INS-1 cells failed to stimulate ATP release from ERYs, which proved the indispensable role of albumin in this process. Channel 4 is identical to channel 1, except the endothelial cells were inhibited, which did not affect the ATP released
Figure 3.7. The amount of ATP in ERYs streams in the four channels, showing the same trend as in Figure 3.6112
Figure 3.8. The released NO from endothelial cells culture in the last insert above each

is with more ATP released, more NO will be produced in endothelial cells. In channel 4, however, though there was a higher ATP release from ERYs, the endothelial cells were pretreated with PPADs, a P2y receptor (ATP receptor in endothelial cells) inhibitor, and thus NO was not increased
Figure 4.1. The 3D-printed cell filter for ERY deformability measurements. (A): the two slabs with O rings on the binding sides. A piece of semipermeable membrane is the key part of the filter device, which was 5 µm pore size polycarbonate membrane. (B): A view of the assembled device, with the membrane between the slabs. The assembling was achieved by simply binding the two slabs on the four wings with binder clips. (C): The view of a real filtration experiment. A sample was introduced by a pump into the top slab, which would be forced to go through the membrane and was then collected for subsequent cell counting. (D): The schematic cross view of a filtration process. A pressure was applied to push cells to deform to pass through the membrane between the O rings. However, only cells with sufficient deformability can go through, otherwise they will be blocked by the membrane
Figure 4.2. The technical drawings of the top slab, bottom slab and O rings of the filtration device, achieved by the autodesk inventor software. Before sending the files into the printer, the O rings were assembled to both slabs in the software so that they can be printed simultaneously. The unit for all the dimensions is mm140
Figure 4.3. The 3D-printed i.v. injection device. (A): the device comprises three parts: a flow splitter, a flow controller, and a stop cock. Screw threads were printed on each part for easy but tight connection. When the hole that goes through the stopcock was adjusted along the channel in the flow controller, liquid can be injected through. Otherwise, the flow will be stopped. (B): Injection of fluorescein into a water circulation. Water was circulating in the loop that connects the low branch of the splitter and the other end of a channel, while fluorescein was injected in by a syringe pump
Figure 4.4. The strategy to study the responsiveness of stored ERYs to $\beta$ -cells. Fresh ERYs with a hematocrit of 5% were circulating in the six channels of the fluidic device, while fresh, AS-1N stored, and AS-1 stored ERYs were injected into the circulations via the i.v. injection device. INS-1 cells were included on the left three channels (green ovals). A 2-hour incubation at 37 °C was applied after the injection, after which, ATP amount in each channel was quantified by the luciferase/luciferin assay in the blue ovals
Figure 4.5. Extracellular glucose levels in AS-1 and AS-1N storage solutions. Throughout the whole 36-day storage, glucose in AS-1 solutions (open circles) stayed at an extremely high level around 40 mM, while AS-1N solutions (filled circles) showed physiological glucose levels around 5 mM. Data present the mean of 7 trials ± S.E.M

Figure 4.6. ATP release reversibility data at different storage days. AS-1N-PSSN trial
referred to ERYs stored in AS-1N (normoglycemic) transfused into normoglycemic PSS;
AS-1-PSSH trial represented ERYs stored in AS-1 (hyperglycemic) transfused into
hyperglycemic PSS; AS-1-PSSN trial was ERYs stored in AS-1 but transfused into
normoglycemic PSS. During the 36 storage days, AS-1N-PSSN ERYs released higher ATP
at a constant level, while AS-1-PSSH ERYs released less ATP. The AS-1-PSSN ERYs,
however, could reverse the ATP release before 15 days (complete reverse before Day
5 and partial reverse on Day 8 and 12). Seven biological replica were analyzed and the
data represent mean ± S.E.M150

#### **KEY TO ABBREVIATIONS**

ATP: Adenosine triphosphate

AS-1: Additive solution 1

AS-1N: Additive solution 1 (normoglycemic)

bPAECs: Bovine pulmonary artery endothelial cells

CPD: Citrate-phosphate-dextrose solution

CPD-N: Citrate-phosphate-dextrose (normoglycemic)

CE: Capillary electrophoresis

CFTR: Cystic fibrosis transmembrane conductance regulator

ERY: Erythrocyte

HBSS: Hank's buffered salt solution

i.v.: Intravenous

INS-1: Rat insulinoma beta cells

LOM: Laminated object manufacturing

NO: Nitric oxide

PBS: Phosphate buffered salt solution

PDMS: Poly-(dimethyl siloxane)

PPADS: pyridoxalphosphate-6-azophenyl-2',4'-disulfonic acid

PSS: Buffered physiological salt solution

#### Chapter 1 – Introduction

## 1.1 Erythrocytes Regulated Vasodilation

Erythrocytes (ERYs), also referred to as red blood cells or RBCs, are the most abundant cells in the blood stream and play an important role in oxygen delivery to other tissues and cells<sup>1</sup>. However, in addition to their oxygen delivery, ERYs also help regulate blood flow by controlling vasodilation via a pathway involving adenosine triphosphate (ATP) and nitric oxide (NO).

The layer of endothelial cells (called endothelium) lining the inside of a vessel can synthesize NO through an endothelial nitric oxide synthase (eNOS) pathway. This NO can diffuse to smooth muscle layers that serve as the main structure of a vessel wall, resulting in a rise in cyclic guanosine monophosphate (cGMP), which leads to a decrease in endoplasmatic Ca<sup>2+</sup> concentration that results in smooth muscle cell relaxation, and subsequent vasodilation<sup>2</sup>.

Increased shear stress is a major stimulus for NO release from the endothelium<sup>3</sup>. However, Sprague and colleagues found that in isolated perfused rabbit lungs, in the absence of ERYs, alteration of sheer stress alone did not evoke NO release. They concluded that in the rabbit pulmonary circulation there must be some interactions between the ERYs and the endothelium, resulting in NO-mediated vasodilation<sup>4</sup>. The authors reported that shear stress induces deformability of ERYs, which increases ATP release from ERYs through a pathway involving a G protein coupled receptor (GPCR) and the cystic fibrosis transmembrane conductivity regulator (CFTR)<sup>5</sup>. They also

proposed that the ATP released from ERYs plays a major role in stimulating NO production in endothelial cells; numerous studies proved the role of ATP as a stimulus of NO production<sup>6</sup>. For example, Bogel and colleagues found that ERY derived ATP can bind the P<sub>2y</sub> receptor on endothelial cells resulting in Ca<sup>2+</sup> influx and the formation of calmodulin, which activates endothelial nitric oxide synthase (eNOS); the eNOS then converts arginine to citrulline, with NO as a byproduct<sup>7</sup>. Figure 1.1 depicts the interaction between ERYs and endothelial cells in the process of NO production and release.

Disturbance of this NO induced vasodilation can cause pathophysiological consequences. People with any form of diabetes will likely experience at least one chronic complication, such as nerve damage (neuropathy), blindness (retinopathy), kidney damage (nephropathy), or cardiovascular disease, which may result in endless pain or mortality<sup>8</sup>. A common theme in many of these conditions is the dysfunction that occurs at the interface between the blood stream and peripheral tissues, or the vessels. For example, Low et al. suggested that poor blood flow results in endoneurial hypoxia, decreasing nerve signaling and leading to neuropathy<sup>9</sup>. In the retina of diabetic patients, restricted vasodilation causes poor oxygen circulation, which stimulates retinal cells to form new but fragile vessels via a vascular endothelial growth factor mechanism. The breaking of the new, weak vessels can cloud the vitreous, and high vessel density may lead to detachment of the retina and eventually result in blindness<sup>10, 11</sup>. In diabetic nephropathy, the glomerulus undergoes partial sclerosis or failure to dilate, which causes hyper filtration and protein leakage. Some

other diseases such as hypertension, atherosclerosis, and restenosis also relate to impaired NO-induced vasodilation<sup>12</sup>.

Interestingly, the release of ATP from ERYs obtained from diabetic patients is significantly lower than that from healthy controls<sup>13, 14</sup>. Given the role of ERY-derived ATP in regulating vasodilation via stimulating endothelium derived NO production, therapies involving stimulation of ATP release from these cells might ameliorate some diabetic complications. However, under *in vivo* conditions, ERYs circulate under multiple physical (e.g. shear stress)<sup>15</sup> and biochemical (e.g. cell-cell interaction)<sup>16</sup> factors. Therefore, a dynamic platform that can mimic the physiological conditions of ERYs will be needed. Microfluidic technology enables precise control of sample (*e.g.* ERYs) and reagent flow and, can recapitulate a vascular microenvironment for *in vitro* ERY studies<sup>17</sup>. In recent years, many studies used microfluidics for vasculature investigations, including hemodynamics<sup>18, 19</sup>, ERYs under shear stress<sup>20, 21</sup>, endothelial barrier function<sup>22</sup>, and angiogenesis<sup>23</sup>.

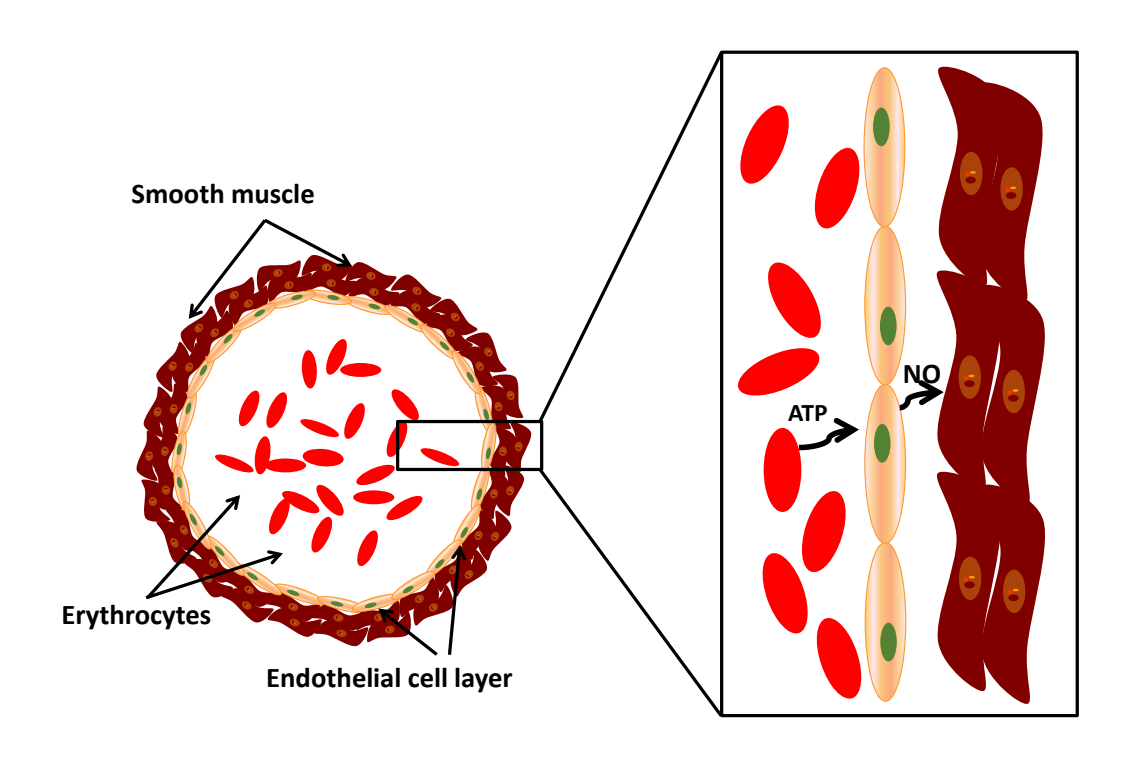


Figure 1.1. The process by which ERYs help regulate blood flow. ERYs-released ATP binds to the P2y receptor on endothelial cells and evokes NO synthesis and release. NO diffuses to smooth muscle layers, the main structural component of a vessel wall, resulting in relaxation of these cells, and subsequent vasodilation.

#### 1.2 Microfluidics

# 1.2.1 Concept and Development

Microfluidics is the science and technology of miniaturized devices for analysis of small amounts of liquids in channels with dimensions at micrometer levels. Microfluidic devices have many benefits in chemical and biological analyses, including reducing the amount of sample and reagents, decreasing experiment time, and enabling experiments to occur under dynamic conditions<sup>24</sup>. The ultimate goal of microfluidic technologies is to develop a lab-on-a-chip or total analysis system, where miniaturized sample pretreatment, separation and detection occur in an integrated fashion on a single device<sup>25</sup>.

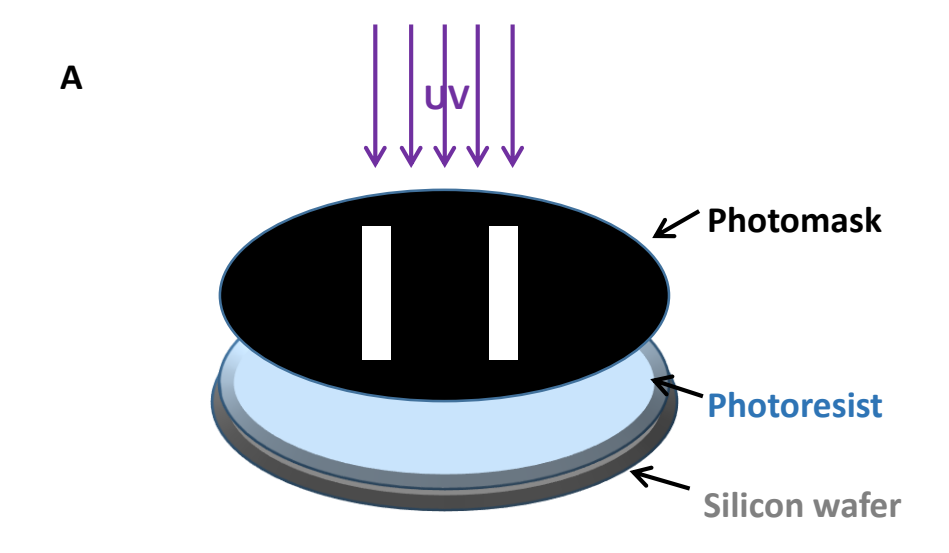
In 1979, Terry and colleagues invented the first microfluidic device, a gas chromatograph fabricated on a silicon wafer for air analysis<sup>26</sup>. Ruzicka developed this concept by creating flow injection analysis systems on plastic milled devices in the 1980's<sup>27,28</sup>. In the 1990's, when biological and chemical weapons started to become a major terrorist threat, the US Department of Defense initiated and supported a series of studies on microfluidic devices for in-field biological and chemical detection, which greatly facilitated the development of the field of microfluidics<sup>24</sup>. During this period, the use of a polymer, poly(dimethyl siloxane) (PDMS) greatly simplified fabrication of microfluidic devices<sup>29</sup>.

Although the first generation of microfluidic devices relied on hard substrates such as silicon wafers and glass, fabrication was costly and time consuming. The use

of soft polymers as device substrates potentially reduces operation time and cost, and introduces new material characteristics, such as elasticity, transparency and easy molding to a microfluidic device<sup>30</sup>. After its introduction by the Whitesides group at Harvard University, PDMS became the most common substrate for microfluidic devices, because of its superior advantages, which include: (i) the simplicity of introducing micro scale features on PMDS with soft lithography; (ii) a relatively inert surface; (iii) curing at relatively low temperatures; (iv) transparency, which enables optical detection; and (v) no toxicity to biological cells<sup>31, 32</sup>.

PDMS based microfluidic devices are commonly fabricated by soft lithography, enabling rapid prototyping based on replica molding<sup>33</sup>. Rapid prototyping creates a master (on a silicon wafer) with a convex feature as a mold for subsequent PDMS casting. This process starts by drawing desired features using computer aided design (CAD) software and printing these features on a transparent plastic film, which serves as a photomask. The photomask is placed on a silicon wafer pre-coated with a photoresistant polymer. SU-8 is a commonly used photoresist that cures upon exposure to ultraviolet (UV) light<sup>34</sup>. The photomask allows UV light to pass through the transparent region only, which leads to selective curing of photoresist on the silicon wafer, thus createing the desired features. The featured master serves as a mold for PDMS device fabrication. PDMS prepolymer (mixed with curing reagent) is cast onto the master. After curing, the PDMS replica is peeled from the master, and creating a negative replica of the master can be fabricated in PDMS<sup>35</sup>. The low instrument requirements for this process make it widely used in many laboratories.

Moreover, it is rapid and low cost, which makes it possible to test or optimize different device designs in a short time. (Figure 1.2)



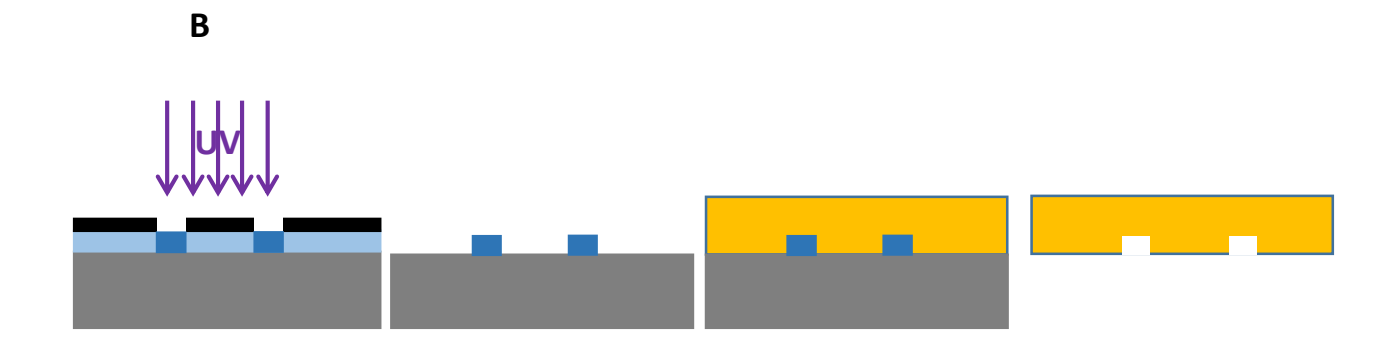


Figure 1.2. A scheme for rapid prototyping and replica molding of microfluidic devices in PMDS. (A), a photomask with desired transparent features (white parts) is placed on a photoresist layer coated on a silicon wafer, which is exposed to UV light. (B), after the photoresist under the transparent feature areas is cured and the rest photoresist removed (called a master), PDMS prepolymer (the yellow part) is poured onto the master. After curing, the PDMS layer is peeled off the master, with negative replication of the features.

## 1.2.2 On-chip Fluidic Component Integration

A functional microfluidic device must contain not only channels, but also components such as mixers and valves necessary to assist liquid delivery, facilitate reaction and enhance experimental efficiency. The following is a brief review of each of these critical components of a microfluidic system.

Liquid flow in a micro scale channel is usually laminar and without convective mixing. When two fluids are flowing in a microchannel simultaneously, they flow in parallel, forming a clear interface between them, without turbulent mixing. The only mixing that will occur results from diffusion at the interface of the two reagents. The tendency for a fluid to develop turbulent flow patterns can be characterized by the Reynolds number (Re), which is proportional to flow speed and channel dimensions and inversely proportional to liquid viscosity, as shown in Equation 1.1<sup>36</sup>.

$$Re = \frac{\rho vL}{\mu}$$
 Equation 1.1

Where  $\rho$  is the density of the fluid (kg/m<sup>3</sup>), v is the mean velocity of the fluid (m/s), L is the travelled length of the fluid (m), and  $\mu$  is the viscosity of the fluid (kg/(m•s))

Because of the small dimensions of microfluidic channels, the Re for microfluidic devices is almost always less than 1, which makes it impossible to be turbulent in character (which requires Re > 4000)<sup>37, 38</sup>. For applications such as on-chip chemical reactions or biological studies, laminar flow is often not very useful, and thus on-chip

mixers that can homogenize flows are often required. There have been several on-chip mixers reported, which predominantly rely on a chaotic advection effect that is realized by increasing contact area and contact time between flows<sup>39, 40</sup>. A classical microfluidic mixer developed by the Whitesides group applies asymmetric herringbone grooves on the floor of a microchannel. A flow will be stretched in a groove and then folded to one another, which significantly increases contact area and time between the flowing species, and thus achieves high mixing efficiency<sup>41</sup>. There are some other on-chip mixer designs such as zigzag channels<sup>42</sup> or twisted channels<sup>43</sup>, or embedding barriers<sup>44</sup> in channels, all of which make it possible to increase mixing on a microfluidic platform.

Valves are important components in any fluidic system to control and regulate flow patterns, and this is also true for microfluidics<sup>45</sup>. On-chip pneumatic valves were invented by Quake's group from the California Institute of Technology, taking advantage of the elastic property of PDMS<sup>46</sup>. The main idea of the valve design is pressure driven occlusion between stacked channels in two PDMS layers. The top channel, which is made within a thin (40 µm) layer of PDMS, is crossed with a bottom channel that is in a thicker PDMS layer (4 mm). The liquid flows in the bottom channel, while the top one will be connected to a pneumatic pressure source. When proper pneumatic pressure is applied through the top channel, it will be inflated and deflect down to occlude the bottom channel (Figure 1.3A). An array of such pneumatic valves was also used to produce peristaltic force across a microfluidic channel to drive flow on a chip <sup>47</sup>. For example, the Landers group used on-chip pneumatic pump arrays to

drive samples through a side channel, directly into an electrophoretic channel for separation and analysis (Figure 1.3B)<sup>48</sup>. Martin further optimized this application by incorporating a reduced-volume pneumatic valve that actuates (on the order of hundreds of milliseconds) to allow analytes from a continuously flowing sampling channel to be injected into a separation channel for electrophoresis (Figure 1.3 C)<sup>49</sup>.

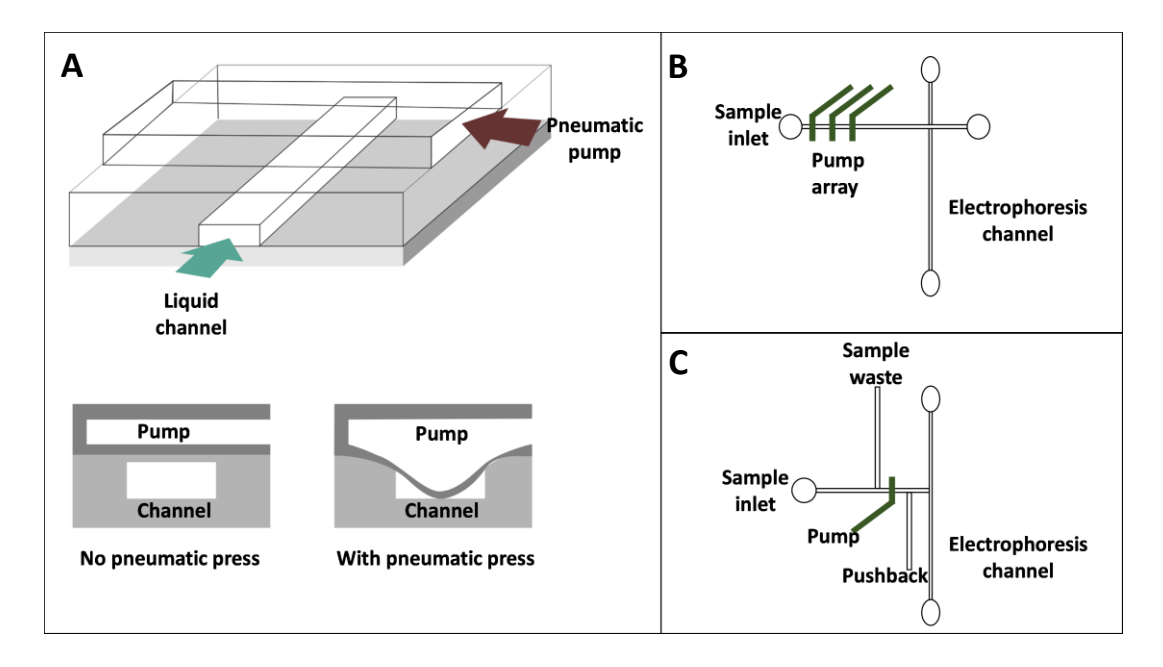


Figure 1.3. (A), a scheme for an on-chip pneumatic pump. A top channel in a thin PDMS layer is placed across a bottom channel in another PDMS layer. When proper pressure is applied in the top channel, it inflates and deflects down to occlude the bottom channel. (B), in Lander's device, an array of pneumatic pumps are integrated to create peristaltic force that drives sample forward into the separation channel. (C), in Martin's device, the pneumatic pump enables accurate injection of a sample plug into the electrophoresis channel from a continuous sample stream. The design of a pushback channel prevents stagnant samples from entering the channel in the next injection.

Porous membranes integrated in PDMS microfluidic devices can act as molecule exchange media and cell culture supports<sup>50</sup>. By simply placing a piece of organic membrane between two PDMS slabs, the membrane binds tightly with PDMS by inter molecular forces, to form a sandwiched microfluidic device<sup>51</sup>. Membranes have

greatly expanded the functions of microfluidic devices in applications such as biosample analysis and on-line sample treatment. <sup>52,53</sup>.

The ultimate goal of building "Lab-on-a-Chip" systems requires on-chip detection methods. Due to the miniaturized features of microfluidic devices, optical and electrochemical detectors are most common. Optical fibers enable detection based on absorbance, fluorescence and chemiluminescence<sup>54</sup>. Chabinyc developed on-chip fluorescence detection by embedding an optical fiber in the microfluidic device and using an offline blue LED and a polymeric light filter for protein detection<sup>55</sup>. Compared to optical methods, which requires external components (light source, filters, photomultiplier tubing) and a dark environment<sup>56</sup>. Embedding of electrodes in PDMS layers during the casting process provides a much simpler detection platform<sup>57</sup>. Biologically relevant analytes such as cocaine<sup>58</sup>, antioxidants<sup>59</sup>, and neurotransmitters have been detected on electrochemically-based integrated microfluidic platforms.

# 1.2.3 Applications of Microfluidics

The development of soft lithography and on-chip integration greatly reduced the time and cost of fabricating microfluidic devices, and enhanced the function of microfluidics, making this technology a powerful tool in many research areas. It also allowed microfluidic devices to be fabricated in any laboratory, as sophisticated etching and ablation equipment was no longer required. This chapter discusses the applications of microfluidics in biochemical engineering.

A complete analytical cycle includes sample pretreatment, separation and detection, which is usually time consuming and labor intensive. The concept of micro total analytical systems ( $\mu$ TAS) that integrate the multiple analytical steps on a miniaturized flow system for faster and automated analysis has gained increasing interest. Sample separation can be a key part in an analytical cycle, and one of the earliest examples of  $\mu$ TAS was the integration of electrophoresis on an etched glass chip invented by Manz and colleagues in 1992, which shows the great potential of electrophoresis-based separation on a microfluidic device<sup>60</sup>.

Electrophoresis is easy to implement in microfluidic technology and thus has remained the primary separation technique on microfluidic devices. With integrated electrodes, an electrical field can drive flow electrokinetically, without the assistance of external bulky pumps, which makes such microfluidic devices a step forward towards automated analytical systems. With a shorter channel on a microfluidic device, the electrophoretic separation can be more efficient than traditional capillary electrophoresis. Ramsey once reported a microfluidic device used for sub-millisecond electrophoresis, which was ~100 times faster than conventional methods<sup>61</sup>. Because a microfluidic channel can be simplified as a thick wall capillary without polyimide coating, the heat dissipation on a microfluidic device is more efficient that in a capillary. Microfluidics also enables parallel and high throughput electrophoresis on one device, making it attractive when proteomics and genomics analyses are needed. For example, Simpson reported a high throughput genetic analysis on a microfluidic electrophoresis platform<sup>62</sup>.

Another advantage of on-chip electrophoresis is the short and controllable sample injection plug. For on-chip sample introduction, electrokinetic injection is the preferred method, which is achieved by two steps, loading and dispensing<sup>63, 64</sup>. The basic principle of this technique is to use two crossing channels, one for sample loading and the other for separation. After a sample is injected in the sample channel, the sample plug at the crossing zone will be driven through the separation channel by an applied voltage (Figure 1.4). This sample injection method was first reported by Manz on his etched glass device<sup>60</sup>. To increase separation efficiency, Ramsey minimized the injection plug by narrowing the sample channel size at the crossing on his device to separate rhodamine B and dichlorofluorescein<sup>61</sup>.

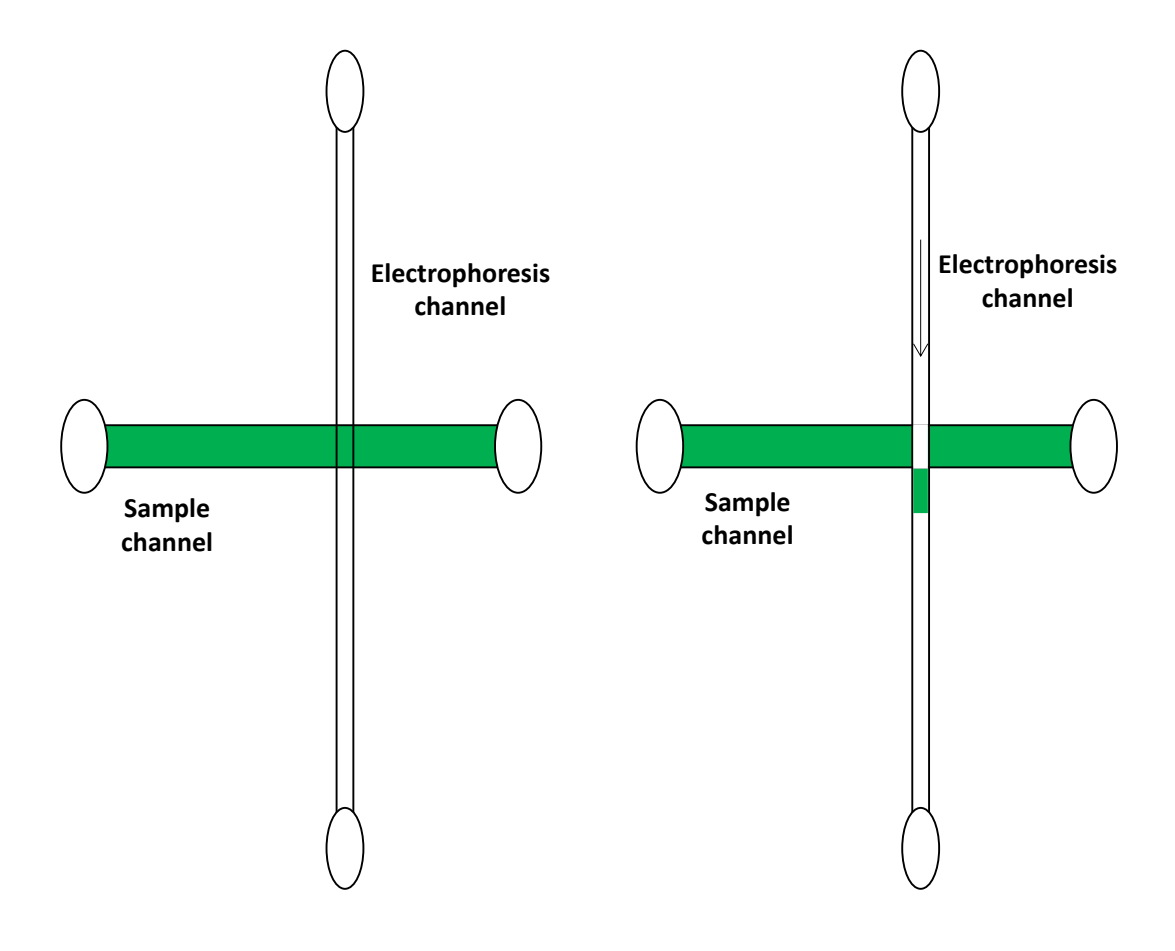


Figure 1.4. Electrokinetic injection of a sample on an electrophoresis microfluidic platform. The sample channel crosses the electrophoresis channels where a potential will applied across. After the sample channel is filled, the plug at the crossing area will be driven into the electrophoresis channel when the potential is applied across the electrophoresis channel.

However, this injection method possesses limitations. First, sample dispersion into the electrophoresis channel occurs during sample loading, leading to uncontrolled plug length. The other problem is continuous sample leakage into the electrophoresis channel during the separation process, which will result in peak tailing<sup>65</sup>. To avoid these problems, Ramsey developed the electric pinched injection that can inhibit leakage of samples by using the electrical field from the separation channel to the sample waste channel as a virtual valve<sup>66</sup>. Furthermore, pneumatic pumps were applied on electrophoresis devices for more accurate and frequent sample injections. For example, Mecker reported a coupled on-chip electrophoresis device that enables online continuous sampling and injection<sup>67</sup>. As shown in Figure 1.5, microdialysed samples were introduced to the sample inlet of the electrophoresis chip. Two pneumatic valves control the injection of sample into the separation channel. For example, if valve 2 is open while valve 1 closed, sample is injected. Then both valves are closed and separation will occur. This work was the first microfluidic system that coupled microdialysis and continuous injection of samples, electrophoretic separation, and detection on a single device.

Another important feature of on-chip elelctrophoresis is the detection technique. Multiple optical detection methods such as laser induced fluorescence (LIF) and UV absorbance have been developed<sup>68, 69</sup>. Because electrode embedding in a microfluidic device has become a mature technique that can be easily performed in many laboratories, electrochemical detection (e.g. amperometry) is widely used for on-chip

electrophoresis detection, without the requirements for bulky optical detectors or dark environments, which potentially makes it more portable<sup>70</sup>.

Besides pure engineering and technique development, on-chip elelctrophoresis has become a practical tool for many applications. It has been applied to the separation of small molecules such as neurotransmitters<sup>71</sup>, amino acids<sup>69</sup>, phenolic compounds<sup>72</sup>, and flavonoids<sup>73</sup>; and macromolecules such as DNA<sup>74,75</sup>, proteins<sup>75</sup>, and glycans<sup>76</sup>. Cell and cell content separation by on-chip electrophoresis has also been reported<sup>77,78</sup>.

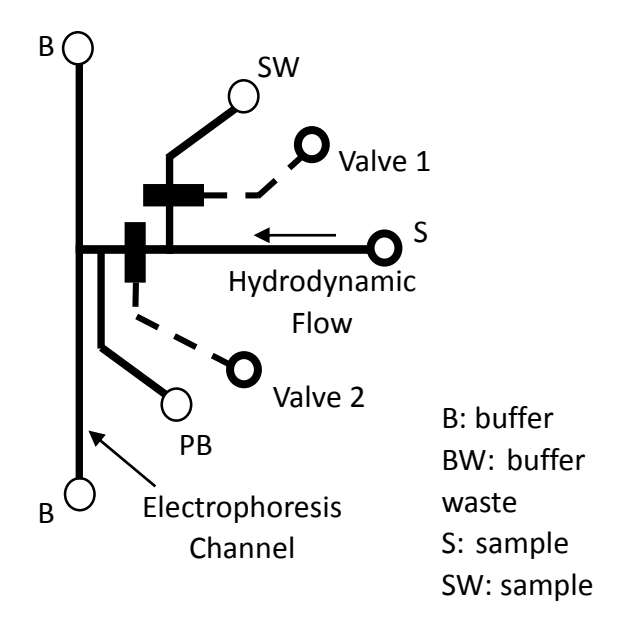


Figure 1.5. A microfluidic electrophoresis device that contains valves to manipulate sample injection. When Valve 1 is closed and Valve 2 open, a sample is injected to the electrophoresis channel. By applying the two valves, accurate sample introduction can be achieved.

Particle separation is an important tool in biological and chemical studies, including tumor cell screening, cell sorting and tissue engineering. However, conventional particle separation methods such as centrifugation, chromatography, and immunoisolation, are time consuming, are not efficient, non-continuous and low throughput. Microfluidic devices have been developed for particle separation, to overcome the shortcomings of existing methods. Acoustic wave based separation, also referred to as acoustophoresis, is a commonly used on-chip particle separation method. The first microfluidic acoustophoresis device was invented by Kapishnikov and colleagues to separate blood cells<sup>79</sup>. Acoustophoresis applies an axial acoustic primary radiation force so that larger particles will move closer to the center of the channels while smaller particles move further from the center, and thus particles of different sizes can be separated<sup>80</sup>. Other forces such as gravity<sup>81</sup> and inertia<sup>82</sup> have also been reported to apply particle separation on microfluidic devices.

### 1.2.3.2 Analytical Science

In contrast to lab-scale chemical analyses, microfluidics are miniaturized systems with continuous but controllable flow and integration capabilities, which have made it an ideal platform for rapid, high throughput chemical analysis. Immunoassay techniques have been widely used on microfluidic devices for protein detection<sup>83</sup>. Microliter and nanoliter scale channels can serve as an immunoreaction chamber that can significantly decrease experimental time and the usage of expensive antibodies. The high surface-to-volume ratio in microchannels, as well as the ease of modifying

the PDMS surface, makes it feasible to immobilize antibodies on the surface of a channel. There have been several antibody immobilization methods reported, among which, Sebra and colleagues made an impressive immobilization by grafting acrylated antibodies on PDMS in the presence of poly(ethylene glycol)<sup>84</sup>. Due to the transparent characteristic of PDMS, optical detection (fluorescence and absorbance) can be performed. By conjugating electrochemical sensitive probes on the secondary antibodies, electrochemical detection with embedded electrodes can also be applied. Enzyme assays, cell-based assays, DNA detection and amplification have also been successfully developed on microfluidic devices<sup>85</sup>.

Since Martinez and colleagues developed several methods to fabricate microfluidic devices on paper, the concept of paper-based microfluidic diagnostic tools has become an active research area<sup>86</sup>. Previous work mainly focused on integrating assays (mainly colorimetric assays) on paper fabricated devices. Although glucose and albumin have been successfully detected, which can potentially serve as a diagnostic tool for diabetes and kidney disease<sup>87</sup>, more research regarding assay development and on-chip detection needs to be performed before paper microfluidics can realize its ultimate goal of providing an inexpensive diagnosis tool for global health, especially for resource limited areas<sup>88</sup>.

Another attractive feature of performing analyses using microfluidic device technology is its ability in sample preparation and for complex biological sample analysis. Kim and colleagues have reviewed microfluidic devices for on-chip cell lysis

and intracellular molecule extraction and purification<sup>89</sup>. With membrane integrated sandwich microfluidic devices, some complex samples do not need to be pretreated prior to detection. Figure 1.6 shows a blood analysis device developed by Halpin<sup>52</sup>. The porous membrane, which only allows molecules such as ATP and nitric oxide (NO) to diffuse through, rather than blood cells, serves as a natural separation unit so that molecules of interest can be directly detected in the well above membrane, without sample separation or pretreatment.

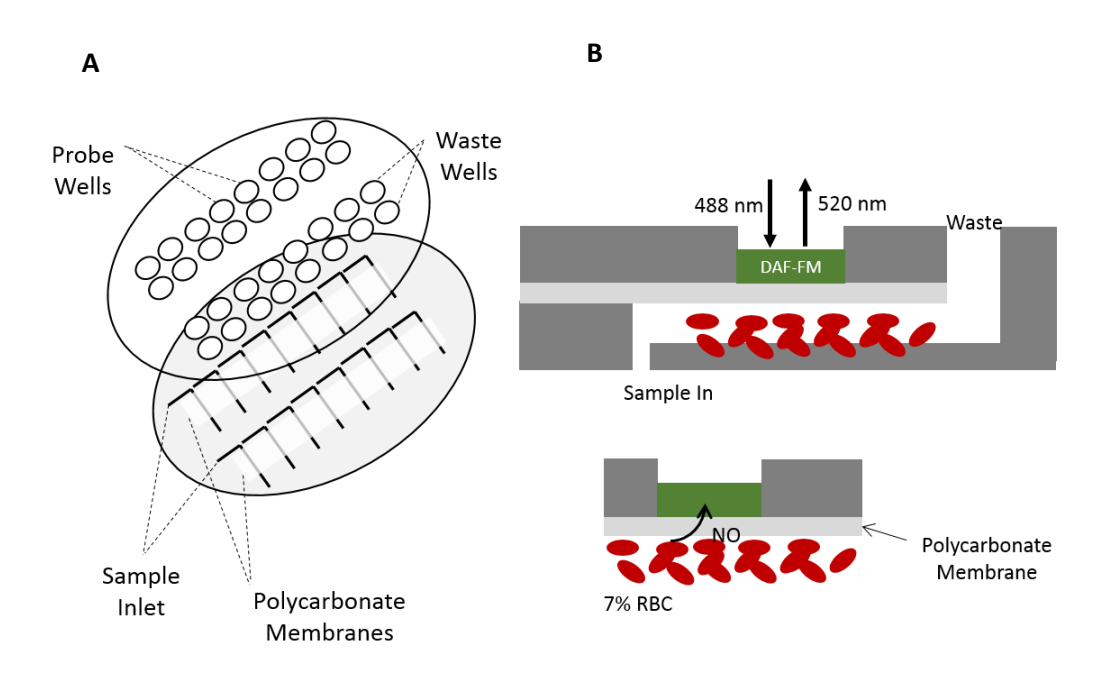


Figure 1.6. A sandwich PDMS microfluidic device for blood analysis. A), device design. Porous membrane was placed between two layers of PDMS, the bottom channel layer of channels and the top layer of wells. B), the schematic side view of a channel. While RBCs were flowing through the channel, produced molecules such as NO will diffuse through the membrane and be collected in the above well, where fluorescence detection can be performed to quantify NO.

## 1.2.3 Advantages and Disadvantages of PDMS Based Microfluidics

The development of microfluidics in the past two decades has turned this field into a very active and dynamic research area, which is reflected by the abundant publications. A Web of Science search revealed that there are more than 13,000 publications since 2000, with "microfluidic" in the title. However, this large body of publications has not helped realize the initial goal of building true micro total analysis systems. Real-world application of the technology in industry is one method to judge the maturity or true beneficial utility of a technology. In the case of microfluidics, the amount of practical and applicable devices does not indicate utility. The market for microfluidics is fairly small, with few simple commercialized devices<sup>90</sup>.

Although PDMS has many advantages, it also has some inevitable disadvantages<sup>91</sup>. For example, microfluidic devices made from PMDS usually lack of ruggedness, causing fluid management difficulties due to leaking and/or uneven pressure. PDMS devices are typically single-use, which reduces the reproducibility of measurements by introducing inter-device errors. These disadvantages also include lack of fabrication standardization (*e.g.* there are no standard production protocols for a specific microfluidic device; most current devices are highly lab-dependent) and practical integration, which enlarges the gap between academic research and real-life applications.

The reproducibility of PDMS microfluidic device fabrication is usually poor between laboratories. Even researchers within the same laboratory, but with different

skill proficiency, can sometimes produce different results. The main reasons behind this is the lack of reusability of PDMS devices and the complicated multiple fabrication steps, as well as the fluid introduction problems via the soft and weak punched ports<sup>92</sup>. For the former problem, a researcher has to fabricate multiple devices for a single measurement (a typical calibration and triplicate measurement will use eight devices), which increases the possibility of introducing error. For the latter problem, even though a different laboratory can have identical CAD designs of the device, the multiple fabrication steps can still inevitably introduce errors, which leads to inter-lab irreproducibility. Though many academic devices have integrated functional parts on a chip, each of them focused on integrating one part (*e.g.* either liquid manipulation or detection). There have been few devices that can integrate several units on one device to realize a real Lab-on-a-Chip platform.

Summarily, microfluidics has immense potential due to its unique characteristics of miniaturized reagent/sample usage, flow based measurement and integration. However, to move out of the academic realm and into applications, novel fabrication methods need to be developed to overcome the inherent drawbacks of PDMS or other fabrication methods involving multi-step production. Other polymers such as poly (methyl methacrylate) (PMMA)<sup>93</sup> and polystyrene (PS)<sup>94</sup> have been studied to make microfluidic devices, which showed advantages over PDMS, but did not essentially solve the problems. 3D-printing, a novel prototyping technology, has emerged as an alternative to fabricate microfluidic devices, and can potentially solve irreproducibility and integration issues seen with PDMS, PMMA and PS-based devices.

## 1.3 Three Dimensional (3D)-printing and Microfluidics

## 1.3.1 3D-printing

3D-printing, which is achieved using an additive process, where successive layers of materials are laid down to build a three dimensional object, has been recently used in academic research laboratories<sup>95</sup>. The idea of 3D-printing was initiated in the early 1980's, when Hideo Kodama of Nagoya Municipal Industrial Research Institute created two additive manufacturing methods for 3D plastic model fabrication with photocurable plastics<sup>96</sup>. Charles Hull further improved this manufacturing process by inventing the classical 3D-printing method, stereolithography, in which layers were created by curing photopolymers with ultraviolet (UV) lasers. Another contribution by Hull to the field of 3D-printing is the invention of the .STL file format that has become the gold standard for data transfer to 3D-printers<sup>97</sup>. A design that is created by computer aid design (CAD) programs (e.g. AutoCAD, AutoDesk, SolidWorks) can be exported to .STL format, where the surface of a 3D model will be broken down to close-packed arrays of triangles, where the coordinates of the vertices can be defined in a text file, and thus be interpreted by a 3D-printer98. The resolution can be controlled by adjusting the numbers of the triangles that compose a surface<sup>99</sup>.

#### 1.3.2 3D-printing Methods

During the past three decades, several 3D-printing methods have been commercialized. Stereolithography (SLA), created by Hull, was the first commercialized 3D-printing method<sup>100</sup>. Although there are different apparatus

designs for SLA from different companies, all of them share the core parts including a polymer reservoir, curing laser optics, and a support stage (Figure 1.7 A). The stage is immersed in a polymer reservoir, which is on the top (surface) of the reservoir at the beginning, and will lower as the printing process continues. A UV light beam traces a 2D cross section on the stage, which will cure a layer of polymer into a specific shape. The stage then lowers by a predefined distance, and another layer of polymer will be cured in the same way on top of the previous layer. This process will be repeated, layer by layer, until the 3D object is finished 101, 102.

Inkjet printing is another prototyping method for 3D-printing. The term of "ink" refers to the material being used to build a 3D object, such as a polymer 103. Figure 1.7B illustrates the principle of an inkjet 3D-printer that uses a liquid binding material as its ink. A layer of polymer particles will be distributed evenly from the powder supply state onto the fabrication stage by a roller, after which, the printing head drops the liquid binding material at desired areas to solidify it. After the first layer is finished, the fabrication stage will drop by a predefined distance, and a second layer will be distributed and selectively solidified by the binding liquid. The steps will be repeated until the 3D model is generated 104-106. Compared to SLA, this technique has a wider material choice. For example, in addition to polymers, some inorganic materials, such as ceramic powders can also be combined with proper binding materials to create a 3D object. However, this powder-based method also possesses some obvious drawbacks. The introduction of liquid binding materials, which are often biologically toxic, may disable such 3D-printed devices for biological applications, such as cell

culture and tissue engineering. The degree of binding of the particles is also questionable, which may result in porosity problems and surface roughness<sup>107</sup>. To overcome these disadvantages, powder-free inkjet printing methods have been developed<sup>108</sup>. For example, Stratasys produces several 3D-printers that can use liquid photopolymers as the ink, which however, will need UV lights for curing.

There is another powder-based, yet glue free 3D-printing method, known as selective laser sintering (SLS)<sup>109</sup>. The main setup of this method is similar to that of inkjet printing, except that a laser system is used to bind the powders through thermal sintering, instead of injecting liquid glue materials<sup>110</sup>. (Figure 1.7C) This method can be applied with a very wide range of materials, including metals. However, a main problem is the shrinkage and deformation of printed objects, caused by laser heating and immediate cooling afterwards<sup>111, 112</sup>.

The most widely used 3D-Printing method today is a technique called fused deposition modeling (FDM), which fabricates a 3D model by depositing semi-fused materials (e.g. thermoplastics) on a stage layer by layer<sup>113</sup>. (Figure 1.7D) The setups of this method are more simplified than SLA and inkjet printing, which enables the production of compact, benchtop 3D-printers. Another advantage of this method is it can be applied to any thermoplastic material, such as glass and certain ceramics. However, the resolution of objects fabricated with this method is fair, which is mainly determined by the size of the filaments of feeding materials<sup>114</sup>.

Helysis developed a method of directly stacking sheet materials such as paper, plastic and metal to create a 3D model, which is called laminated object manufacturing (LOM)<sup>115</sup>. As shown in Figure 1.7E, two rollers keep supplying a sheet material under a laser optics setup, which can selectively cut an outline on a layer that is stacked on the previous layer by a subsequent heating/glue treatment. LOM can only be used with materials that can be processed into sheets. Delamination is also a common problem with this method<sup>116, 117</sup>.

In 2015, DeSimmone reported a modification to 3D-printing that can achieve high resolution (below 100  $\mu$ m) with shorter fabrication time<sup>118</sup>. This method is derived from SLA (Figure 1.7F). In this technique, an oxygen-permeable window is incorporated between the polymer reservoir and UV light, to form a continuous liquid interface, which enables a continuous sequence of UV light to cure the polymer. Some examples show that hundreds of millimeters can be built within an hour, which significantly shortens 3D fabrication time.

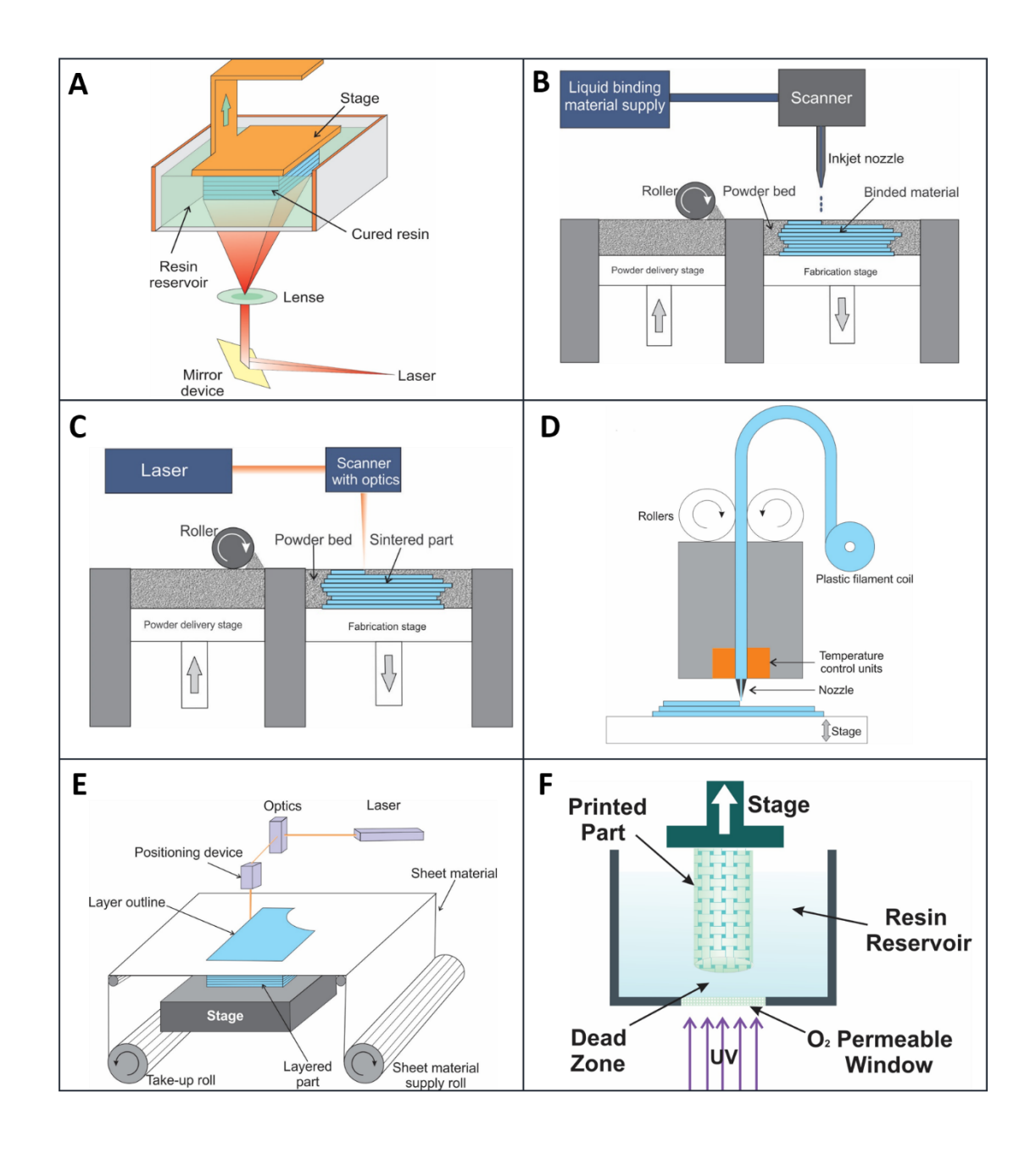


Figure 1.7. Current 3D-printing methods. A), stereolithography; B), inkjet printing; C), selective laser sintering; D), fused deposition modeling; E), laminated object manufacturing; F) continuous printing model

## 1.3.3 3D-printed Microfluidics

As discussed previously, microfluidics are powerful tools for many scientific applications that can be potentially developed to miniaturized lab-on-a-chip interfaces. However, certain disadvantages of PDMS and fabrication methods have prohibited this technique from being practically useful by the end-user. In addition to the poor ruggedness and mechanical strength of PDMS, most of the devices were prepared during a multi-step fabrication, which not only increases fabrication time (especially given the fact that most of the devices are not reusable), but also makes it difficult to reproduce results between different laboratories. Therefore, some researchers have advocated to use one-step manufacturing methods, such as 3D-printing, to fabricate the next generation of microfluidic devices. The first 3D-printed microfluidic device was created by Cronin in 2012, which is a flow-based micro reactor for the synthesis of imine. Subsequently, this concept has been further developed by Spence and other researchers in the past a few years, with the generation of a number of novel microfluidic devices that demonstrate superior features over PDMS devices.

#### 1.3.3.1 Advantageous Features of 3D-printed Microfluidic Devices

The poor ruggedness of PDMS usually results in uneven pressure distribution and flow problems (e.g. accumulation of liquid around inlet ports). Even though hard polymers such as polystyrene have been used to avoid these problems, the fabrication process is time consuming, and the failure rate during experiments is high. 3D-printing, however, enables fabrication of a rugged microfluidic device in one step. With proper

materials, such as acrylates, 3D-printed microfluidic devices can be reusable because they can be treated with harsh chemicals (e.g. bleach) and cleaning methods (e.g. ultra sonication), which significantly increases the reliability of results acquired on these devices<sup>102</sup>.

3D-printed microfluidic devices can also facilitate robust analytical method development, as evidenced by the device reported by Chen and colleagues<sup>119</sup>. 3D-printing enabled the authors to shape the fluidic device in the format of a standard 96-well plate, which is amenable to plate readers for high throughput analysis. With static wells printed on the device, simultaneous calibration can also be acquired on the same device.

Inter-lab reproducibility can also be enhanced by 3D-printed microfluidic devices. By sharing the engineering sketches of a design, with detailed data information, another researcher can easily achieve an identical device. Moreover, as more and more laboratories are using 3D-printing to fabricate their devices, a library database that collects all the device designs and parameters can be built, which can potentially leverage academic sharing, communication and mutual development.

Although integrated components have been realized on PDMS microfluidic devices, the poor ruggedness of PDMS increases the difficulty, time, and cost to integrate units on a device. Integrated devices using PDMS also suffer because the device itself is typically discarded after single use. Because 3D-printing can fabricate

any feature or shape based on user's demand, on-chip functional features such as connectors and mixers can be easily achieved<sup>120</sup>.

Microfluidic devices usually need to be connected to external tubing for liquid transport. A common technique for connecting tubing to a PDMS microfluidic device include directly inserting tubing into holes punched into PDMS and using adhesive to seal tubing into PDMS slabs<sup>121, 122</sup>. Frazier also created a locking mechanism by soft lithography that can form removable and tight connections, although this method was not widely implemented, partially because of the complexity of the fabrication process<sup>123</sup>. However, the lack of reliability and flexibility of these protocols can cause fatal problems for the devices. For example, inserting tubing directly into punched holes is susceptible to leakage or even ejection of the tubing. For 3D-printed devices, these problems and concerns can be removed by designing proper connection mechanisms. In Chen's device, the ends of each channel were printed with screw threads that fit standard finger tight adapters, via which external tubing can be connected. Hardin and colleagues also performed a thorough study by physical modeling and calculations that proved the reliability of printed threads 124. Moreover, with multi-material printing, O rings can also be printed on a microfluidic device for tight sealing or connection 125.

Lee and colleagues recently reported an integrated 3D-printed microfluidic device for biomarker detection. This single device contains mixers, reaction chambers, gradient generators and connectors, which enables sample pretreatment, reaction

and detection on the same chip, without skilled handling. Though this device was designed with different modules, 3D-printed alignments and O rings make it easy to combine, which meets the starting point of the research to develop an end-user detection device<sup>120</sup>.

With soft lithography, only channels with rectangular cross sections can be fabricated in PDMS. In the case of on-chip vasculature studies, because leukocytes preferentially migrate at the corners of a rectangular channel, the behaviors of these cells on such a device do not represent the *in vivo* conditions<sup>126</sup>. However, 3D-printing can easily fabricate channels with circular cross sections.

Electrophoresis and on-chip electrochemical detection is widely used as a step closer to the goal of lab-on-a-chip. Although electrodes have been successfully incorporated or deposited in PDMS microfluidic devices, the non-reusability of these devices increases research cost (especially when using expensive metals as electrodes), but reduces reliability of results due to inter-device error propagation. A 3D-printed electrochemical device that was developed by the Spence group and the Martin group avoided these problems by applying a flexible electrode system<sup>127</sup>. To be specific, electrodes were embedded in a hollow plastic screw nut with Nafion, which were then integrated into a female threaded port in a microfluidic device. After a measurement, the electrodes and the microfluidic device can be separated by screwing the nut off, and cleaned for reusing. Krejcova et al. recently also reported a 3D-printed

microfluidic device that combines electrodes and magnetic beads for the detection of influenza hemagglutinin<sup>128</sup>.

#### 1.3.4 Current Challenges and Future Directions

Although 3D-printed microfluidic devices possess a number of advantages as discussed above, current 3D-printing technologies are not advanced enough to fabricate perfect microfluidic devices. The resolution of current 3D-printers is usually at the level of tens to hundreds of microns, which is not sufficient for certain applications that require smaller sizes. Another problem resulting from the relatively poor resolution is surface roughness. Many 3D-printed objects need further polishing prior to use, which is not a problem for bulk surfaces, but may represent drawbacks for surfaces of small features and interior structures. The void spaces (channels, chambers etc.) are usually printed with pre-filling of supporting materials (e.g. waxlike compounds) that need to be completely removed before using, which is time consuming and labor intensive. Unfortunately, there isn't any literature that reports an easy way to clean the supporting materials. Also, most materials used in current 3D-printers are not elastomers. For certain studies that need to include mechanical factors, such as stretching, these hard devices will not be the appropriate choices. There is also a lack of studies evaluating the bio-toxicity of these materials.

The development of novel 3D-printing techniques can naturally solve some of the problems. However, the philosophy of combining PDMS and 3D-printing can be an immediate solution to the problems, which combines the strong points of other

fabrication methods to make up for its own shortcomings. For example, to avoid the surface roughness problem and the bio-toxicity concern, Gross recently reported a 3D-printed microfluidic device with a PDMS coated channel for cell culture<sup>129</sup>. Wu's group recently reported a creative concept, which is to use 3D-printing to fabricate complicated masters that cannot be easily achieved by soft lithography, to cast PDMS devices. With this method, they demonstrated several designs that include complicated 3D channel systems for flow regulating. This innovation enlightens the applications that have to be achieved on PDMS devices<sup>130</sup>. Also, 3D-printing can be used to produce rigid connection parts and sample pretreatment units that can be combined with PDMS devices.

## 1.4 Dissertation Motivation and Overview

In vivo, ERYs circulate under shear stress, and interact with other cell types. Therefore, to investigate ERY in a physiologically relevant way, an *in vitro* vasculature mimic device that can integrate other cell types and hemodynamics needs to be developed. Because microfluidic devices allows the samples to flow or even circulate, and micro-channels can be fabricated with dimensions <10 μm, which potentially replicates the geometry and dimensions of microcirculation, microfluidic devices can be a powerful tool to study *in vivo* physiology of ERYs on an *in vitro* device. PDMS based microfluidic devices have been widely used to create vasculature models that can mimic certain physiological factors such as hemodynamics, physiological relevance, and cell integration. However, due to the inherent drawbacks of PDMS

devices, such as lack of ruggedness and reproducibility, most of the currently developed microfluidic vasculature devices only include one physiological factor. Also, these complicated devices are not reusable, which not only increases fabrication cost and time, but also reduces reproducibility.

One-step fabrication of microfluidic devices with more rugged materials has thus been proposed by researchers, and 3D-printing appears to be a promising technique to fabricate the next generation of microfluidics. Some pioneering research work by the Spence group and others has proven 3D-printed microfluidic devices can be more integrated, rugged, reusable, and reproducible than PDMS based devices. More importantly, features such as threads and connection ports can also be easily achieved with 3D-printing. The design of a device with CAD software can also be shared between laboratories for device reproduction.

Therefore, there are two goals for the research work presented in this dissertation. The first goal is relevant to engineering and attempts to develop a standard *in vitro* circulation/vasculature device by 3D-printing, to investigate ERY physiology. This 3D-printed fluidic device demonstrates some important advantages over its PDMS counterpart. For example, screw threads are printed at the ends of each channel for simple, yet tight connection to external tubing. The design of static wells enables simultaneous on-chip calibration, which promotes experiment efficiency and increases reliability. Moreover, the dimensions of the device, as well as the locations of the wells follow a standard 96-well plate geometry so that the whole device can be

placed directly in a plate reader for high content readout. The device is rugged and reusable, which enables the valuation of stored ERY samples on the same device during an experiment period of six weeks. The device also shows its versatility to be developed to an Organs-on-a-Chip model for inter-tissue communication studies. By simply plugging membrane inserts that contain cultured cells into the wells on the device, different cell types can be combined to investigate cell-cell interactions. In this study, pancreatic  $\beta$ -cells (INS-1 cell line) that can secret C-peptide, and endothelial cells that can mimic a blood vessel barrier will be integrated, and be connected by circulating ERYs. Although PMDS-based Organs-on-a-Chip platforms have been developed, they were mainly single-cell models, and had to be discarded after single use. This 3D-printed model demonstrates an innovative way to fabricate more integrated (e.g. multiple cells), standard (e.g. using membrane inserts to culture cells), and versatile (e.g. any cell type that can be cultured in membrane inserts can be integrated and studied) Organs-on-a-Chip platforms. In this research work, 3Dprinting also shows its capability in fabrication of demand-based and customized analytical devices.

From a physiological perspective, these 3D-printed devices facilitate the investigation of ERYs, with the ultimate goals of developing a therapy for diabetic complications, and improving the quality of stored ERYs. By circulating ERYs under different conditions through different channels on the 3D-printed fluidic device, the efficacy of C-peptide, Zn<sup>2+</sup> and albumin in stimulating ATP release from ERYs is confirmed, which can be potentially developed to a therapy for diabetic complications.

This single device also enables long-term evaluation of stored ERYs, suggesting that a normoglycemic storage condition is more beneficial to stored ERYs than currently approved hyperglycemic solutions. The results acquired from a 3D-printed homemade cell filtration device proved that hyperglycemia can permanently diminish ERY deformability.

REFERENCES

#### **REFERENCES**

- 1. Fairbanks, G., Steck, T.L. & Wallach, D.F. Electrophoretic analysis of the major polypeptides of the human erythrocyte membrane. *Biochemistry* 10, 2606-2617 (1971).
- 2. Cooke, J.P. & Dzau, V.J. Nitric oxide synthase: Role in the genesis of vascular disease. *Annu Rev Med* 48, 489-509 (1997).
- 3. Buga, G.M., Gold, M.E., Fukuto, J.M. & Ignarro, L.J. Shear-Stress Induced Release of Nitric-Oxide from Endothelial-Cells Grown on Beads. *Hypertension* 17, 187-193 (1991).
- 4. Sprague, R.S. et al. Effect of L-NAME on pressure-flow relationships in isolated rabbit lungs: Role of red blood cells (vol 38, pg H1941, 1995). *Am J Physiol-Heart C* 270, U33-U33 (1996).
- 5. Sprague, R.S., Ellsworth, M.L., Stephenson, A.H., Kleinhenz, M.E. & Lonigro, A.J. Deformation-induced ATP release from red blood cells requires CFTR activity. *Am J Physiol-Heart C* 275, H1726-H1732 (1998).
- 6. Sprague, R.S., Ellsworth, M.L., Stephenson, A.H. & Lonigro, A.J. ATP: The red blood cell link to NO and local control of the pulmonary circulation. *Am J Physiol-Heart C* 271, H2717-H2722 (1996).
- 7. Bergfeld, G.R. & Forrester, T. Release of Atp from Human Erythrocytes in Response to a Brief Period of Hypoxia and Hypercapnia. *Cardiovasc Res* 26, 40-47 (1992).
- 8. Rich, S.S. Genetics of diabetes and its complications. *J Am Soc Nephrol* 17, 353-360 (2006).
- 9. Low, P.A., Schmelzer, J.D., Ward, K.K., Curran, G.L. & Poduslo, J.F. Effect of Hyperbaric Oxygenation on Normal and Chronic Streptozotocin Diabetic Peripheral-Nerves. *Exp Neurol* 99, 201-212 (1988).
- 10. Pierce, E.A., Avery, R.L., Foley, E.D., Aiello, L.P. & Smith, L.E.H. Vascular Endothelial Growth-Factor Vascular-Permeability Factor Expression in a Mouse Model of Retinal Neovascularization. *P Natl Acad Sci USA* 92, 905-909 (1995).
- 11. Sheetz, M.J. & King, G.L. Molecular understanding of hyperglycemia's adverse effects for diabetic complications. *Jama-J Am Med Assoc* 288, 2579-2588 (2002).
- 12. Craven, P.A., Caines, M.A. & Derubertis, F.R. Sequential Alterations in Glomerular Prostaglandin and Thromboxane Synthesis in Diabetic Rats -

- Relationship to the Hyperfiltration of Early Diabetes. *Metabolism* 36, 95-103 (1987).
- 13. Carroll, J. et al. An altered oxidant defense system in red blood cells affects their ability to release nitric oxide-stimulating ATP. *Mol Biosyst* 2, 305-311 (2006).
- 14. Sprague, R.S., Stephenson, A.H., Bowles, E.A., Stumpf, M.S. & Lonigro, A.J. Reduced expression of G(i) in erythrocytes of humans with type 2 diabetes is associated with impairment of both cAMP generation and ATP release. *Diabetes* 55, 3588-3593 (2006).
- 15. Chiu, J.J. & Chien, S. Effects of Disturbed Flow on Vascular Endothelium: Pathophysiological Basis and Clinical Perspectives. *Physiol Rev* 91, 327-387 (2011).
- 16. Abaci, H.E., Hanjaya-Putra, D. & Gerecht, S. Hypoxia and Matrix Manipulation for Vascular Engineering. *Biol Med Phys Biomed*, 127-165 (2011).
- 17. Wong, K.H.K., Chan, J.M., Kamm, R.D. & Tien, J. Microfluidic Models of Vascular Functions. *Annual Review of Biomedical Engineering, Vol* 14 14, 205-230 (2012).
- 18. Shevkoplyas, S.S., Gifford, S.C., Yoshida, T. & Bitensky, M.W. Prototype of an in vitro model of the microcirculation. *Microvasc Res* 65, 132-136 (2003).
- 19. Shevkoplyas, S.S., Yoshida, T., Gifford, S.C. & Bitensky, M.W. Direct measurement of the impact of impaired erythrocyte deformability on microvascular network perfusion in a microfluidic device. *Lab Chip* 6, 914-920 (2006).
- 20. Wan, J.D., Ristenpart, W.D. & Stone, H.A. Dynamics of shear-induced ATP release from red blood cells. *P Natl Acad Sci USA* 105, 16432-16437 (2008).
- 21. Sprung, R., Sprague, R. & Spence, D. Determination of ATP release from erythrocytes using microbore tubing as a model of resistance vessels in vivo. *Anal Chem* 74, 2274-2278 (2002).
- 22. Shao, J.B. et al. Integrated microfluidic chip for endothelial cells culture and analysis exposed to a pulsatile and oscillatory shear stress. *Lab Chip* 9, 3118-3125 (2009).
- 23. Bouhadir, K.H. & Mooney, D.J. Promoting angiogenesis in engineered tissues. *J Drug Target* 9, 397-406 (2001).
- 24. Whitesides, G.M. The origins and the future of microfluidics. *Nature* 442, 368-373 (2006).

- 25. Abgrall, P. & Gue, A.M. Lab-on-chip technologies: making a microfluidic network and coupling it into a complete microsystem a review. *J Micromech Microeng* 17, R15-R49 (2007).
- 26. Terry, S.C., Jerman, J.H. & Angell, J.B. Gas-Chromatographic Air Analyzer Fabricated on a Silicon-Wafer. *Ieee T Electron Dev* 26, 1880-1886 (1979).
- 27. Ruzicka, J. & Hansen, E.H. Flow-Injection Analysis and Its Early History. *Talanta* 29, 157-157 (1982).
- 28. Ruzicka, J., Hansen, E.H. & Ramsing, A.U. Flow-Injection Analyzer for Students, Teaching and Research Spectrophotometric Methods. *Anal Chim Acta* 134, 55-71 (1982).
- 29. Whitesides, G.M. & Stroock, A.D. Flexible methods for microfluidics. *Phys Today* 54, 42-48 (2001).
- 30. Mijatovic, D., Eijkel, J.C.T. & van den Berg, A. Technologies for nanofluidic systems: top-down vs. bottom-up a review. *Lab Chip* 5, 492-500 (2005).
- 31. McDonald, J.C. et al. Fabrication of microfluidic systems in poly(dimethylsiloxane). *Electrophoresis* 21, 27-40 (2000).
- 32. McDonald, J.C. & Whitesides, G.M. Poly(dimethylsiloxane) as a material for fabricating microfluidic devices. *Accounts Chem Res* 35, 491-499 (2002).
- 33. Xia, Y.N. & Whitesides, G.M. Soft lithography. *Annu Rev Mater Sci* 28, 153-184 (1998).
- 34. Lorenz, H. et al. SU-8: a low-cost negative resist for MEMS. *J Micromech Microeng* 7, 121-124 (1997).
- 35. Whitesides, G.M., Ostuni, E., Takayama, S., Jiang, X.Y. & Ingber, D.E. Soft lithography in biology and biochemistry. *Annu Rev Biomed Eng* 3, 335-373 (2001).
- 36. Fredsoe, J. Turbulent Boundary-Layer in Wave-Current Motion. *J Hydraul Eng-Asce* 110, 1103-1120 (1984).
- 37. Suh, Y.K. & Kang, S. A Review on Mixing in Microfluidics. *Micromachines-Basel* 1, 82-111 (2010).
- 38. Squires, T.M. & Quake, S.R. Microfluidics: Fluid physics at the nanoliter scale. *Rev Mod Phys* 77, 977-1026 (2005).
- 39. Hessel, V., Lowe, H. & Schonfeld, F. Micromixers a review on passive and active mixing principles. *Chem Eng Sci* 60, 2479-2501 (2005).
- 40. Nguyen, N.T. & Wu, Z.G. Micromixers a review. *J Micromech Microeng* 15, R1-R16 (2005).

- 41. Stroock, A.D. et al. Chaotic mixer for microchannels. *Science* 295, 647-651 (2002).
- 42. Mengeaud, V., Josserand, J. & Girault, H.H. Mixing processes in a zigzag microchannel: Finite element simulations and optical study. *Anal Chem* 74, 4279-4286 (2002).
- 43. Jen, C.P., Wu, C.Y., Lin, Y.C. & Wu, C.Y. Design and simulation of the micromixer with chaotic advection in twisted microchannels. *Lab Chip* 3, 77-81 (2003).
- 44. Kim, D.S., Lee, S.W., Kwon, T.H. & Lee, S.S. A barrier embedded chaotic micromixer. *J Micromech Microeng* 14, 798-805 (2004).
- 45. Hong, J.W. & Quake, S.R. Integrated nanoliter systems. *Nat Biotechnol* 21, 1179-1183 (2003).
- 46. Thorsen, T., Maerkl, S.J. & Quake, S.R. Microfluidic large-scale integration. *Science* 298, 580-584 (2002).
- 47. Quake, S. The chips are down microfluidic large-scale integration. *Trac-Trend Anal Chem* 21, Xii-Xiii (2002).
- 48. Karlinsey, J.M., Monahan, J., Marchiarullo, D.J., Ferrance, J.P. & Landers, J.P. Pressure injection on a valved microdevice for electrophoretic analysis of submicroliter samples. *Anal Chem* 77, 3637-3643 (2005).
- 49. Li, M.W., Huynh, B.H., Hulvey, M.K., Lunte, S.M. & Martin, R.S. Design and characterization of poly(dimethylsiloxane)-based valves for interfacing continuous-flow sampling to microchip electrophoresis. *Anal Chem* 78, 1042-1051 (2006).
- 50. de Jong, J., Lammertink, R.G.H. & Wessling, M. Membranes and microfluidics: a review. *Lab Chip* 6, 1125-1139 (2006).
- 51. Srigunapalan, S., Lam, C., Wheeler, A.R. & Simmons, C.A. A microfluidic membrane device to mimic critical components of the vascular microenvironment. *Biomicrofluidics* 5 (2011).
- 52. Halpin, S.T. & Spence, D.M. Direct Plate-Reader Measurement of Nitric Oxide Released from Hypoxic Erythrocytes Flowing through a Microfluidic Device. *Anal Chem* 82, 7492-7497 (2010).
- 53. Vogel, P.A., Halpin, S.T., Martin, R.S. & Spence, D.M. Microfluidic Transendothelial Electrical Resistance Measurement Device that Enables Blood Flow and Postgrowth Experiments. *Anal Chem* 83, 4296-4301 (2011).
- 54. Kuswandi, B., Nuriman, Huskens, J. & Verboom, W. Optical sensing systems for microfluidic devices: A review. *Anal Chim Acta* 601, 141-155 (2007).

- 55. Chabinyc, M.L. et al. An integrated fluorescence detection system in poly(dimethylsiloxane) for microfluidic applications. *Anal Chem* 73, 4491-4498 (2001).
- 56. Erickson, D. & Li, D.Q. Integrated microfluidic devices. *Anal Chim Acta* 507, 11-26 (2004).
- 57. Li, X.H., Klemic, K.G., Reed, M.A. & Sigworth, F.J. Microfluidic system for planar patch clamp electrode arrays. *Nano Lett* 6, 815-819 (2006).
- 58. Swensen, J.S. et al. Continuous, Real-Time Monitoring of Cocaine in Undiluted Blood Serum via a Microfluidic, Electrochemical Aptamer-Based Sensor. *J Am Chem Soc* 131, 4262-4266 (2009).
- 59. Kovachev, N., Canals, A. & Escarpa, A. Fast and Selective Microfluidic Chips for Electrochemical Antioxidant Sensing in Complex Samples. *Anal Chem* 82, 2925-2931 (2010).
- 60. Harrison, D.J., Manz, A., Fan, Z.H., Ludi, H. & Widmer, H.M. Capillary Electrophoresis and Sample Injection Systems Integrated on a Planar Glass Chip. *Anal Chem* 64, 1926-1932 (1992).
- 61. Jacobson, S.C., Culbertson, C.T., Daler, J.E. & Ramsey, J.M. Microchip structures for submillisecond electrophoresis. *Anal Chem* 70, 3476-3480 (1998).
- 62. Simpson, P.C. et al. High-throughput genetic analysis using microfabricated 96-sample capillary array electrophoresis microplates. *P Natl Acad Sci USA* 95, 2256-2261 (1998).
- 63. Jacobson, S.C., Ermakov, S.V. & Ramsey, J.M. Minimizing the number of voltage sources and fluid reservoirs for electrokinetic valving in microfluidic devices. *Anal Chem* 71, 3273-3276 (1999).
- 64. Raymond, D.E., Manz, A. & Widmer, H.M. Continuous Sample Pretreatment Using a Free-Flow Electrophoresis Device Integrated onto a Silicon Chip. *Anal Chem* 66, 2858-2865 (1994).
- 65. Wu, D.P., Qin, J.H. & Lin, B.C. Electrophoretic separations on microfluidic chips. *J Chromatogr A* 1184, 542-559 (2008).
- 66. Jacobson, S.C., Hergenroder, R., Koutny, L.B., Warmack, R.J. & Ramsey, J.M. Effects of Injection Schemes and Column Geometry on the Performance of Microchip Electrophoresis Devices. *Anal Chem* 66, 1107-1113 (1994).
- 67. Mecker, L.C. & Martin, R.S. Integration of Microdialysis Sampling and Microchip Electrophoresis with Electrochemical Detection. *Anal Chem* 80, 9257-9264 (2008).

- 68. Mayers, B.T., Vezenov, D.V., Vullev, V.I. & Whitesides, G.M. Arrays and cascades of fluorescent liquid-liquid waveguides: Broadband light sources for spectroscopy in microchannels. *Anal Chem* 77, 1310-1316 (2005).
- 69. Ma, B. et al. A hybrid microdevice with a thin PDMS membrane on the detection window for UV absorbance detection. *Electrophoresis* 28, 2474-2477 (2007).
- 70. Wang, J., Ibanez, A., Chatrathi, M.P. & Escarpa, A. Electrochemical enzyme immunoassays on microchip platforms. *Anal Chem* 73, 5323-5327 (2001).
- 71. Sandlin, Z.D., Shou, M.S., Shackman, J.G. & Kennedy, R.T. Microfluidic electrophoresis chip coupled to microdialysis for in vivo monitoring of amino acid neurotransmitters. *Anal Chem* 77, 7702-7708 (2005).
- 72. Shiddiky, M.J.A., Park, H. & Shim, Y.B. Direct analysis of trace phenolics with a microchip: In-channel sample preconcentration, separation, and electrochemical detection. *Anal Chem* 78, 6809-6817 (2006).
- 73. Schulze, P., Ludwig, M., Kohler, F. & Belder, D. Deep UV laser-induced fluorescence detection of unlabeled drugs and proteins in microchip electrophoresis. *Anal Chem* 77, 1325-1329 (2005).
- 74. Effenhauser, C.S., Paulus, A., Manz, A. & Widmer, H.M. High-Speed Separation of Antisense Oligonucleotides on a Micromachined Capillary Electrophoresis Device. *Anal Chem* 66, 2949-2953 (1994).
- 75. Blazej, R.G., Kumaresan, P. & Mathies, R.A. Microfabricated bioprocessor for integrated nanoliter-scale Sanger DNA sequencing. *P Natl Acad Sci USA* 103, 7240-7245 (2006).
- 76. Dang, F.Q. et al. Hybrid dynamic coating with n-dodecyl beta-D-maltoside and methyl cellulose for high-performance carbohydrate analysis on poly(methyl methacrylate) chips. *Anal Chem* 78, 1452-1458 (2006).
- 77. Ye, N.N., Qin, J.H., Shi, W.W. & Lin, B.C. Characterizing doxorubicin-induced apoptosis in HepG2 cells using an integrated microfluidic device. *Electrophoresis* 28, 1146-1153 (2007).
- 78. Qin, J.H. et al. Simultaneous and ultrarapid determination of reactive oxygen species and reduced glutathione in apoptotic leukemia cells by microchip electrophoresis. *Electrophoresis* 26, 1155-1162 (2005).
- 79. Kapishnikov, S., Kantsler, V. & Steinberg, V. Continuous particle size separation and size sorting using ultrasound in a microchannel. *J Stat Mech-Theory E* (2006).

- 80. Shi, J.J., Huang, H., Stratton, Z., Huang, Y.P. & Huang, T.J. Continuous particle separation in a microfluidic channel via standing surface acoustic waves (SSAW). *Lab Chip* 9, 3354-3359 (2009).
- 81. Huh, D. et al. Gravity-driven microfluidic particle sorting device with hydrodynamic separation amplification. *Anal Chem* 79, 1369-1376 (2007).
- 82. Kuntaegowdanahalli, S.S., Bhagat, A.A.S., Kumar, G. & Papautsky, I. Inertial microfluidics for continuous particle separation in spiral microchannels. *Lab Chip* 9, 2973-2980 (2009).
- 83. Phillips, K.S. & Cheng, Q. Microfluidic immunoassay for bacterial toxins with supported phospholipid bilayer membranes on poly(dimethylsiloxane). *Anal Chem* 77, 327-334 (2005).
- 84. Jiang, H., Weng, X.A. & Li, D.Q. Microfluidic whole-blood immunoassays. *Microfluid Nanofluid* 10, 941-964 (2011).
- 85. Livak-Dahl, E., Sinn, I. & Burns, M. Microfluidic Chemical Analysis Systems. *Annu Rev Chem Biomol* 2, 325-353 (2011).
- 86. Martinez, A.W. et al. Simple telemedicine for developing regions: Camera phones and paper-based microfluidic devices for real-time, off-site diagnosis. *Anal Chem* 80, 3699-3707 (2008).
- 87. Ellerbee, A.K. et al. Quantifying Colorimetric Assays in Paper-Based Microfluidic Devices by Measuring the Transmission of Light through Paper. *Anal Chem* 81, 8447-8452 (2009).
- 88. Martinez, A.W., Phillips, S.T., Whitesides, G.M. & Carrilho, E. Diagnostics for the Developing World: Microfluidic Paper-Based Analytical Devices. *Anal Chem* 82, 3-10 (2010).
- 89. Kim, J., Johnson, M., Hill, P. & Gale, B.K. Microfluidic sample preparation: cell lysis and nucleic acid purification. *Integr Biol* 1, 574-586 (2009).
- 90. Volpatti, L.R. & Yetisen, A.K. Commercialization of microfluidic devices. *Trends Biotechnol* 32, 347-350 (2014).
- 91. Mukhopadhyay, R. Hard-soft microfluidic device bypasses drawbacks of PDMS. *Anal Chem* 81, 5108-5108 (2009).
- 92. Coltro, W.K.T., Lunte, S.M. & Carrilho, E. Comparison of the analytical performance of electrophoresis microchannels fabricated in PDMS, glass, and polyester-toner. *Electrophoresis* 29, 4928-4937 (2008).
- 93. Galloway, M. et al. Contact conductivity detection in poly(methyl methacylate)-based microfluidic devices for analysis of mono- and polyanionic molecules. *Anal Chem* 74, 2407-2415 (2002).

- 94. Shadpour, H. et al. Multichannel microchip electrophoresis device fabricated in polycarbonate with an integrated contact conductivity sensor array. *Anal Chem* 79, 870-878 (2007).
- 95. Gross, B.C., Erkal, J.L., Lockwood, S.Y., Chen, C.P. & Spence, D.M. Evaluation of 3D Printing and Its Potential Impact on Biotechnology and the Chemical Sciences. *Anal Chem* 86, 3240-3253 (2014).
- 96. Kodama, H. Automatic Method for Fabricating a 3-Dimensional Plastic Model with Photo-Hardening Polymer. *Rev Sci Instrum* 52, 1770-1773 (1981).
- 97. Hull, C.W. Apparatus for production of three-dimensional objects by stereolithography. *us patent* 4,929,402 (1986).
- 98. Landers, R. et al. Fabrication of soft tissue engineering scaffolds by means of rapid prototyping techniques. *J Mater Sci* 37, 3107-3116 (2002).
- 99. Pandey, P.M., Reddy, N.V. & Dhande, S.G. Slicing procedures in layered manufacturing: a review. *Rapid Prototyping J* 9, 274-288 (2003).
- 100. Melchels, F.P.W., Feijen, J. & Grijpma, D.W. A review on stereolithography and its applications in biomedical engineering. *Biomaterials* 31, 6121-6130 (2010).
- 101. Stereolithography: Materials, Processes and Applications. *Stereolithography: Materials, Processes and Applications*, 1-340 (2011).
- 102. Waldbaur, A., Rapp, H., Lange, K. & Rapp, B.E. Let there be chip-towards rapid prototyping of microfluidic devices: one-step manufacturing processes. *Anal Methods-Uk* 3, 2681-2716 (2011).
- 103. Calvert, P. Inkjet printing for materials and devices. *Chem Mater* 13, 3299-3305 (2001).
- 104. Pfister, A. et al. Biofunctional rapid prototyping for tissue-engineering applications: 3D bioplotting versus 3D printing. *J Polym Sci Pol Chem* 42, 624-638 (2004).
- 105. Keyser, E.L., Sears, S. B. Method and apparatus for recording with writing fluids and drop projection means therefor. *us patent* 3,946,398 (1976).
- 106. Breen, J., Nottrot, R. & Stellingwerff, M. Tangible virtuality perceptions of computer-aided and physical modelling. *Automat Constr* 12, 649-653 (2003).
- 107. Lam, C.X.F., Mo, X.M., Teoh, S.H. & Hutmacher, D.W. Scaffold development using 3D printing with a starch-based polymer. *Mat Sci Eng C-Bio S* 20, 49-56 (2002).
- 108. de Gans, B.J., Duineveld, P.C. & Schubert, U.S. Inkjet printing of polymers: State of the art and future developments. *Adv Mater* 16, 203-213 (2004).

- 109. Beaman, J.J., Deckard, C. R. Selective laser sintering with assisted powder handling. *US PATENT* 4,938,816 (1990).
- 110. Kumar, S. Selective laser sintering: A qualitative and objective approach. *Jom-J Min Met Mat S* 55, 43-47 (2003).
- 111. Kruth, J.P., Mercelis, P., Van Vaerenbergh, J., Froyen, L. & Rombouts, M. Binding mechanisms in selective laser sintering and selective laser melting. *Rapid Prototyping J* 11, 26-36 (2005).
- 112. Song, Y.A. & Koenig, W. Experimental study of the basic process mechanism for direct selective laser sintering of low-melting metallic powder. *Cirp Annals* 1997 Manufacturing Technology, Volume 46/1/1997 46, 127-130 (1997).
- 113. Zhong, W.H., Li, F., Zhang, Z.G., Song, L.L. & Li, Z.M. Short fiber reinforced composites for fused deposition modeling. *Mat Sci Eng a-Struct* 301, 125-130 (2001).
- 114. Jafari, M.A. et al. A novel system for fused deposition of advanced multiple ceramics. *Rapid Prototyping J* 6, 161-174 (2000).
- 115. Feygin, M.S., A.; Diamond M. N.; Dvorskiy, E Laminated object manufacturing system. *US patent* 5,730,817 (1998).
- 116. Mueller, B. & Kochan, D. Laminated object manufacturing for rapid tooling and patternmaking in foundry industry. *Comput Ind* 39, 47-53 (1999).
- 117. Rengier, F. et al. 3D printing based on imaging data: review of medical applications. *Int J Comput Ass Rad* 5, 335-341 (2010).
- 118. Tumbleston, J.R. et al. Continuous liquid interface production of 3D objects. *Science* 347, 1349-1352 (2015).
- 119. Chen, C.P., Wang, Y.M., Lockwood, S.Y. & Spence, D.M. 3D-printed fluidic devices enable quantitative evaluation of blood components in modified storage solutions for use in transfusion medicine. *Analyst* 139, 3219-3226 (2014).
- 120. Lee, K.G. et al. 3D printed modules for integrated microfluidic devices. *Rsc. Adv.* 4, 32876-32880 (2014).
- 121. Tsai, J.H. & Lin, L.W. Micro-to-macro fluidic interconnectors with an integrated polymer sealant. *J Micromech Microeng* 11, 577-581 (2001).
- 122. Lo, R. & Meng, E. Integrated and reusable in-plane microfluidic interconnects. *Sensor Actuat B-Chem* 132, 531-539 (2008).
- 123. Han, K.H. & Frazier, A.B. Reliability aspects of packaging and integration technology for microfluidic systems. *Ieee T Device Mat Re* 5, 452-457 (2005).

- 124. Hardin, J.O., Ober, T. J., Valentine, A. D., Lewis, J. A Microfluidic Printheads for Multimaterial 3D Printing of Viscoelastic Inks. *Adv Mater* 10.1002/adma.201500222 (2015).
- 125. Paydar, O.H. et al. Characterization of 3D-printed microfluidic chip interconnects with integrated O-rings. *Sensor Actuat a-Phys* 205, 199-203 (2014).
- 126. Burns, J.M., Yang, X.X., Forouzan, O., Sosa, J.M. & Shevkoplyas, S.S. Artificial microvascular network: a new tool for measuring rheologic properties of stored red blood cells. *Transfusion* 52, 1010-1023 (2012).
- 127. Erkal, J.L. et al. 3D printed microfluidic devices with integrated versatile and reusable electrodes. *Lab Chip* 14, 2023-2032 (2014).
- 128. Krejcova, L. et al. 3D printed chip for electrochemical detection of influenza virus labeled with CdS quantum dots. *Biosens Bioelectron* 54, 421-427 (2014).
- 129. Bethany C Gross , K.B.A., Jayda E Meisel , Megan I McNitt , Dana M Spence Polymer Coatings in 3D Printed Fluidic Device Channels for Improved Cellular Adherence Prior to Electrical Lysis. *Anal Chem* DOI: 10.1021/acs.analchem.5b01202 (2015).
- 130. Chan, H.N., Chen, Y., Shu, Y., Chen, Y., Tian, Q., Wu, H. Direct, one-step molding of 3D-printed structures for convenient fabrication of truly 3D PDMS microfluidic chips. *Microfluidics and Nanofluidics* DOI 10.1007/s10404-014-1542-4 (2015).

Chapter 2 – Study of C-peptide Stimulated ATP Release from Erythrocytes on a 3Dprinted Circulation-mimic Fluidic Device

## 2.1 Background

## 2.1.1 Diabetes Complications

Diabetes mellitus is a medical condition that is characterized by uncontrolled and elevated blood glucose levels. It currently affects more than 20 million people in the United States, but this number may increase to 48.3 million people by the year  $2050^1$ . Based on different pathologies, there are three main types of diabetes: type 1, type 2 and gestational diabetes. Type 1 diabetes stems from a lack of insulin production due to destruction of pancreatic  $\beta$ -cells. These patients are dependent on exogenous insulin therapy and type 1 diabetics make up about 10 % of all reported cases of diabetes. Type 2 diabetes, or non-insulin dependent diabetes, resulting from a resistance to insulin. Overall, it accounts for about 85% of all reported cases of diabetes. The third type of diabetes is gestational diabetes, or pregnancy-induced diabetes, which accounts for about 5% of diabetes in the United States<sup>2-4</sup>.

Diabetes typically leads to chronic complications, which may result in endless pain and increased mortality. These complications may include nerve damage (neuropathy), blindness (retinopathy), kidney damage (nephropathy), or cardiovascular disease<sup>5</sup>. Nearly all people with diabetes in the United States suffer some form of neuropathy<sup>6</sup>. Some symptoms of the onset of neuropathy include numbness, loss of dexterity, burning, hypersensitivity and difficulty in rising from a

seated position<sup>7</sup>. Diabetic retinopathy (DR) is reported to be the leading cause of new cases of blindness<sup>8</sup>, and people with diabetics are about 30 times more likely than a healthy individual to become blind<sup>9</sup>. Kidney disease is another severe result of diabetes, which leads to leakage of protein into urine and eventually kidney failure<sup>10</sup>.

The direct cause of most diabetic complications lies in the dysfunction of the interface between the blood stream and peripheral tissues, or blood vessel barriers <sup>11</sup>. Low and colleagues suggested that neuropathy results from poor blood flow that lead to endoneurial hypoxia, which decreases nerve signaling <sup>12</sup>. Retinopathy stems from diminished blood flow that causes poor oxygen supply, which triggers retinal cells to form new but fragile vessels via a vascular endothelial growth factor mechanism. The new fragile vessels can cloud a patient's vision by leaking blood into the vitreous, and will eventually detach the retina and cause blindness <sup>13, 14</sup>. Nephropathy occurs when the glomerulus undergoes partial sclerosis or failure to dilate, resulting in hyper filtration and resulting protein leakage <sup>15</sup>. All of these studies indicate that restoration of vasodilation and/or blood flow can be a potential therapy for diabetic complications.

# 2.1.2 C-peptide and Vasodilation

C-peptide and insulin are produced simultaneously from proinsulin in pancreatic  $\beta$ -cells<sup>16</sup>. As shown in Figure 2.1, in a proinsulin molecule, the insulin chains A and B are linked by a connecting segment, which will subsequently form C-peptide. Two endopeptidases are involved in cleaving the proinsulin molecule to produce insulin, one cleaving exclusively on the C-terminal side of Arg 31/Arg 32 (B-chain/C-peptide

junction), the other on the C-terminal side of Lys 64/Arg 65 of proinsulin (C-peptide/A-chain junction)<sup>17</sup>. Therefore, the 31 amino acid peptide (C-peptide) is produced and secreted in equimolar amounts with insulin. Since this process was discovered in  $1967^{18}$ , C-peptide had long been regarded as a by-product of insulin production, with no physiological relevance. Due to the longer half-life of C-peptide (30min) compared with insulin (3min), the main application of C-peptide is its use in monitoring the function of  $\beta$ -cells of diabetic patients<sup>19</sup>.

In the past two decades, studies have shown that C-peptide can reduce diabetic complications. The Diabetes Control and Complications Trial Research Group reported that treatment of hyperglycemia decreases diabetic complications, but it is not sufficient to fully reverse diabetes, suggesting that there is a missing therapy for diabetic complications<sup>20</sup>.

Sjoberg and colleagues found that some type 1 diabetic patients who maintained some degree of  $\beta$ -cell activity after the onset of the disease experienced less severe complications than those whose  $\beta$ -cells were completely destroyed<sup>21</sup>. The evidence suggested that other molecule(s) secreted from  $\beta$ -cells are important for control of diabetic complications, and thus C-peptide attracted the attention of a few pioneer researchers. In a recent study, diabetic patients who retained detectable amounts of C-peptide after the onset of the disease exhibited lower levels of complications such as retinopathy, microalbuminuria, and neuropathy<sup>22</sup>.

Johansson performed multiple studies evaluating the effects of the short-term replacement of C-peptide on renal function in type 1 diabetic patients, finding that C-peptide infusion significantly decreased glomerular hyperfiltration. They also observed 40% and 55% decreases in albuminuria (urine protein leakage) at 2 and 4 weeks, respectively, indicating that C-peptide potentially ameliorated diabetic nephropathy<sup>23-25</sup>. Also, Forst reported that diabetes-induced cardiovascular complications, such as decreased blood flow in the extremities, were ameliorated by C-peptide therapy<sup>26</sup>. Furthermore, C-peptide prevents diabetic neuropathy via improving endoneural blood flow and preventing axonal swelling<sup>27</sup>.

Evidence indicates that C-peptide increases blood flow and decrease diabetic complications. However, the mechanism of how C-peptide enhances blood flow remains unknown. Previous studies from the Spence group reported that C-peptide may regulate blood flow via stimulating ATP release from ERYs. However, the first attempts to correlate C-peptide with increased ATP release were not reproducible. It was later discovered that only when C-peptide was administered with a metal ion, such as  $Fe^{2+}$  and  $Cr^{3+}$ , which are common impurities in commercial C-peptide, could an increase of ATP release from ERYs be observed<sup>28</sup>. Subsequent experiments with HPLC-purified C-peptide further confirmed this discovery<sup>29</sup>. Considering the physiological process by which C-peptide is produced and secreted, another metal ion,  $Zn^{2+}$ , gained interest because of its high abundance<sup>30</sup> (at mM level) in pancreatic  $\beta$ -cell granules. Our group initially hypothesized that upon secretion from  $\beta$ -cells, C-peptide and  $Zn^{2+}$  were somehow bound and it was this ensemble of C-peptide and  $Zn^{2+}$  that

increases ERY derived ATP. While our group was able to confirm that C-peptide and Zn<sup>2+</sup> were indeed required for biological activity on ERYs, we were never able to confirm that the two species bind to each other.

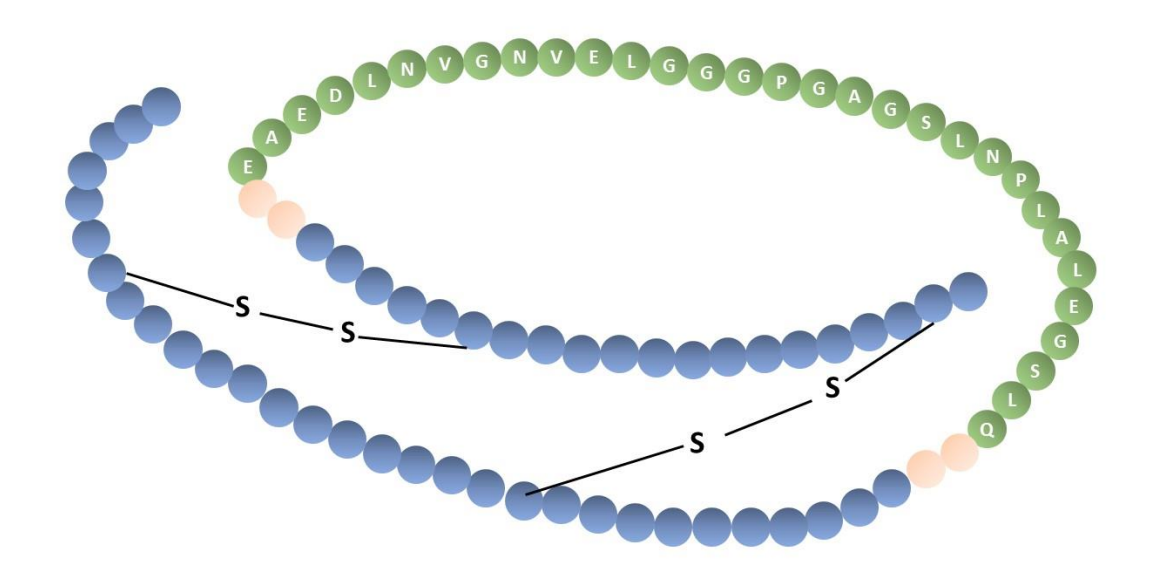


Figure 2.1. Proinsulin. Each sphere represent an amino acid. The labeled amino acids represent C-peptide. Upon cleavage, the two chains connected with disulfide bond forms insulin, while the connecting segment forms C-peptide.

# 2.1.3 Chapter Motivation and Overview

Previous studies about C-peptide's effect on ERYs were based on static experiments, in which, ERYs were incubated in a static buffer under different conditions (e.g. with/without C-peptide). However, under *in vivo* conditions, ERYs are circulating under shear stress, which is an important physical factor that affects ATP release from these cells<sup>31</sup>. Therefore, a fluidic device that enables long-term (e.g. hours) *in vitro* ERY circulation is needed to mimic *in vivo* conditions. As discussed in the first chapter, given the drawbacks of PDMS-based microfluidic devices, 3D-printing will be explored to fabricate such a device.

Although previous research showed the indispensable role of Zn<sup>2+</sup> in this process, numerous binding studies of C-peptide and Zn<sup>2+</sup> were unsuccessful, which indicates that there is not direct binding between the two species. However, under *in vivo* conditions, albumin is a common carrier protein, which can transport numerous molecules to cells<sup>32</sup>. Therefore, the hypothesis that albumin carries C-peptide and Zn<sup>2+</sup> to ERYs will also be examined.

#### 2.2 Methods

## 2.2.1 The Design and Fabrication of the Fluidic Device

The device was printed on an Objet Connex 350 printer (Stratasys Ltd, Eden Prairie, MN) in the department of Electrical and Computer Engineering at Michigan State University. The 3-D design (Figure 2.2) was created using the CAD based engineering software package AutoDesk Inventor Professional (Autodesk, Inc., San Francisco, CA). The device was printed using Objet VeroClear material (Stratasys Ltd, Eden Prairie, MN) whose exact composition is proprietary, but approximately contains isobornyl acrylate (15-30%), acrylic monomer (15-30%), urethane acrylate (10-30%), acrylic monomer (5-10; 10-15%), epoxy acrylate (5-10; 10-15%), acrylate oligomer (5-10; 10-15%), and a photoinitiator (0.1-1;1-2%). Once printed, the device is translucent and rigid, but becomes optically transparent and ready to use after a simple polish and cleaning with sand paper and water. Commercially available membrane inserts (6.5 mm diameter; Corning, Inc., Horseheads, NY) with polyester membranes (0.4 µm pore diameter; 10 μm membrane thickness; 10<sup>8</sup> pores/cm<sup>2</sup>) were inserted into the dynamic wells above the channels. The inserts function as a semi-permeable barrier between flowing cells or reagents in the channel and reagents that are loaded in the insert (on the opposite side of the membrane). This configuration enables molecular transport through the pores by diffusion. The side of each membrane insert was wrapped by a layer of PTFE seal tape (PL Sourcing, Inc., Newport News, VA) to enhance the seal between the inserts and the wells.

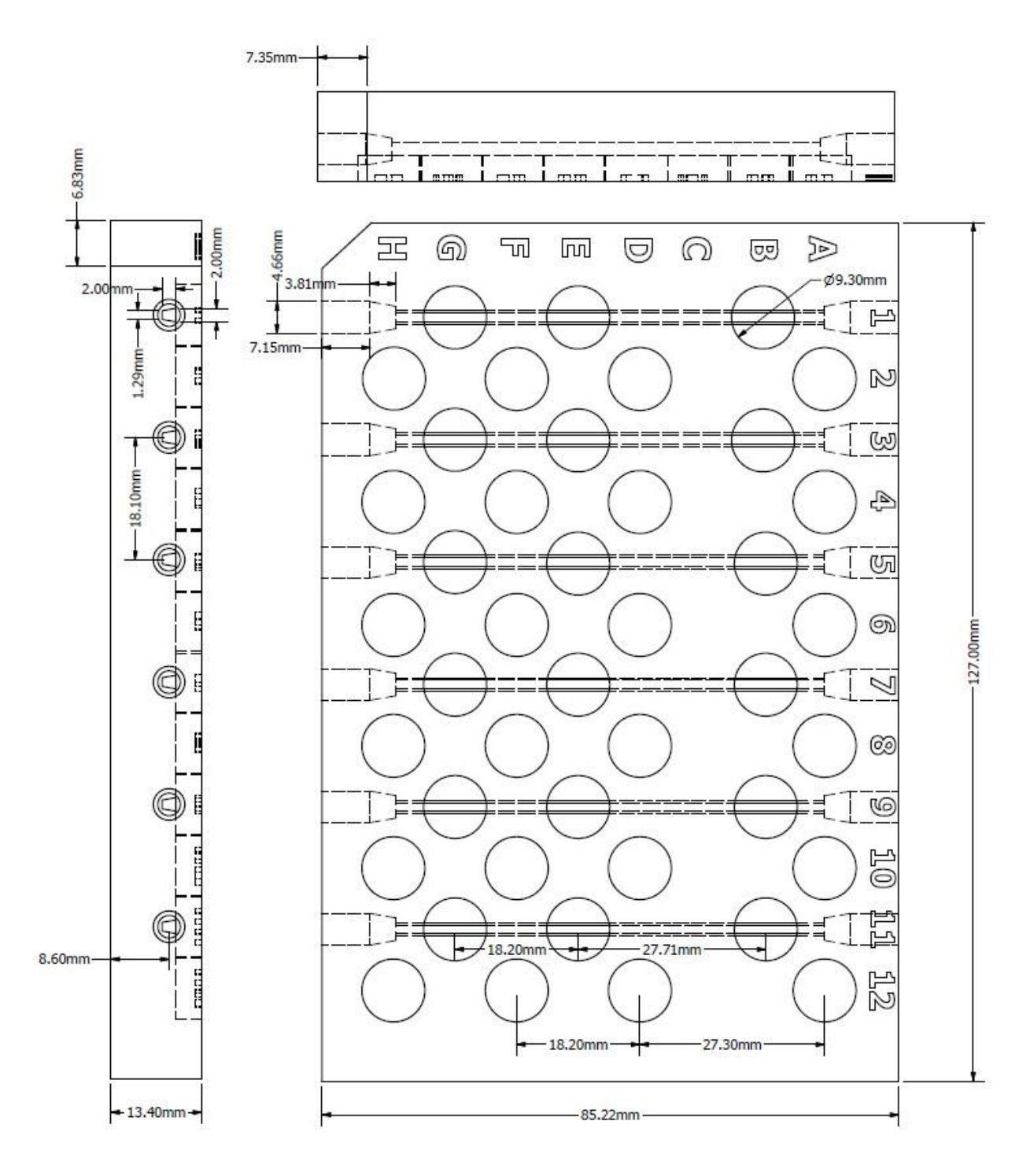


Figure 2.2. The engineering sketch of the fluidic device with detailed dimensions

A section of grafted tubing was prepared by connecting two, 20 cm pieces of 1/8" Tygon tubing (Saint-Gobain PPL Corp, Jackson, MI) to the ends of a piece of 15 cm Ismatec tubing (Cole-Parmer Instrument Company, Vernou Hills, IL). The two ends of the tubing were connected to male finger tight adapters (IDEX Health & Science LLC, Oak Harbor, WA), which can be integrated with the two threaded ends of a channel in the printed device, thus forming a loop. The threads were printed directly from the device design (as opposed to being tapped post-printing) as 10-32 type threads, thus enabling the use of the aforementioned male finger tight adaptors. Fluids or samples were driven through the loop by a 12-roller peristaltic pump (IDEX Health & Science LLC, Oak Harbor, WA).

To confirm the absence of bulk fluid movement through the membrane pores into a channel, a 50  $\mu$ L aliquot of DDW was added to dynamic inserts in wells B1, E1 and G1, while DDW was delivered through the closed loop system at a flow rate of 50  $\mu$ L/min for 2 hours. The amount of water in each insert after pumping was determined by mass measurement. As a control group, the same amount of DDW was loaded into each insert in static wells A2, D2 and F2 (no channels beneath and thus no possible water delivery) for 2 hours. There is no channel underneath the static inserts, thus representing a control group used to account for any change in volumes in the inserts due to evaporation. All other channels were examined in the same way, using static inserts in the next right column as a control set.

To investigate the extent of any leakage of fluids from a channel to the area above membrane inserts, a 30  $\mu$ M fluorescein solution in DDW was circulated at a rate of 50  $\mu$ L/min in the loop for 2 hours. The device was then detached from the pumping system and placed under the objective lens of a fluorescence microscope (Olympus, Japan). Leakage was investigated for all six channels on the device; any detectable quantity of fluorescein on the outside of the trans-well inserts was considered to be indicative of leaking.

#### 2.2.2 ATP Measurement Optimization

The well-established luciferin/luciferase chemiluminescence assay was used for ATP assays<sup>33</sup>. Reagents were prepared by dissolving 2.0 mg of D-luciferin (Sigma Aldrich, St. Louis, MO) in 5 mL of DDW, and adding the resultant solution into a single 100 mg vial of firefly extract (Sigma Aldrich, St. Louis, MO). Five ATP (Sigma Aldrich, St. Louis, MO) standards ranging in concentration from 0 nM to 800 nM were prepared by dissolved in DDW and diluting in a physiological salt solution (PSS, containing 4.7 mM KCl, 2.0 mM CaCl<sub>2</sub>, 1.2 mM MgSO<sub>4</sub>, 140.5 mM NaCl, 21.0 mM tris-hydroxymethyl aminomethane, 5.5 mM glucose, and 5% bovine serum albumin at pH = 7.4; all reagents were from Sigma Aldrich). A 50  $\mu$ L aliquot of PSS was loaded in the insert located in well B. The PSS served as a solution to collect ATP diffusing from the channel through the membrane of the insert. After 10 min, 20 min or 30 min of pumping the various ATP standards, the device was detached and placed in the sample holder of the plate reader (Molecular Devices LLC, Sunnyvale, CA). A 50  $\mu$ L aliquot of 20 nM ATP

standard solution was pipetted into insert in static well 2A as a calibrator, thereby minimizing possible indeterminate error. A 10  $\mu$ L of luciferin/luciferase was then added into inserts in wells 2A and 1B, simultaneously. After 15 s, the chemiluminescence intensity from both inserts was detected simultaneously, followed by the evaluation of the detection background, detection limit, sensitivity and linearity for the different pumping times under investigation.

To determine the optimal volume of luciferin/luciferase mixture for each assay, ATP standards were prepared and circulated in a channel, as described above, with 50  $\mu$ L of PSS loaded in the insert in well 1B. ATP standards circulated for 20 min at a rate 50  $\mu$ L/min. Next, 10  $\mu$ L to 30  $\mu$ L aliquots of the luciferin/luciferase mixture were added to the membrane inserts in dynamic well 1B, as well as static well 2A (containing 50  $\mu$ L of 20 nM ATP standard as a calibrator) simultaneously. The device was detached and placed in the plate reader sample holder and the optimal assay amount was determined by an evaluation of detection limit, linearity and sensitivity.

## 2.2.3 Evaluation of Analytical Features of the Device

ATP solutions of 0, 0.2, 0.3, 0.4, 0.5, 0.8  $\mu$ M were prepared in PSS and circulated randomly through 6 channels, simultaneously, at a rate of 50  $\mu$ L/min for 20 min after 50  $\mu$ L of PSS were loaded in the membrane inserts in wells B above each channel. The device was then detached from the tubing and placed in the plate reader for chemiluminescence detection with the optimal ATP quantitation parameters determined above, on all wells in the row labeled as "B" (Figure 2.4). A curve of

chemiluminescence intensity versus ATP concentration was obtained, and the resulting regression statistics (slope, y-intercept, and coefficient of determination) were calculated.

ATP standards of 150 nM and 250 nM were prepared and circulated in channel 1 at a rate of 50  $\mu$ L/min for 20 min, with 50  $\mu$ L of PSS buffer loaded in the membrane insert in well B (dynamic wells) above the channel to collect ATP by diffusion. A 50  $\mu$ L aliquot of 20 nM ATP was then added into the membrane insert in wells found in row labeled as "A" (static wells). The device was then detached from tubing and placed in the sample holder of the plate reader. Chemiluminescence was detected 15 s after adding 10  $\mu$ L of the luciferin/luciferase assay into dynamic and static wells to quantify the ATP, using calibration curves prepared in advance in a similar manner as described above. Two more identical measurements were performed on channel 3 and channel 5.

ATP standards having concentrations ranging from 0 to 800 nM were prepared and simultaneously circulated through channels 1, 3 and 5 at a rate 50  $\mu$ L /min for 20 min, while 50  $\mu$ L of PSS buffer were loaded in the membrane inserts in wells B above each channel. After adding 50  $\mu$ L of 20 nM ATP to wells 2A, 4A and 6A (as static calibrators for measurements on channels 1, 3, and 5, respectively), the device was detached and placed in the sample holder of the plate reader. An aliquot of 10  $\mu$ L of the luciferin/luciferase mixture was simultaneously added into inserts above the dynamic and static wells, and chemiluminescence was detected by the plate reader

after 15 s. A comparison of sensitivity, detection limit and linearity of results from the 3 channels was performed to determine if the device channels and inserts are statistically equivalent. Precision was also investigated by performing identical measurements as those described above while changing well inserts in between studies.

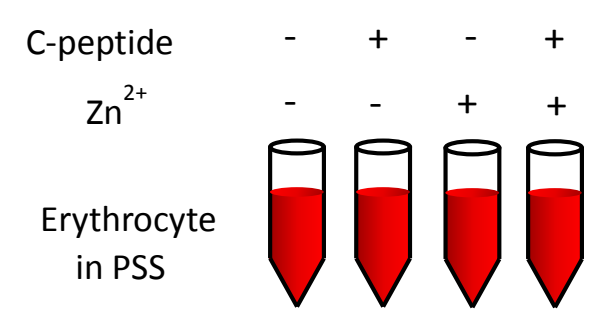
# 2.2.4 ERY Sample Preparation

Whole blood was obtained from healthy human donors by venipuncture and collected into heparinized tubes. Blood was then centrifuged at 500 g for 10 min and the plasma and buffy coat were removed by aspiration. ERYs were washed 3 times in PSS<sup>34</sup>. For all albumin free experiments, ERYs were washed in albumin-free PSS. The hematocrit was determined using a hematocrit measurement device (CritSpin, Iris Sample Processing, Westwood, MA).

Four samples were prepared containing ERYs at a 7% hematocrit in different conditions: buffer only, buffer with C-peptide, buffer with both C-peptide and  $Zn^{2+}$  ( $ZnCl_2$ ), and buffer with  $Zn^{2+}$ . Buffer choices included PSS and albumin-free PSS in order to study the effect of albumin on C-peptide and  $Zn^{2+}$  delivery to the ERYs, as well as subsequent ATP release from the ERYs. Human C-peptide and  $Zn^{2+}$  stock solutions (800 nM for both) were prepared in doubly deionized water (DDW, 18.2 M $\Omega$ ). The working samples (10 nM) were then pumped to fill four randomly chosen channels on the device, after which each channel and corresponding tubing were closed to form a loop. The samples with different C-peptide treatments were then introduced into the device

to form four circulating loops. The whole setup was then placed in a 37 °C incubator for 2 hours, during which, C-peptide/Zn<sup>2+</sup>/albumin that were mixed in circulating ERY samples would exert their effect on the cells. The entire setup of pump, device, and closed loops with circulating samples were placed in an incubator at 37 °C. The samples were allowed to circulate through the system for 1.5 h, after which, aliquots of 50  $\mu$ L of PSS were loaded in the inserts in row E to collect ATP from samples via diffusion through the pores in the insert membrane. ERY-derived ATP was determined in the same manner as the ATP standards, other than the fact that a stream of ERYs was delivered through the channels as opposed to ATP standards. (Figure 2.3)





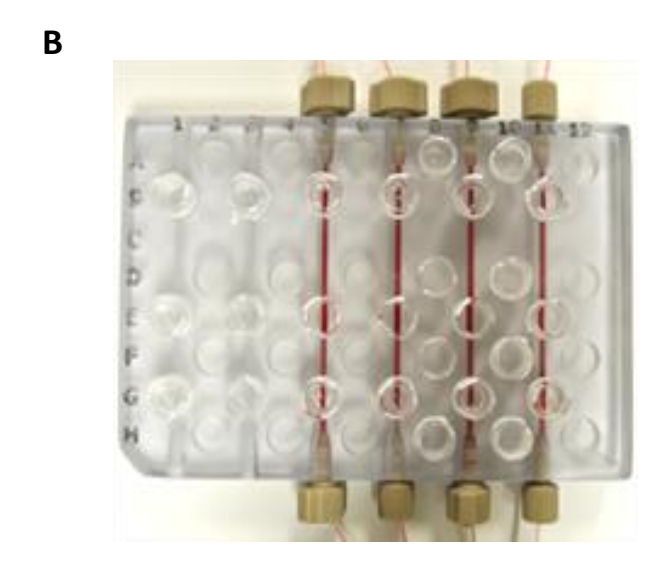


Figure 2.3. ERY sample preparation and measurement. A), four ERY samples were prepared with different treatments: without C-peptide or  $Zn^{2+}$ ; only with C-peptide; only with  $Zn^{2+}$ ; and with both C-peptide and  $Zn^{2+}$ , the concentrations of C-peptide and  $Zn^{2+}$  were both 10 nM. B), the four samples were introduced into four channels of the fluidic device. After the samples circulated for 1.5 hours in the fluidic device that was placed in a 37 °C incubator, aliquots of 50  $\mu$ L of PSS were loaded in the wells in row E to collect ATP from the flowing via diffusion, which was then quantified with the luciferin/luciferase assay by a plate reader.

### 2.2.5 ERY Derived ATP Determination

ATP was quantified by the luciferase/luciferin chemiluminescence assay on the 3-D printed fluidic device. The device design was modeled as a 96-well plate for subsequent measurement on a standard plate reader. Six channels were fabricated in the device, with wells above these channels that align with the internal robotics of the plate reader for measurement convenience. A 6.5 mm diameter transwell insert whose bottom is porous polyester (0.4 micron) is placed in each of the wells. During use, ERY samples flow through the channels and released ATP is able to diffuse through the membrane pores into buffer that was pre-loaded in the insert above the membrane. Aliquots (10  $\mu$ L) of the luciferin/luciferase mixture were then injected into each well, and the entire device was placed in the plate reader for chemiluminescence measurement.

Before measuring ERY samples, a calibration curve was obtained by circulating four ATP standards prepared in PSS (concentrations of 0, 100, 200 and 400 nM) in four randomly chosen channels at a flow rate of 50  $\mu$ L/min using a peristaltic pump (IDEX Health & Science LLC, Oak Harbor, WA) as part of the pumping mechanism. To facilitate ATP diffusion through the membrane pores and into the well insert, 50  $\mu$ L of PSS was loaded in the membrane inserts on row E above each channel. After flowing for 20 minutes, the 3D-printed device was detached from the peristaltic pump tubing and was placed on the holder of a plate reader (Molecular Devices LLC, Sunnyvale, CA), followed by the simultaneous addition of 10  $\mu$ L of L/L assay mixture into each insert to measure chemiluminescence intensity values resulting from the reaction of the L/L

mixture with ATP. A standard curve was generated by plotting the chemiluminescence intensity values against the known concentrations of ATP.

#### 2.3 Results

## 2.3.1 Device Design and Fabrication

As shown in Figure 2.4A, the device is modeled after the dimensions of a standard 96-well plate, making it suitable for direct analysis on a plate reader and use with automated fluidic handling systems. The printed column (1 to 12) and row (A to H) markers make it easy to identify and label wells. This particular device enables parallel analyses as it consists of six channels, each with 3 wells. Membrane inserts, which are removable trans-well inserts often used in cell culture applications, were plugged into the wells (Figure 2.4B). 3D-printed threads were designed for both ends of each channel to allow for an amenable connection to external tubing via male finger tight adapters (Figure 2.4C). The static wells between channels enable simultaneous calibration and/or internal standards when necessary. In this current application, all 3 wells above each channel were used for dynamic determination of ATP release from ERYs flowing through the channel, while the 4 wells not over a channel were used for calibration by performing static measurements of ATP standards. In this construct, quantitative determinations of ATP could be performed, facilitated by a generated working curve on a single device. Figure 2.4D displays the cross section of a single channel, enabling a view of each membrane insert after placement into the device. An evaluation of Figure 2.4D also shows how diffusion of the analytes could occur, moving from the channel, across the membrane, and to the area above the insert for eventual measurement.

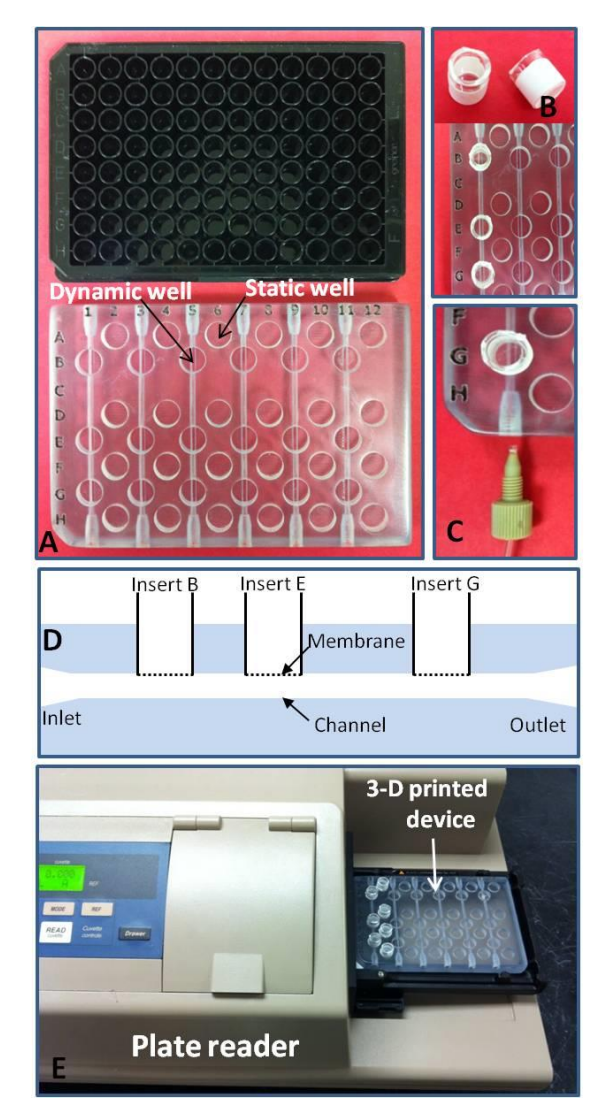


Figure 2.4. (A): The 3D-printed fluidic device (bottom) used in this study is modeled after the dimensions of a 96-well plate (top). Column and row markers make it convenient to localize wells. Six channels were printed on the odd number columns, with three wells corresponding to each channel. Static wells, printed on the even number columns allow for internal standards or calibration. (B): Membrane inserts (top), which have a semi-permeable polyester membrane, are inserted into wells (bottom) of the 3-D printed device. (C): Threads, printed at both ends of the channel, connect external tubing through a finger tight adaptor. (D): A schematic cross section of a channel and the membrane inserts. (E): The device locks into the sample holder of the commercial plate reader.

In this study, ATP diffuses from channels to wells across the porous membrane, where it is collected into buffer already loaded into the well insert prior to commencement of pumping. Based on diffusion, the amount of ATP accumulated in the well (at some fixed pumping time) is proportional to the concentration in the channel, thereby enabling ATP that is in the channel to be quantitatively determined. After flow of samples in the channels, the device was detached from tubing and directly placed into the plate reader for measurements (Figure 2.4E).

Since this device was designed amenable to a plate reader for convenient and high content readouts, the alignment of the device and the wells with the plate reader was characterized and validated prior to studies involving ATP measurements. Six fluorescein standard solutions with concentrations ranging from 0 to 20  $\mu$ M were loaded in the six wells in rows B, E and G, respectively, followed by fluorescence detection over the wells by the plate reader (ex. 494 nm; em. 521 nm). Figure 2.5 shows the fluorescence intensity over the wells in row B, as a function of fluorescein concentration. The fluorescence intensity is linearly proportional to the concentration of fluorescein loaded in the wells, which indicates correct alignments of the wells with the optical detectors in the plate reader.

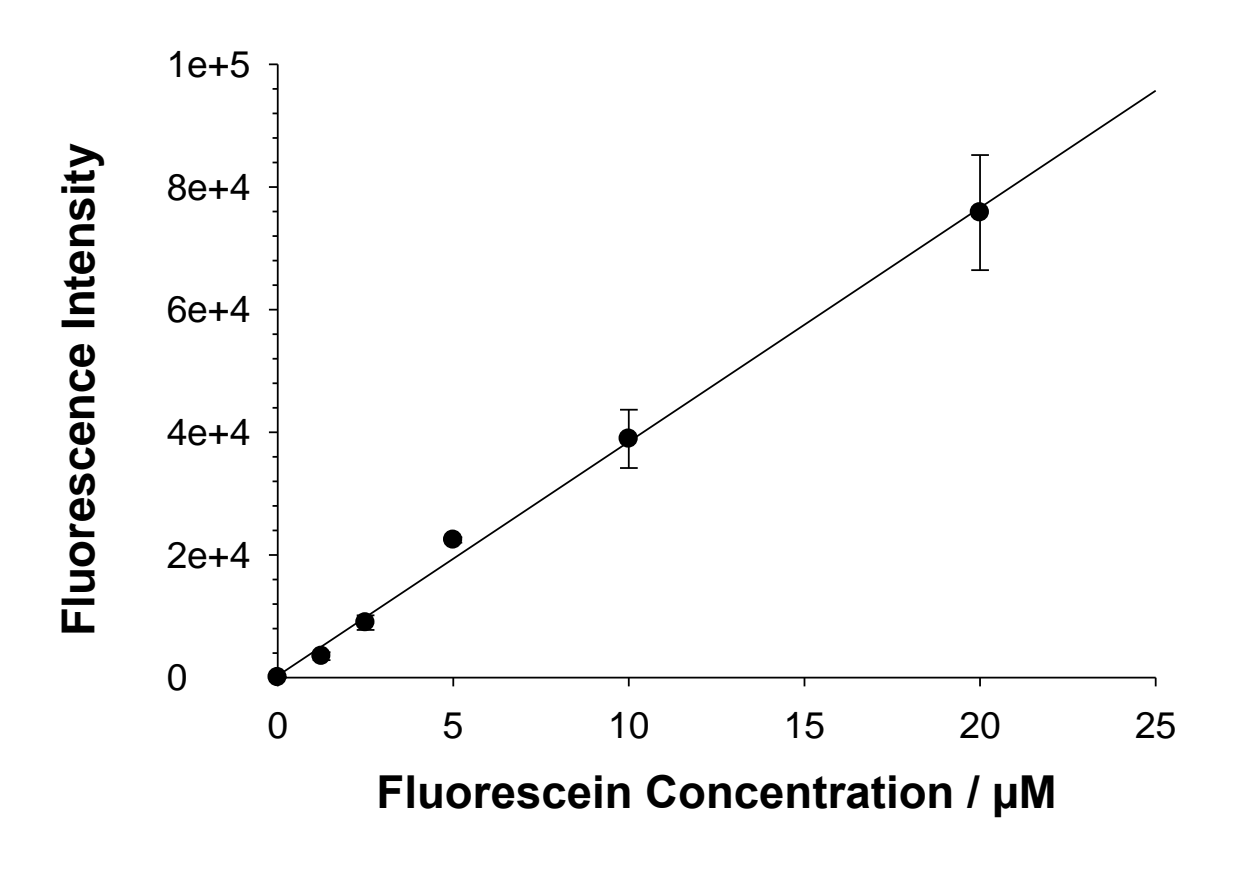


Figure 2.5. Validation of the alignment of the device and printed wells in the plate reader. Six fluorescein solutions (concentrations ranging from 0 to 20  $\mu$ M) were prepared and were loaded into the six inserts in wells B above each channel, respectively. Fluorescence intensity above these inserts was detected by plate reader and was plotted versus fluorescein concentration. The good linearity ( $r^2$  = 0.99) shows that the device and wells are aligned well with the plate reader. n = 3, Error = stdev.

The trans-well inserts are not fixed into place by any type of glue or epoxy adhesives that lead to permanent combination. There is, however, a wrap of PTFE tape around the side of inserts to help them seal onto the bulk device tightly, yet remain removable if needed. However, to confirm that bulk fluid movement is not occurring from the channel to the area above the membrane insert, or vice-versa, 50 µL of doubly deionized water (DDW) were added into membrane inserts in wells B1, E1 and G1 above channel 1. After circulating DDW through the channel for 2 hours at a rate of 50 μL/min, the remaining volumes of water in the inserts were measured. A control set was performed by adding 50 µL of DDW in inserts placed in static wells A2, D2 and F2, and then measuring the remaining volumes after two hours of loading. As shown in Table 2.1, though a minimal loss of liquid volume in the dynamic inserts (B1, E1 and G1, with flowing underneath) was observed, the lost volume was not likely due to liquid transfer into the channel for a minimal liquid loss was also shown in static inserts (A2, D2 and F2), beneath which, there is no channel. There is no significant difference in remaining volumes between dynamic and static inserts. The results suggest that loaded liquid can be firmly held in dynamic inserts without being drawn into the underlying flow channel for the time duration investigated. The other five channels were examined in the same way, and no bulk liquid transfer was observed.

The leakage of fluids from the flowing channel across the membrane and into any pre-loaded reagents on the other side of the membrane has the potential to be detrimental to the quality of analysis using this fluidic device. For example, the device detects ATP that has diffused from the channel to the inserts, any direct leakage of

fluids across the membrane will cause false signals and thus make the detected results unreliable. Also, dilution effect caused by leakage can potentially hinder detection limits of ATP. To determine if flowing fluids leak across membrane (as opposed to movement of an analyte by diffusion alone), a 20 µM fluorescein solution was circulated through channel 1, with nothing loaded in the membrane inserts above the channel. After 2 hours of pumping this solution, fluorescence images above the channel were obtained. Figure 2.6 was integrated by images observed on separate parts of the channel because of the limited camera view. As shown, there is some fluorescein at the bottom of each well shaped in rectangular. This fluorescence was on the apical side of the membrane (the bottom side, touching the channel), on the channel area, resulting from remaining fluorescein in the channel. If there is any liquid leakage across the membrane, a "circle" of fluorescence emission in the well would be expected. Due to the lack of fluorescein entering the well, it was concluded that leakage of fluids was not occurring. The other five channels were verified with the same method and none showed any leakage of liquid across membrane. This is important because it will help ensure that only molecules can diffuse or move through the membrane to the other side of inserts.

**Table 2.1. Remaining Volumes of Water in Inserts** 

Well	Remaining volume after 2 hour pumping/μL <sup>a</sup>	Well	Remaining volume after 2 hour pumping// μL <sup>b</sup>
B1	49.5 ± 4.5	A2	48.7 ± 3.8
E1	48.6 ± 3.5	D2	49.4 ± 1.3
G1	46.8 ± 6.2	F2	47.6 ± 2.5

a: n=10, error=stdev; b: n=5, error=stdev

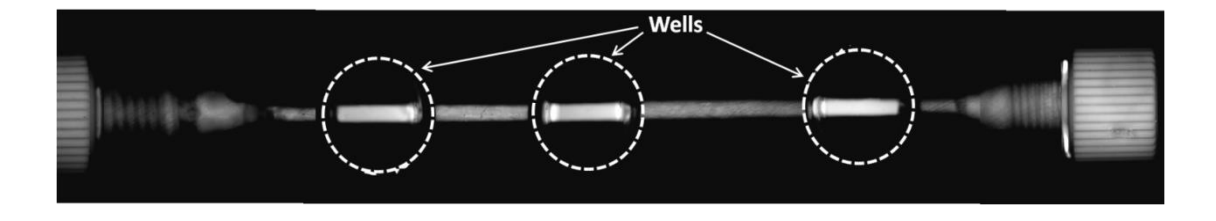


Figure 2.6. A fluorescence image of a channel after flowing fluorescein. The dotted circles indicate the well areas. The image implies that leakage of liquid from channel across the membranes did not occur. Due to the limited scope view, images on separate parts of the channel were obtained and integrated into a single image.

# 2.3.2 ATP Measurement Optimization

Multiple factors can affect the overall quantitative determination of ATP release from the stored ERYs flowing through the device channels. One of the first factors we investigated was the amount of time the ERYs flowed through the device channel prior to determination of ATP. As the ERYs pass through the channel, they release ATP that diffuses through the porous membrane on the bottom of the trans-well insert. Thus, an increase in the amount of time the ERYs pass through the device channels would increase the collection time and amount of ATP in the well above the channel. To determine the optimal ATP collection time, ATP standards (0 to 800 nM) were circulated for 10 min, 20 min or 30 min through a device channel having a well insert that was loaded with 50 µL of PSS. This circulation time enabled ATP from the ERYs to diffuse through the membrane pores. After the various circulation times of the ERYs (or the collection time of ERY-derived ATP), an aliquot of a luciferin/luciferase mixture was added to the well insert and the resultant chemiluminescence was recorded using the multi-well plate reader. Calibration curves were prepared to investigate such figures of merit as analytical sensitivity and limits of detection for each collection time. The resultant data, which are summarized in Table 2.2, show that lower limits of detection and higher sensitivity can be achieved as the collection time increased. Although quantifiable results were obtained even after 10 minutes of pumping, the 20 minute collection period was utilized for subsequent studies because of its precision and significant reduction in the limit of detection in comparison to the 10 minute pumping period and its suitability for measurements of ERY-derived ATP, which is typically in a range of 90 to 400 nM, depending on the health status of the donor.

**Table 2.2. Optimization of ATP Collection Time** 

Collection time/min	Y intercept	Slope	r <sup>2</sup>	Detection limit/nM
10	20.9 ± 5.5	517.5 ± 33.6	0.98 ± 0.00 <sub>5</sub>	136.6 ± 24.0
20	15.8 ± 1.8	565.4 ± 38.6	0.99 ± 0.00 <sub>1</sub>	52.4 ± 7.3
30	19.8 ± 1.0	883.8 ± 69.9	0.99 ± 0.00 <sub>7</sub>	33.3 ± 6.8

(n =3; all errors represent standard deviations)

A mixture consisting of luciferin/luciferase is required in the chemiluminescent determination of ATP. However, this mixture also contributes to high background luminescence during the measurement portion of the analysis. Thus, a study was performed to determine the volume of luciferin/luciferase mixture added during the assay that provided the best analytical features (detection limit, sensitivity, etc.). To perform this study, ATP standards of identical concentration were circulated in a channel for 20 min and ATP was allowed to diffuse through the membranes of the trans-well inserts that had already been filled with 50  $\mu$ L of buffer, after which, the device was detached and placed on the sample holder of the plate reader. Aliquots of 10, 20 or 30  $\mu$ L of the luciferin/luciferase mixture were added to the wells and the

chemiluminescence from each trial was acquired. The data from these studies, shown in Table 2.3, suggest that 10  $\mu$ L of the luciferin/luciferase mixture yielded the lowest background (y-intercept), and the best linearity, as measured by the coefficient of determination,  $r^2$ . In fact, larger volumes of the luciferin/luciferase mixture added to the wells lowered analysis quality, likely due to higher background emission. Additionally, when adding the 20 or 30  $\mu$ L volumes of the luciferin/luciferase mixture, the signals from 100 nM or 200 nM ATP standards were not statistically different and exhibited reduced linearity and higher detection limits.

Table 2.3. Optimization of Luciferin/luciferase Assay Volume

Assay volume/μL	Y intercept	Slope	R <sup>2</sup>	Detection limit/nM
10	15.8 ± 1.8	565.4 ± 38.6	0.99 ± 0.0 <sub>01</sub>	52.4 ± 7.3
20	36.8 ± 3.7	515.9 ± 21.0	0.97 ± 0.0 <sub>2</sub>	120.1 ± 13.6
30	43.8 ± 1.9	549.0 ± 32.0	0.97 ± 0.0 <sub>1</sub>	167.7± 39.4

(Each assay volume was performed on 5 ATP standards; the resultant calibration curves were evaluated for y-intercept, slope, and linearity which, in turn, were used to determine the detection limit. n = 3; all errors represent standard deviations)

# 2.3.3 Evaluation of Analytical Features of the Device

With six channels integrated into the 3-D printed device, all of which were amenable to a commercial plate reader, high-throughput applications were explored. Six ATP standards (0 to 0.8  $\mu$ M) were circulated in the six channels, but in a random order. The membrane inserts in wells B on each channel were loaded with 50  $\mu$ L of PSS to collect ATP by diffusion. The chemiluminescence intensity detected from each insert was plotted as a function of the concentration of ATP flowing in the channels. The linearity ( $r^2$ =0.99) and precision of measurement demonstrated the device can perform 6 quantitative analyses, simultaneously.

Under optimal conditions, ATP standards of known concentrations (150 nM and 250 nM) were evaluated with the device. These two concentrations were determined because a 7% solution of ERYs release ~200 nM ATP. Such measurements were performed on channels 1, 3 and 5. Data shown in Table 2.4 indicate that the levels of ATP can be detected quantitatively, and the detection results from the three channels did not show any statistically significant difference, which further suggests that quantitation on different channels will yield statistically similar results. Such results are expected due to all channels being printed on the same printer using the same prototype dimensions. To confirm precision between channels, ATP standards were circulated in three channels and resultant calibration curves were compared. As shown in Table 2.4, these channels were statistically equal in terms of background, sensitivity, linearity, detection limit and accuracy. This intra-channel reproducibility is another outstanding advantage of the 3-D printed device, as it helps reduce variability

of devices from different manufactures and fabrication protocols. Another key advantage is the reusability of the 3-D printed device; the same device was used for all reported experiments and was cleaned with a simple rinse with DDW. Data in Figure 2.5, Table 2.2 and Table 2.3 were obtained using the same channel on the same device. The error bars, which represent standard deviation, support the reusability of the device, which not only reduces use of materials, but also enables repeated measurements of the same sample on the same device in a reproducible manner.

Table 2.4. Observed quantitative detection of 150 nM and 250 nM ATP from channel 1, channel 3 and channel 5

Known concentration/nM		150			250	
Observed	Ch1	Ch3	Ch5	Ch1	Ch3	Ch5
Concentration/nM	140.6 ±	154.4 ±	159.4±	245.5 ±	253.7 ±	251.6±
	5.8	7.2	8.6	15.6	18.7	14.0

ATP standards of known concentrations were introduced to channels 1, 3, and 5 (Ch1, Ch3, and Ch5) in the fluidic device, and were subsequently quantified with the luciferin/luciferase assay by a plate reader. The observed concentrations are the average ± stdev of 5 experiments. Calibration curve was made each time for quantitation purpose.

# 2.3.4 Investigation of ERY Derived ATP Release stimulated by C-peptide

As shown by the black bars in Figure 2.7 ERYs incubated with C-peptide and  $Zn^{2+}$  in PSS stimulated the highest ATP release (319.8  $\pm$  15.2 nM), which was significantly higher than the ERYs in the absence of C-peptide/ $Zn^{2+}$  in PSS as a control group (194.9  $\pm$  19.7 nM, p < 0.005). ERYs incubated with C-peptide or  $Zn^{2+}$  alone, however, did not show significant ATP release increase. These results further confirmed that, under hemodynamic conditions, C-peptide can increase ATP release from ERYs, only with the presence of  $Zn^{2+}$ .

However, binding studies using isothermal titration calorimetry (ITC) did not reveal any binding between C-peptide and Zn<sup>2+</sup>, it was then proposed that albumin, which is a common transporter for molecules in a blood stream, delivers C-peptide and Zn<sup>2+</sup> to ERYs. Subsequent ITC experiments proved the binding between albumin and C-peptide and Zn<sup>2+</sup>. However, the effect of C-peptide and Zn<sup>2+</sup> on ERY derived ATP release, in the absence of albumin, remained unknown. Thus, the same sample as aforementioned were prepared, but in albumin-free PSS. The ATP measurements from these samples are summarized in Figure 2.7(grey bars). The data suggest that without albumin, C-peptide and Zn<sup>2+</sup> failed to increase ATP release from ERYs.

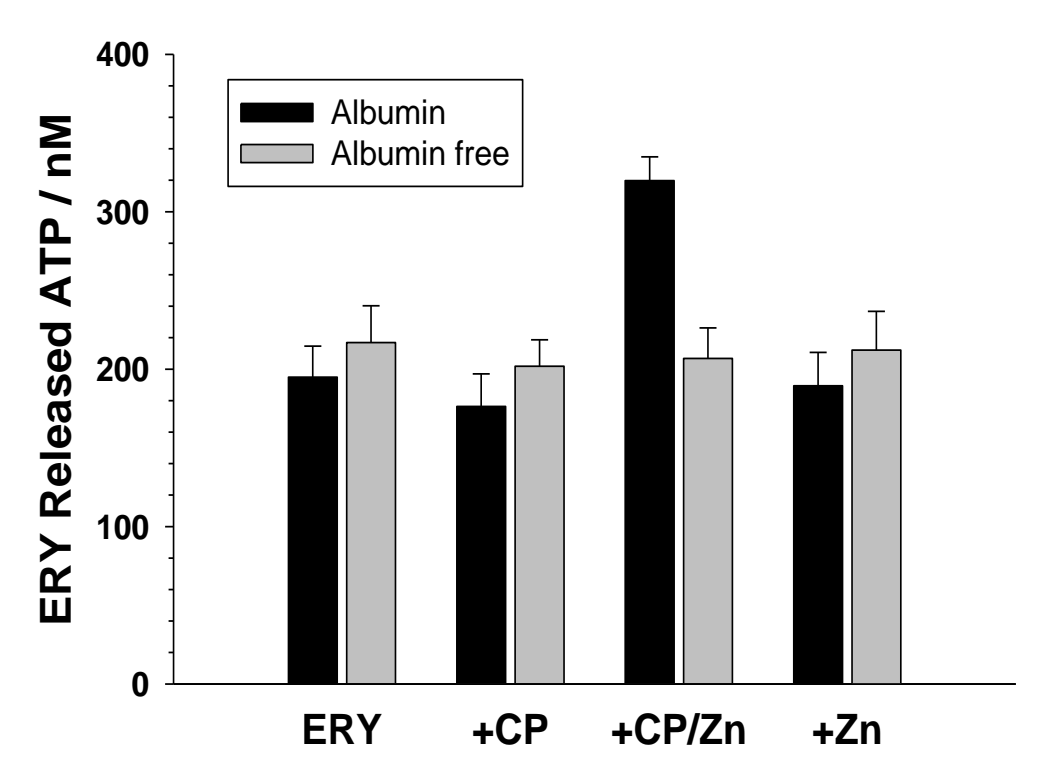


Figure 2.7. ATP release from circulating ERYs with different treatments. The data summarized in black bars were collected from ERYs flowing in PSS, which suggest that C-peptide and Zn<sup>2+</sup> together significantly increased ATP release, while C-peptide or Zn<sup>2+</sup> alone did not show this effect. Without albumin in the ERY streams, however, C-peptide and Zn<sup>2+</sup> fail to stimulate ATP release (grey bars), which confirmed the role of albumin in the ATP stimulation process. In this experiment, 10 nM C-peptide and Zn<sup>2+</sup> were used to treat ERY samples. (N=5, error=S.E.M)

It has been reported that the amino acid at position 27 in C-peptide, glutamic acid, plays a crucial role in its physiological efficacy. Therefore, the mutant E27A (replaced glutamic acid with alanine) was applied to observe if it can increase ATP release from ERYs. Figure 2.8 shows with or without albumin, E27A failed to enhance ERY-released ATP.

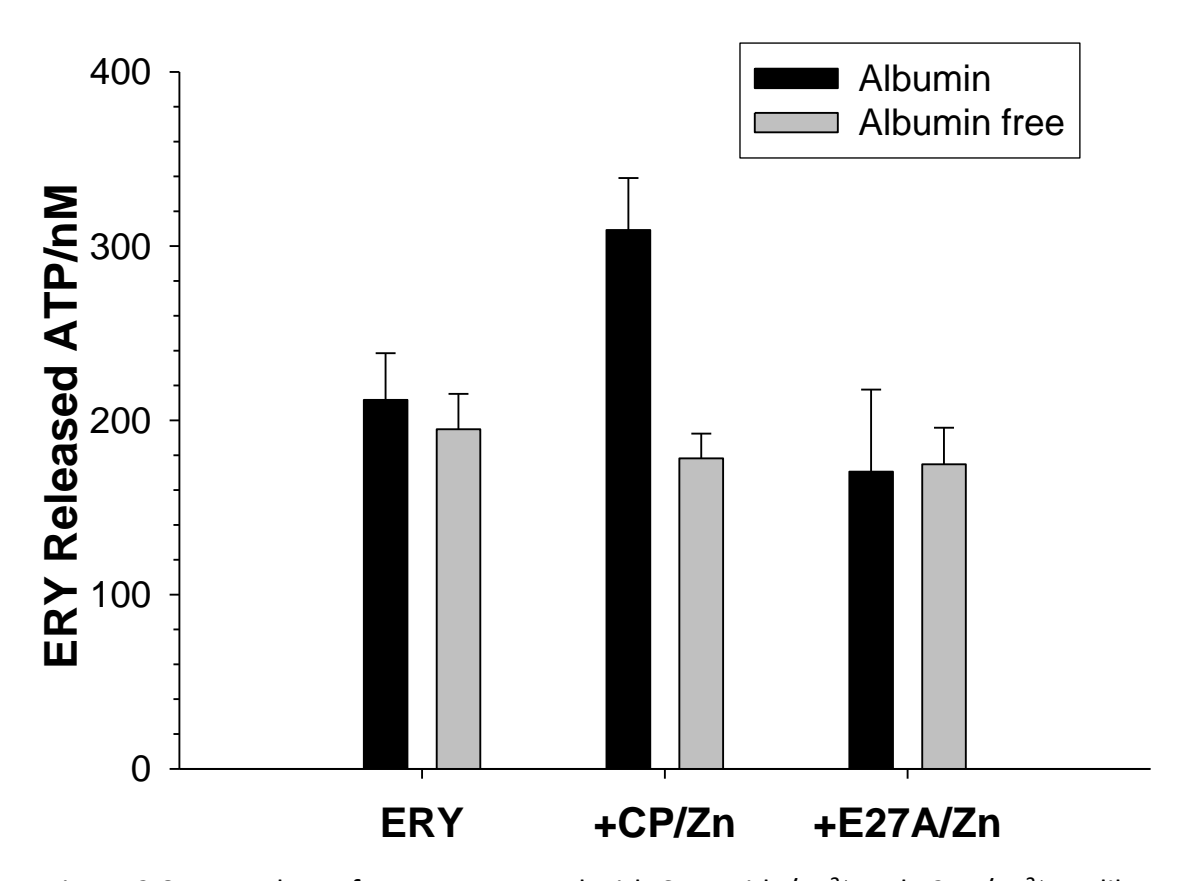


Figure 2.8. ATP release from ERYs treated with C-peptide/Zn<sup>2+</sup> and E27A/Zn<sup>2+</sup>. Unlike C-peptide/Zn<sup>2+</sup>, E27A/Zn<sup>2+</sup> cannot stimulate ATP release from ERYs.

## 2.4 Discussion

A 3D-printed fluidic device was designed and implemented for *in vitro* studies of ATP release from circulating ERYs. Compared to conventional PDMS-based fluidic devices, the 3D-printed device is more rugged and robust, and is capable of multiple uses over a month-long study, which enhances reproducibility of experimental results. To be specific, the leakage examination showed that there was no leakage or bulk liquid transfer occurred across porous membranes on the device, which in contrast, is a common problem/concern for PDMS based devices. Also, the six channels on the device and its reusability significantly enhance throughput and experiment efficiency.

With 3D-printing, the device was easily modeled after a 96-well plate, which is amenable to a commercial plate reader for efficient and high throughput analysis. Moreover, the design of static wells on the device enables simultaneous on-chip calibration, which not only simplifies experimental procedures, but also guarantees result reliability. The device also possesses some other features that cannot be easily achieved in PDMS. For example, threads were directly printed at the ends of each channel, allowing it to be connected to external tubing by standard finger tight adapters.

This 3D-printed device facilitates the progress of developing C-peptide to be a potential therapy for type 1 diabetic (T1D) complications. In the past few decades, numerous animal tests and small scale clinical surveys have proven C-peptide is effective to alleviate T1D complications. However, the underlying mechanism remained unknown, which has hindered subsequent research and clinical studies for the development of C-peptide therapy. The Spence group has found that C-peptide can increase ATP release from ERYs, with the presence of Zn<sup>2+</sup>, which can then enhance vasodilation by stimulating NO production from endothelial cells. However, previous experiments were performed by mixing ERYs with C-peptide/Zn<sup>2+</sup> in a test tube, followed by incubation at 37 °C. In other words, ERYs in these experiments were in a static condition, which cannot represent the actual physiological condition of ERYs, which are circulating under shear stress. With the 3D-printed fluidic device, however, an *in vitro* ERY circulation mimic can be easily achieved. The results shown in Figure 2.7 confirmed previous observations that C-peptide and Zn<sup>2+</sup> are able to stimulate ATP

release from ERYs, while C-peptide or  $Zn^{2+}$  alone does not show the effect. It was then anticipated that there must be a binding between C-peptide and  $Zn^{2+}$ . Unfortunately, numerous attempts to demonstrate C-peptide binding to  $Zn^{2+}$  were unsuccessful, therefore suggesting that another component in the system may be participating in the delivery of C-peptide and  $Zn^{2+}$  to ERYs.

Because of its well-known capability of carrying proteins, drugs and other molecules to cells, albumin was hypothesized to be the missing carrier of C-peptide and Zn<sup>2+</sup>. As discovered by Liu and colleagues, ITC experiments confirmed that albumin can bind C-peptide and Zn<sup>2+</sup> in a two-phase manner. It was also discovered that without albumin in the system, C-peptide and Zn<sup>2+</sup> cannot be delivered to ERYs<sup>35</sup>. All the evidence indicates that albumin is indispensable for C-peptide and Zn<sup>2+</sup> to play the role of increasing ERY-released ATP, which can be confirmed by the data in Figure 2.7 that C-peptide and Zn<sup>2+</sup> failed to stimulate ERY released ATP if albumin is absent in the system. There were also numerous reports showing that the 27 position amino acid of C-peptide, glutamic acid, is required for C-peptide to affect cells<sup>36, 37</sup>. Therefore, an E27 mutant to alanine (E27A) was prepared and ITC experiments suggested this mutant cannot bind albumin. Efficacy studies indicated that this mutant cannot stimulate ATP release from ERYs, even if both Zn<sup>2+</sup> and albumin were present. Collectively, it is the ensemble of albumin, C-peptide, and Zn<sup>2+</sup> that enhances ATP release from ERYs. Although the binding structure is not completely understood yet, the 27 position glutamic acid has proven to be involved.

## 2.5 Conclusion

Microfluidics has become a powerful tool in the field of bioanalytical chemistry. However, traditional microfluidic devices fabricated in PDMS possess some disadvantages, such as lack of ruggedness and reusability, making it almost impossible to move microfluidics out of the academic realm and into real life applications. In this work, however, 3D-printing has been explored to fabricate a novel and functional microfluidic device. This device possesses numerous advantages over PDMS devices. It is rugged, reusable, high throughput and amenable to a plate reader, which significantly enhances the quality of data acquired on the device. Moreover, unlike PDMS microfluidics, device examination experiments showed that no leakage or liquid bulk transfer occurred on the 3D-printed device. The printed threads that fit commercial finger tight adapters also prevent the problems of dead volumes and leakage at connection ports.

The device was then applied to realize an *in vitro* circulation to study the effect of C-peptide and Zn<sup>2+</sup> on circulating hemodynamic ERYs. The results suggest that the three-molecule ensemble that contains C-peptide, Zn<sup>2+</sup>, and albumin can increase ATP release from ERYs, which can then stimulate vasodilation via stimulating NO production from the endothelium. Though the binding structure of the ensemble is not fully understood, the 27 position glutamic acid of C-peptide has proven to be involved in the process. These results reveal a potential therapy for diabetic complications.

**REFERENCES** 

### **REFERENCES**

- 1. Narayan, K.M.V., Saaddine, J.B., Boyle, J.P., Thompson, T.J. & Geiss, L.S. Impact of recent increase in incidence on future diabetes burden US, 2005-2050. *Diabetes Care* 29, 2114-2116 (2006).
- 2. Inzucchi, S. et al. Diagnosis and Classification of Diabetes Mellitus. *Diabetes Care* 33, S62-S69 (2010).
- Medvescek, M. Classification and Criteria for the Diagnosis of Diabetes-Mellitus and Other Categories of Glucose-Intolerance. *Zdrav Vestn* 52, 183-187 (1983).
- 4. Harris, M. Classification and Diagnosis of Diabetes-Mellitus and Other Categories of Glucose-Intolerance. *Diabetes* 28, 1039-1057 (1979).
- 5. Rich, S.S. Genetics of diabetes and its complications. *J Am Soc Nephrol* 17, 353-360 (2006).
- 6. Backonja, M. et al. Gabapentin for the symptomatic treatment of painful neuropathy in patients with diabetes mellitus A randomized controlled trial. Jama-J Am Med Assoc 280, 1831-1836 (1998).
- 7. Airey, M., Bennett, C., Nicolucci, A. & Williams, R. Aldose reductase inhibitors for the prevention and treatment of diabetic peripheral neuropathy. *Cochrane Db Syst Rev* (2005).
- 8. Wilkinson, C.P. et al. Proposed international clinical diabetic retinopathy and diabetic macular edema disease severity scales. *Ophthalmology* 110, 1677-1682 (2003).
- 9. Rubanyi, G.M. & Vanhoutte, P.M. Superoxide Anions and Hyperoxia Inactivate Endothelium-Derived Relaxing Factor. *Am J Physiol* 250, H822-H827 (1986).
- 10. Bennett, P.H. et al. Screening and Management of Microalbuminuria in Patients with Diabetes-Mellitus Recommendations to the Scientific-Advisory-Board of the National-Kidney-Foundation from an Ad-Hoc-Committee of the Council-on Diabetes-Mellitus of the National-Kidney-Foundation. *Am J Kidney Dis* 25, 107-112 (1995).
- 11. Sprague, R.S., Stephenson, A.H., Bowles, E.A., Stumpf, M.S. & Lonigro, A.J. Reduced expression of G(i) in erythrocytes of humans with type 2 diabetes is

- associated with impairment of both cAMP generation and ATP release. *Diabetes* 55, 3588-3593 (2006).
- 12. Low, P.A., Schmelzer, J.D., Ward, K.K., Curran, G.L. & Poduslo, J.F. Effect of Hyperbaric Oxygenation on Normal and Chronic Streptozotocin Diabetic Peripheral-Nerves. *Exp Neurol* 99, 201-212 (1988).
- 13. Pierce, E.A., Avery, R.L., Foley, E.D., Aiello, L.P. & Smith, L.E.H. Vascular Endothelial Growth-Factor Vascular-Permeability Factor Expression in a Mouse Model of Retinal Neovascularization. *P Natl Acad Sci USA* 92, 905-909 (1995).
- 14. Sheetz, M.J. & King, G.L. Molecular understanding of hyperglycemia's adverse effects for diabetic complications. *Jama-J Am Med Assoc* 288, 2579-2588 (2002).
- 15. Craven, P.A., Caines, M.A. & Derubertis, F.R. Sequential Alterations in Glomerular Prostaglandin and Thromboxane Synthesis in Diabetic Rats Relationship to the Hyperfiltration of Early Diabetes. *Metabolism* 36, 95-103 (1987).
- 16. Kitabchi, A.E. Proinsulin and C-Peptide Review. *Metabolism* 26, 547-587 (1977).
- 17. Marques, R.G., Fontaine, M.J. & Rogers, J. C-peptide Much more than a byproduct of insulin biosynthesis. *Pancreas* 29, 231-238 (2004).
- 18. Steiner, D.F., Cunningh.D, Spigelma.L & Aten, B. Insulin Biosynthesis Evidence for a Precursor. *Science* 157, 697-& (1967).
- 19. Wahren, J., Johansson, B.L. & Wallberghenriksson, H. Does C-Peptide Have a Physiological-Role. *Diabetologia* 37, S99-S107 (1994).
- 20. Grp, D.R. Effect of Intensive Diabetes Treatment on the Development and Progression of Long-Term Complications in Adolescents with Insulin-Dependent Diabetes-Mellitus Diabetes Control and Complications Trial. *J Pediatr-Us* 125, 177-188 (1994).
- 21. Sjoberg, S. et al. Residual Insulin Production, Glycemic Control and Prevalence of Microvascular Lesions and Polyneuropathy in Long-Term Type-1 (Insulin-Dependent) Diabetes-Mellitus. *Diabetologia* 30, 208-213 (1987).

- 22. Keenan, H.A. et al. Residual Insulin Production and Pancreatic beta-Cell Turnover After 50 Years of Diabetes: Joslin Medalist Study. *Diabetes* 59, 2846-2853 (2010).
- 23. Johansson, B.L., Sjoberg, S. & Wahren, J. The Influence of Human C-Peptide on Renal-Function and Glucose-Utilization in Type-1 (Insulin-Dependent) Diabetic-Patients. *Diabetologia* 35, 121-128 (1992).
- 24. Johansson, B.L., Kernell, A., Sjoberg, S. & Wahren, J. Influence of Combined C-Peptide and Insulin Administration on Renal-Function and Metabolic Control in Diabetes Type-1. *J Clin Endocr Metab* 77, 976-981 (1993).
- 25. Johansson, B.L. et al. Beneficial effects of C-peptide on incipient nephropathy and neuropathy in patients with Type 1 diabetes mellitus. *Diabetic Med* 17, 181-189 (2000).
- 26. Forst, T., Kunt, T., Pfutzner, A., Beyer, J. & Wahren, J. New aspects on biological activity of C-peptide in IDDM patients. *Exp Clin Endocr Diab* 106, 270-276 (1998).
- 27. Sima, A.A.F., Zhang, W.X. & Grunberger, G. Type 1 diabetic neuropathy and C-peptide. *Exp Diabesity Res* 5, 65-77 (2004).
- 28. Meyer, J.A., Froelich, J.M., Reid, G.E., Karunarathne, W.K.A. & Spence, D.M. Metal-activated C-peptide facilitates glucose clearance and the release of a nitric oxide stimulus via the GLUT1 transporter. *Diabetologia* 51, 175-182 (2008).
- 29. W. Medawala, P.M., A. Giebink, J. Meyer, C. J. Ku, D. M. Spence A Molecular Level Understanding of Zinc Activation of C-peptide and its Effects on Cellular Communication in the Bloodstream. *Rev Diabet Stud* 6, 148-158 (2009).
- 30. Scott, D.A. & Fisher, A.M. The insulin and the zinc content of normal and diabetic pancreas. *J Clin Invest* 17, 725-728 (1938).
- 31. Chien, S., Usami, S., Dellenba.Rj & Gregerse.Mi Shear-Dependent Deformation of Erythrocytes in Rheology of Human Blood. *Am J Physiol* 219, 136-& (1970).
- 32. Elsadek, B. & Kratz, F. Impact of albumin on drug delivery New applications on the horizon. *J Control Release* 157, 4-28 (2012).
- 33. Sevin, B.U. et al. Application of an Atp-Bioluminescence Assay in Human-Tumor Chemosensitivity Testing. *Gynecol Oncol* 31, 191-204 (1988).

- 34. Carroll, J.S., Ku, C.J., Karunarathne, W. & Spence, D.M. Red blood cell stimulation of platelet nitric oxide production indicated by quantitative monitoring of the communication between cells in the bloodstream. *Anal Chem* 79, 5133-5138 (2007).
- 35. Liu, Y.L., Chen, C.P., Summers, S., Medawala, W. & Spence, D.M. C-peptide and zinc delivery to erythrocytes requires the presence of albumin: implications in diabetes explored with a 3D-printed fluidic device. *Integr Biol-Uk* 7, 534-543 (2015).
- 36. Wahren, J. & Larsson, C. C-peptide: New findings and therapeutic possibilities. *Diabetes Res Clin Pr* 107, 309-319 (2015).
- 37. Pramanik, A., Olsson, M., Langel, U., Bartfai, T. & Rigler, R. Fluorescence correlation spectroscopy detects galanin receptor diversity on insulinoma cells. *Biochemistry-Us* 40, 10839-10845 (2001).

# 3.1 Background

The results in chapter 2 show that the ensemble of albumin, C-peptide and Zn<sup>2+</sup> elicits biological activity, increasing ERY-released ATP. However, in these experiments, though ERYs were subject to flow, the C-peptide and Zn<sup>2+</sup> were added exogenously, which may not represent the physiological process by which C-peptide/Zn<sup>2+</sup> interacts with ERYs.

Under *in vivo* conditions, C-peptide and  $Zn^{2+}$  are secreted from pancreatic  $\beta$ -cells continuously into the blood stream<sup>1</sup>. It is difficult to control the amount of exogenously added C-peptide and  $Zn^{2+}$  to mimic the gradually secreted amount *in vivo*. Furthermore, the structure of C-peptide and  $Zn^{2+}$  upon secretion cannot be represented well in static experiments. These shortcomings led us to an *in vitro* platform that combines C-peptide secreting cells and a flowing stream of blood cells. The recent concept of Organs-on-a-Chip facilitates the development of such a device.

## 3.1.1 Organs-on-a-Chip

The development of microfluidic technology has made it possible to integrate and culture cells on microfluidic devices, with manageable liquid or gas flow; these advances gradually developed into a new research field, Organs-on-a-Chip<sup>2</sup>. The concept of Organs-on-a-chip represents a class of micro devices for *in vitro* tissue

culture that can mimic key structures and functions of *in vivo* tissues and organs<sup>3, 4</sup>.

This concept can be further developed to Human-on-a-Chip, which combines different *in vitro* organ models on one device through a circulation mimic, for pharmacology and fundamental physiology studies<sup>5-8</sup> (Figure 3.1).

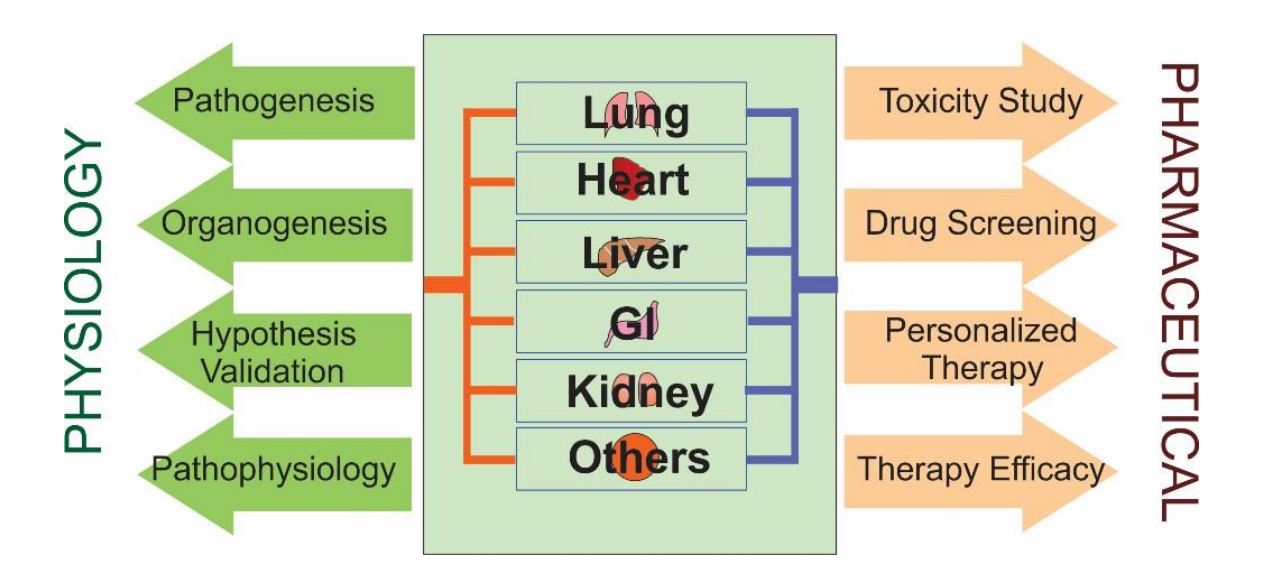


Figure 3.1. The concept of Human-on-a-Chip and its potential applications in fundamental physiological studies and in pharmaceutical research.

# 3.1.2 Cell Selection for Organs-on-a-Chip

To construct an on-chip organ that is functional and representative of *in vivo* conditions, the first technical issue that needs to be addressed is the selection of cell/tissue type to build the organ of interest<sup>5</sup>. There are three types of cells/tissues that are widely used. Each of them has its own advantages and disadvantages, and the most appropriate selection will be based on the specific goals of a study.

Because cell-cell communication, and cell-extracellular matrix (ECM) interaction play an important role in cell physiology, a fresh biopsy, which preserves the original tissue architecture, is the most reliable *in vitro* organ mimics. *Ex vivo* pancreatic islets have been successfully adapted to Organs-on-a-Chip devices by different researchers. For example, Roper monitored hormone secretion from islets on microfluidic chips, with simultaneous on-chip detection<sup>9</sup>. Mohammed reported an islet-on-chip device to characterize islets before transplantation<sup>10</sup>. Some other biopsies such as brain slice and heart tissue have also been successfully integrated onto microfluidic devices<sup>11-14</sup>.

Though biopsies are more representative of *in vivo* environments, they only remain viable for a short time (a few hours) after being extracted<sup>15, 16</sup>. Therefore, Organ-on-Chip integrated with *ex vivo* tissues are limited to assays that do not require much time. Also, the availability of human *ex vivo* tissues is limited, which restricts its application in human-oriented physiological and pharmaceutical studies.

Primary cells are directly isolated from animals, making them a good mimic of *in vivo* conditions. Therefore, primary cells have become the most common cell source for Organ-on-a-Chip platforms. Using proper protocols that have been developed, primary cells can remain viable and functional for weeks after isolation, which enables long term physiological observation and studies<sup>17, 18</sup>. However, primary cells also possess noticeable disadvantages. Although a single primary cell can represent its *in vivo* counterpart, the lack of cell-cell, and cell-ECM interactions, and three dimensional (3D) architectures can compromise the relevance of the results from corresponding studies.

Several advances in the field of cell biology, such as 3D cell culture and cell coculture assays help overcome some of the drawbacks. 3D cell culture models apply
porous ECM gels as scaffolds for living cell cultures, to mimic tissue- and organ-specific
micro architectures<sup>2, 19</sup>. Goral and colleagues have successfully cultured hepatocytes
in a 3D manner and integrated them onto a microfluidic platform<sup>20</sup>. An *in vivo*tissue/organ is comprised of different types of cells, the interaction between which
usually plays an important role in maintaining normal functionality and activity<sup>21</sup>. Cell
co-culture assays enable interactive culture of primary cells that can be applied to
microfluidic platforms, as shown by the recapitulation of an on-chip blood vessel. A
blood vessel consists of two layers, the endothelial cells (EC) that form a continuous
lining for blood flow, and the smooth muscle cell (SMC) layer<sup>22</sup>. The interaction
between EC and SMC regulates vessel dilation and thus is associated with

complications of several diseases including hypertension and diabetes. Wallace and colleagues have developed different co-culture assays for EC and SMC<sup>23</sup>.

Though primary cells can mimic *in vivo* conditions, there are still limitations. The process to isolate primary cells can be labor intensive, time consuming and costly. Moreover, the availability of primary cells is also limited, which is especially true in the case of human studies. Therefore, cell lines, which are less representative than primary cells, but are suitable for large volume pre-tests in a short time period, can be also used for Organs-on-a-Chip fabrication.

Both tissue biopsy and primary cells have the problem of limited availability. With the development of stem cell technology, especially human induced pluripotent stem cells (hiPSCs), it is possible to imagine collecting a body cell from a human and inducing it to hiPSCs, which then differentiate to different tissue/organ models on specific 3D culture scaffolds<sup>24</sup>. The Organ-on-a-Chip studies starting from stem cells are still in their infancy, yet appear to be very promising<sup>25-27</sup>. The pioneering work in this field started from on-chip stem cell culture and differentiation<sup>28</sup>.

It is not easy to culture and differentiate stem cells because many factors such as media flow rate, chemical environments (*e.g.*, gradient of growth factor), and mechanical factors are hard to regulate in conventional cell culture setups<sup>29</sup>. Microfluidics, however, have shown success in stem cell culture by controlling media flow and manipulating the chemical environment well. Recently, Wan and colleagues

obtained functional cardiomyocyte tissue derived from embryonic stem cells on a microfluidic device<sup>30</sup>.

### 3.1.3 Reconstruction of *in vivo* Microenvironments

Mechanical factors, such as shear stress, have long been recognized as a key determinant of tissue/organ function by regulating cell morphological polarization, molecule transportation and pathway activation<sup>31, 32</sup>. Therefore, mechanical factors should be taken into full consideration when establishing an Organ-on-a-Chip system.

The elasticity property of PDMS enables the integration of mechanical effects on a microfluidic chip, a well-known example of which is the lung-on-chip model developed by Ingber<sup>33</sup>. Gas exchange in the lungs occurs at the interface of alveoli and surrounding capillaries. The alveoli are lined with epithelial cells, while the capillaries are lined with endothelial cells. During a respiratory process, with the expansion and contraction of an alveolus, both epithelial cells and endothelial cells experience cyclic stretching, while the endothelial cells are also under forward shear stress caused by blood flow<sup>34</sup>. By applying multiple layers of PDMS and vacuum chambers, Ingber's model mimicked all these mechanical factors. This device mainly consisted of a center channel and two side chambers. The centered channel was used to mimic the alveolicapillary interface, with a piece of elastic membrane between the upper and lower halves of the channel. Epithelial and endothelial cells were cultured on the top and bottom sides of the membrane, which was pre-coated with fibronectin and collagen. Liquid was pumped through the lower half of the channel, in contact with the

endothelial cells, to represent blood flow, while the upper half was filled with air in order to mimic the alveoli-capillary interface. A respiratory process was achieved by stretching the cell loaded membrane, using vacuum through the side chambers. With this device, the effect of mechanical shear stress on nanoparticle translocation was investigated. Another example is an on-chip blood vessel model reported by Zheng that can apply both forward shear stress and cyclic shear stress on endothelial cells<sup>32</sup>.

Because of the difference between *in vitro* experimental conditions and *in vivo* physiological conditions, Organs-on-a-Chip models need to provide appropriate chemical microenvironments for the tissues to perform normally, which is especially true for *ex vivo* biopsy and primary cell culture. These chemical microenvironments mainly include cell nutrient supply, growth factor manipulation and chemotaxis.

The viability of extracted biopsies is usually short (within hours), which makes it difficult to perform long term or time-consuming studies. Microfluidic perfusion can be used to simulate hemodynamics in a tissue biopsy and thus reduce the risk of necrosis in a short time. For example, Sankar and colleagues reported a microfluidic perfusion culture system for isolated mouse pancreatic islet studies that used hydrodynamic traps to maintain the morphology and functions of the tissue<sup>35</sup>. Additionally, oxygen levels are a crucial determinant of the physiology of many cell types. An on-chip oxygen control device has been reported by Goral and colleagues where they applied an oxygen controlling unit in the microfluidic device for human hepatocyte culture<sup>36</sup>.

Most on-chip stem cell studies are still focused on the early stage of characterizing chemical conditions that preserve self-renewal and differentiation, for which on-chip chemical gradient manipulation can be a powerful tool. Chung and colleagues developed a microfluidic device with a concentration gradient control mechanism, to study the effect of growth factor concentrations on neuronal-stem cell behavior; using this system, they discovered a correlation between growth factor concentration and differentiation rates. In some research cases, such as cancer studies, chemotaxis needs to be evaluated<sup>37</sup>. Torisawa reported a double layer PDMS microfluidic device that applied chemical gradients along the channel to study immigration of cancer cells.<sup>38</sup>

As mentioned previously, cell-cell and cell-ECM interaction in the correct micro architecture determines the degree of resemblance of *in vitro* models to *in vivo* conditions. Many 3D cell culture protocols and cell co-culture assays have been invented that have advanced the development of Organs-on-a-Chip models.

## 3.1.4 Current development of Organs-on-a-Chip

Combining the advances in microfluidics and tissue engineering, different Organson-a-Chip models have been developed for pharmaceutical and fundamental science studies, as summarized in Table 3.1.

 Table 3.1. Summary of currently developed Organs-on-a-Chip models

System	Organ model	Study Emphasis
Cardiovascular	Heart	Build contractible cardiomyocytes <sup>39</sup>
		stem cells to cardiomyocytes <sup>40</sup>
		Recapitulation of artery structure <sup>41</sup>
		Angiogenesis <sup>42</sup>
	<b>Blood vessel</b>	Nanoparticle translocation <sup>43</sup>
		EC and SMC co-culture <sup>23</sup>
		Cell interaction and on-chip analysis <sup>44</sup>
Nervous	Brain	Electrophysiology; neural circuits <sup>14</sup>
	Nerve	Axon-glia interaction <sup>45</sup>
		Tumor angiogenesis <sup>46</sup>
	Neuromuscular	Neuromuscular contact <sup>47</sup>
	junction	
	Blood-Brain	The barrier function and drug passage <sup>48</sup>
	Barrier	
Skeletal and	Bone	Lacuna-canalicular network <sup>49</sup>
Skeietai and Muscular	Muscle	Recapitulation of contractible muscle <sup>50</sup>
iviuscular	iviuscie	Exercise inducible muscle response <sup>51</sup>
Digestive		Recapitulation of intestine tissue <sup>52</sup>
	Gastro-	Drug toxicity <sup>53</sup>
	intestine	Substance intestinal absorption <sup>54</sup>
		Recapitulation of intestinal villi <sup>55</sup>
	Liver	Recapitulation of sinusoid <sup>56</sup>
		Serum protein synthesis <sup>57, 58</sup>
		Bile canaliculi <sup>59, 60</sup>
		Assessment of metabolites and toxicity <sup>61</sup>
		Liver intestinal interactions <sup>62</sup>
		Long term repeat dose experiment <sup>63</sup>
Endocrine	Pancreatic	Islet characterization before transplantation <sup>10</sup>
	islet	Monitoring of secretion <sup>16</sup>
Respiratory	Lung	Mechanophysiological factors <sup>33</sup>
Lymphatic	Spleen	Recapitulation of spleen tissue <sup>64</sup>
	drainage	Lymphatic drainage system on chip <sup>65</sup>
	Breast	Malignant tumor invasion <sup>66</sup>
		Cancer metastasis <sup>38, 67</sup>
Disease		Blood supply in tumor <sup>68</sup>
Models	3D cultured	Drug assessment <sup>69</sup>
	tumor cells	Drug dosing <sup>70</sup>
		Photodynamic therapy <sup>71</sup>

# 3.1.5 Challenges and Future Directions

Previously developed microfluidic Organs-on-a-Chip models have proven capable of simulating parts of human physiology, which can potentially facilitate fundamental studies such as physiology, pathogenesis and organogenesis, as well as pharmaceutical studies such as drug screening, assessment, and toxicity tests.

Although some organ-organ interaction proof-of-concept models have been developed, most of the reported Organ-on-a-Chip systems are single organ/tissue models<sup>5</sup>. To enhance the applicability of such devices, multiple organs that are physiologically relevant need to be integrated to realize the Human-on-a-Chip concept<sup>72</sup>. Paradoxically, almost all Organs-on-a-Chip devices are currently fabricated in PDMS (some are in other soft materials such as hydrogels), which limits the integration capacity of multiple organs on a device because of the poor rigidness of the material. Other disadvantages of PDMS microfluidic devices, such as poor reproducibility and single use, make it nearly impossible to develop a standard and universal method to fabricate Organs-on-a-Chip devices, leading to inter-lab irreproducibility and prevention of such devices from being used for practical and industrial applications<sup>2</sup>. Therefore, new techniques that can fabricate more rugged and standard microfluidic devices, such as 3D-printing, need to be explored to make Organs-on-a-Chip models.

Organs-on-a-Chip is an exciting research area that is highly interdisciplinary between biology, chemistry and engineering. Thus, advances in these fields need to

be effectively leveraged to build novel Organs-on-a-Chip systems. The integration of stem cells on microfluidic devices is a good example, with the potential to produce physiologically representative tissues/organs on a chip. The development of hiPSCs makes it possible to establish patient-specific Human-on-a-Chip systems, for more accurate and personalized drug assessment and dosing determination. Also, to achieve the full potential of Organs-on-a-Chip devices, bioanalytical sensors such as optical sensors, electrodes and label free indicators need to be incorporated, all controlled by the appropriate software.

Summarily, Organs-on-a-Chip can be a revolutionary technique in the fields of physiology and human healthcare because of its potential applications in fundamental biological research and pharmaceutical sciences. The development of Organs-on-a-Chip in the past decade has progressed based on different proof-of-concept organ models. However, it is time to advance this technique from cutting-edge regeared towards real applications.

# 3.1.6 Chapter Overview

As discussed above, the platform that will be used to study the interactions between endogenous C-peptide and flowing blood will contain C-peptide secreting cells, blood cells (ERYs) and endothelial cells as a blood barrier mimic. Currently developed Organs-on-a-Chip models, based on PDMS microfluidic devices, are mainly single organ models that cannot achieve the desirable features of the multiple organ platform. Also, the lack of ruggedness and robustness of PDMS will significantly hinder

the establishment of such a platform. Therefore, the development of a novel Multi-Organs-on-a-Chip model based on 3D-printed fluidic devices will be investigated.

Human ERYs will be used as part of the blood flow mimic, and commonly used bovine pulmonary artery endothelial cells (bPAECs) will be used to mimic the endothelium<sup>73</sup>. Rat insulinoma cells (INS-1 cells) will be used for the C-peptide secreting cells.

Although great efforts have been exerted into isolating a pancreatic β-cell line that can respond to glucose normally, a normal β-cell line of human origin has not yet been established. The most widely used β-cell lines, including RIN (rat insulinoma cell line), HIT (hamster pancreatic beta cells), MIN (transgenic C57BL/6 insulinoma cell line), INS-1, and βTC (beta tumor cells) originated from mammals such as hamsters and rats<sup>74</sup>. Among these cell lines, the INS-1 represents many important characteristics of the pancreatic β-cells, including high insulin content and responsiveness to glucose at physiological range<sup>75</sup>. This cell line was isolated from rat insulinoma induced by X-ray irradiation by Asfari and colleagues in 1992 $^{76}$ . Rat  $\beta$ -cells, however, contain two types of proinsulins, which will subsequently produce two Cpeptides (the 8 position amino acid is either proline or alanine) in equimolar amounts<sup>75</sup>. Though these C-peptides are different than human C-peptide, the acidic amino acids with carboxyl groups, which have proven to be vital for C-peptide's biological effects<sup>44</sup>, are at the same position in both forms of the secreted peptide.

A multi-Organs-on-a-Chip model, based on a 3D-printed fluidic device is reported. Specifically, INS-1 cells will be integrated as a mimic of endocrine  $\beta$ -cells that will secrete molecules such as C-peptide and Zn<sup>2+</sup> into an ERY circulation where cell-cell interactions will be explored. An endothelium mimic will also be included to study endothelial cell-derived molecules that may be determinants of blood flow and vessel dilation *in vivo*.

### 3.2 Methods

### 3.2.1 Culture of INS-1 Cells in Membrane Inserts

Trans-well membrane inserts (Corning Inc., Horseheads, NY) were prepared for cell culture by coating the membrane with 30  $\mu$ L of a fibronectin solution (50  $\mu$ g/mL), and subsequent drying in a cell hood and sterilization by exposure to UV light. Rat INS-1 cells were cultured in RPMI-1640 medium (Life Technologies, Carlsbad, CA) supplemented with 1 mM sodium pyruvate, 100 U/mL penicillin, 100  $\mu$ g/mL streptomycin, 55  $\mu$ M mercaptoethanol, 10% fetal bovine serum, 2 mM L-glutamine and 10 mM HEPES. When the cells were confluent, as verified by optical microscopy, they were detached from the flask with trypsin/EDTA and centrifuged at 1000 g for 4 min. The pellet was resuspended in 400  $\mu$ L of the RPMI-1640 medium. Cell density was measured by a hemacytometer (Reichert, Buffalo, NY) and further diluted to a cell density of  $10^5/\mu$ L. An aliquot of 200  $\mu$ L of the cell suspension was added into a coated membrane insert (6.5 mm diameter; 0.4  $\mu$ m pore size) that was placed in an incubator with 5% CO<sub>2</sub> at 37 °C. After two hours, the medium in the inserts was removed and

200  $\mu$ L of fresh medium were added. The cells were allowed to grow to confluence before use on the 3D-printed fluidic device, which takes about 24 hours.

### 3.2.2 Culture of Endothelial Cells in Membrane Inserts

Endothelial cell culture was accomplished using bovine pulmonary arterial endothelial cells (bPAECs) that were cultured in T-75 flasks with DMEM media containing 5.5 mM glucose, 10% (v/v) fetal bovine penicillin/streptomyocin. When the cells were confluent, as verified with optical microscopy, they were detached from the flask with trypsin/EDTA and centrifuged at 1500 q for 5 min. The pellet was then resuspended in 400  $\mu$ L of the DMEM media. Cell density was determined by a hemacytometer, and the cell suspension was then diluted to a density of 0.05 million/µL. An aliquot of 200 µL of the cell suspension was added into a coated membrane insert and placed in an incubator with 5% CO<sub>2</sub> at 37 °C. After two hours, the medium in the inserts was removed and 200 μL of fresh medium were added. The cells were grown to confluence before use on the 3D-printed fluidic device.

### 3.2.3 Integration of Cells onto the Fluidic Device

Prior to use, the medium for INS-1 cells was removed and 200  $\mu$ L Krebs buffer containing 12 mM glucose and 0.1 % albumin were added to stimulate secretion of these cells for 1 hour.

Before integrating endothelial cell inserts into the fluidic device, the cell culture media was removed. Then after rinsing the cells three times with Hank's Buffered Salt Solution (HBSS, Sigma), 200  $\mu$ L of HBSS were added into each endothelial cell insert. PPADS (pyridoxalphosphate-6-azophenyl-2', 4'-disulfonic acid) was used for the experiments involving inhibition of P2y receptors on endothelial cells. A PPADS working solution was prepared by diluting 50  $\mu$ L of 100 mM PPADS stock solution (in DMSO) with 450  $\mu$ L of HBSS to create a final concentration of 10 mM. Next, 50  $\mu$ L of the PPADS working solution was added to the insert. After a 30 min incubation at 37 °C, the cells were then rinsed with HBSS to remove extra PPADS solution, after which, 200  $\mu$ L of HBSS were added into the inserts.

Membrane inserts with INS-1 cells and bPAECs were then placed in the first and third wells above a channel, respectively. A clean insert with no cells was plugged in the middle well for ATP collection via diffusion. ERY samples circulated through the channels at a flow rate of 200  $\mu$ L/min (Figure 3.2). ATP and NO standards were added to the static wells in columns 8 and 10, for on-chip calibration. The entire setup was then placed in a 37 °C incubator with the inserts covered by moist napkins to prevent evaporation of the solutions inside. An experiment time of 2 hours was employed to observe the physiological interactions between the cells.

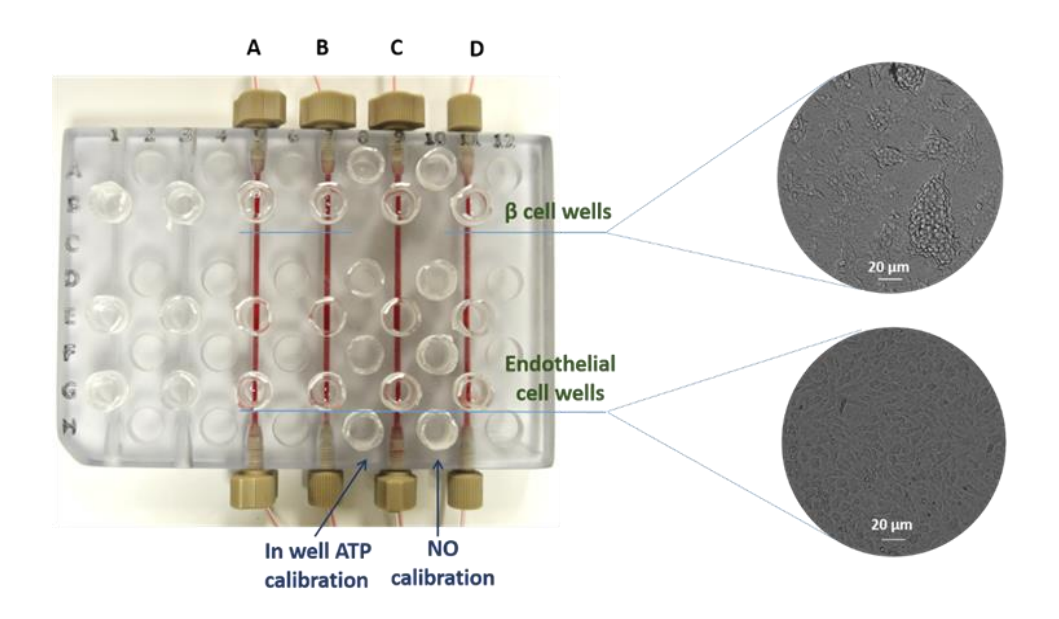


Figure 3.2. The setup of the Organs-on-a-Chip device. This study used four channels, above which, inserts cultured with INS-1 cells ( $\beta$ -cells) and bPAECs (endothelial cells) were integrated. The static wells in columns 8 and 10 contained ATP and NO standards for on-chip simultaneous calibration.

### 3.2.4 INS-1 Cell Secretion Profile Measurement

The secretion profiles of INS-1 cells were measured by an ELISA kit for rat C-peptides (Mercodia, Uppsala, Sweden). Kreb's buffer containing 12 mM glucose and 0.1% albumin was used to stimulate the INS-1 cells. Because albumin-free buffer will be used in one experimental trial, albumin-free stimulating solutions (Kreb's buffer with 12 mM glucose only) were also prepared.

After adding 200  $\mu$ L of stimulating solution into each INS-1 cell cultured insert, an aliquot of 5  $\mu$ L of the solution was sampled at 0, 10, 30, 60, 90, 120, and 180 min, which was subsequently diluted to 50  $\mu$ L with DI water. Following the instructions of the ELISA kit, the concentration of C-peptide in the samples at different times were quantified.

INS-1 cell inserts were integrated onto the device, followed by the circulation of PSS through the channels to measure the amount of C-peptide that diffused into the ERY circulation. At 0, 10, 30, 60, 90, 120, and 180 min, the tubing was opened and 5  $\mu$ L of the flowing solution were collected, diluted in DI water (to 50  $\mu$ L) and quantified by the ELISA kit. For the cells that were stimulated by albumin-free solution, albumin-free PSS was used to measure diffused C-peptides.

# 3.2.5 ATP Quantification

For ATP measurements, 50  $\mu$ L of PSS were loaded in the middle inserts above each channel, 20 min prior to measurement to collect ATP. Next, 10  $\mu$ L of luciferase/luciferin assay mixture were added into the ATP collection inserts

simultaneously by a multi-channel pipet, followed by chemiluminescence detection in a plate reader. A calibration curve was obtained before integrating the cells on the device, by circulating ATP standards of 0, 100, 200, 300, and 400 nM in five channels, and taking the measurements the same way as described above.

# 3.2.6 NO Quantification

NO was determined by using the fluorescent probe DAF-FM (4-Amino-5-methylamino-2',7'-difluorofluorescein), which shows enhanced fluorescence after reacting with NO, with an excitation wavelength of 485 nm and emission wavelength of 515 nm. In this study, 1 mg of DAF-FM was dissolved in DMSO to make a 5 mM solution, which was diluted to 25  $\mu$ M in HBSS immediately before use. Once the Organs-on-a-Chip setup was placed in the 37 °C incubator, 50  $\mu$ L of DAF-FM were added into each endothelial cell insert, to react with released NO for the whole experiment period. A black box was applied to cover the device, to prevent photobleaching of the fluorescent probe.

The NO donor Spermine NONOate (Cayman Chemicals, Ann Arbor, MI) has a half-life of 37 min at 37 °C and was used to prepare NO standard solutions. Spermine NONOate was dissolved in 0.01 M NaOH as a 1 mM stock solution, which can be stored at -20 °C for months. This stock solution was diluted in HBSS to four standard solutions of 0, 0.5, 1, and 2  $\mu$ M, followed by the immediate addition of 25  $\mu$ M DAF solution (100  $\mu$ L of DAF solution into 400  $\mu$ L of Spermine NONOate solution). The mixed solutions were then kept in the dark and placed in a 37 °C incubator for 37 min.

After the 37 min incubation, 250  $\mu$ L of the prepared NONOate (with DAF-FM) were added into four static wells in column 10 of the fluidic device, which was then placed in a plate reader. Fluorescence intensity (ex. 485, em. 515) above the endothelial cell inserts and the four static inserts were detected simultaneously. A calibration curve was obtained by plotting the fluorescence intensity of the four static wells versus the concentration of NO standards, by which, the amount of NO released from endothelial cells was quantitatively determined .

#### 3.3 Results

#### 3.3.1 Cell culture in Membrane Inserts

The INS-1 cells and endothelial cells cultured in membrane inserts were examined under a microscope. Both cells can grow to a high degree of confluence on the membrane inserts. Figure 3.3 shows that the morphology of the INS-1 cells (A) and bPAECs (B) are normal in the membrane inserts.

To count the number of cells that were cultured in membrane inserts, the medium was removed and 200  $\mu$ L of 0.25% trypsin were added into an insert. After 5 min, the cell suspension (in trypsin) was removed and cell numbers were determined by hemacytometer. In a membrane insert used in this study (6.5 mm diameter, polyester memebrane, 0.4  $\mu$ m pore size), 0.17±0.0079 million INS-1 cells and 0.036±0.0011 million bPAECs can be cultured (results represent average of 5 measurements ± S.E.M.). The reason that there are more that INS-1 cells than bPAECs on the same area

in the membrane insert is INS-1 cells can form pseudo islets, or multi-layer aggregates (Figure 3.3A) while bPAECs can only grow along the surface.

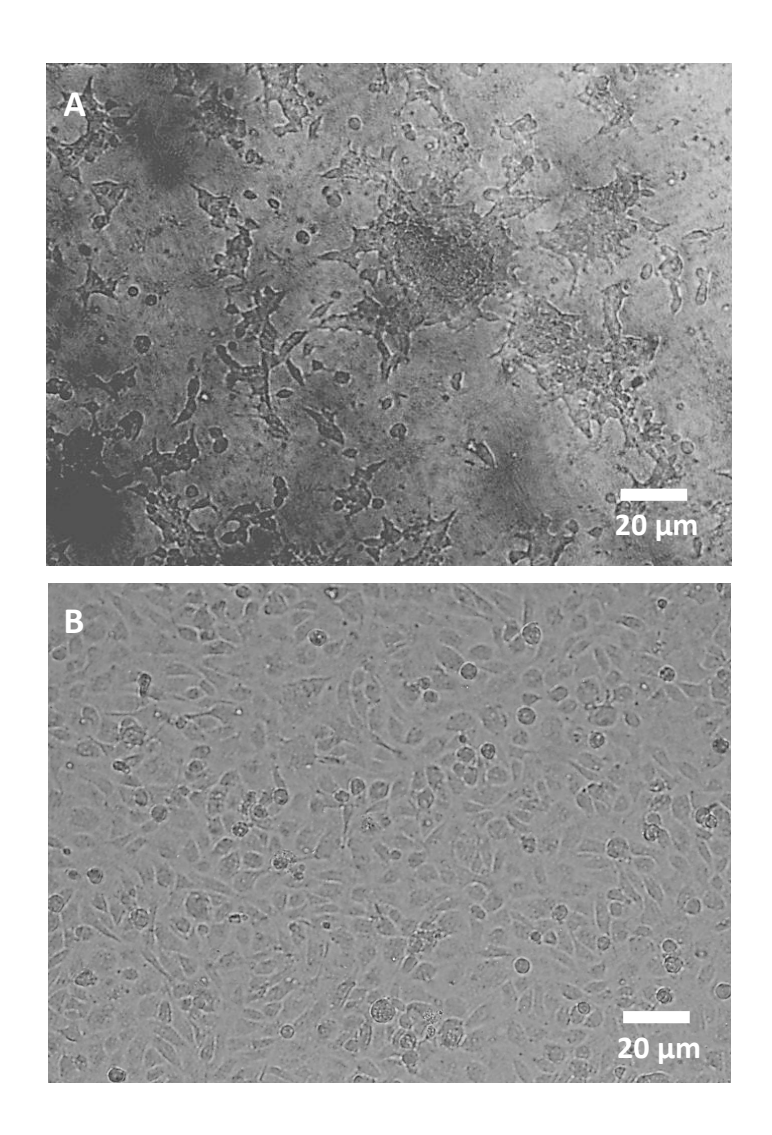


Figure 3.3. (A), microscope images cells cultured in a membrane insert. (A) INS-1 cells; (B) bPAECs.

### 3.3.2 INS-1 cell Secretion Profile

Figure 3.4A (with albumin in the stimulating solution) and Figure 3.4B (without albumin in the stimulating solution) show the secretion pattern of C-peptide after INS-1 cells were stimulated. The results suggest that albumin does not affect the stimulation of C-peptide secretion from INS-1 cells. After 60 min of stimulation, the amount of C-peptide measured reached a maximum at 26.04±1.93 nM (n=4 inserts, error=S.E.M.). After these INS-1 cells were stimulated for 60 min, the inserts were then plugged into the fluidic device, above different channels. For the inserts that had albumin containing stimulation solution, albumin containing PSS was circulated underneath. For INS-1 cells stimulated with albumin free solution, albumin free PSS was pumped through the corresponding channels. C-peptide in channels at different time points was quantified by the ELISA kit. Figure 3.4(C, D) show the diffusion profiles of C-peptide from stimulated INS-1 cells to the flowing stream under the membrane. The diffusion profiles did not show a significant difference between albumin containing (C) and albumin free (D) trials. The concentration range of C-peptide in the flow was at sub- to single digit nanomolar levels, which is consistent with reported physiological concentration range.

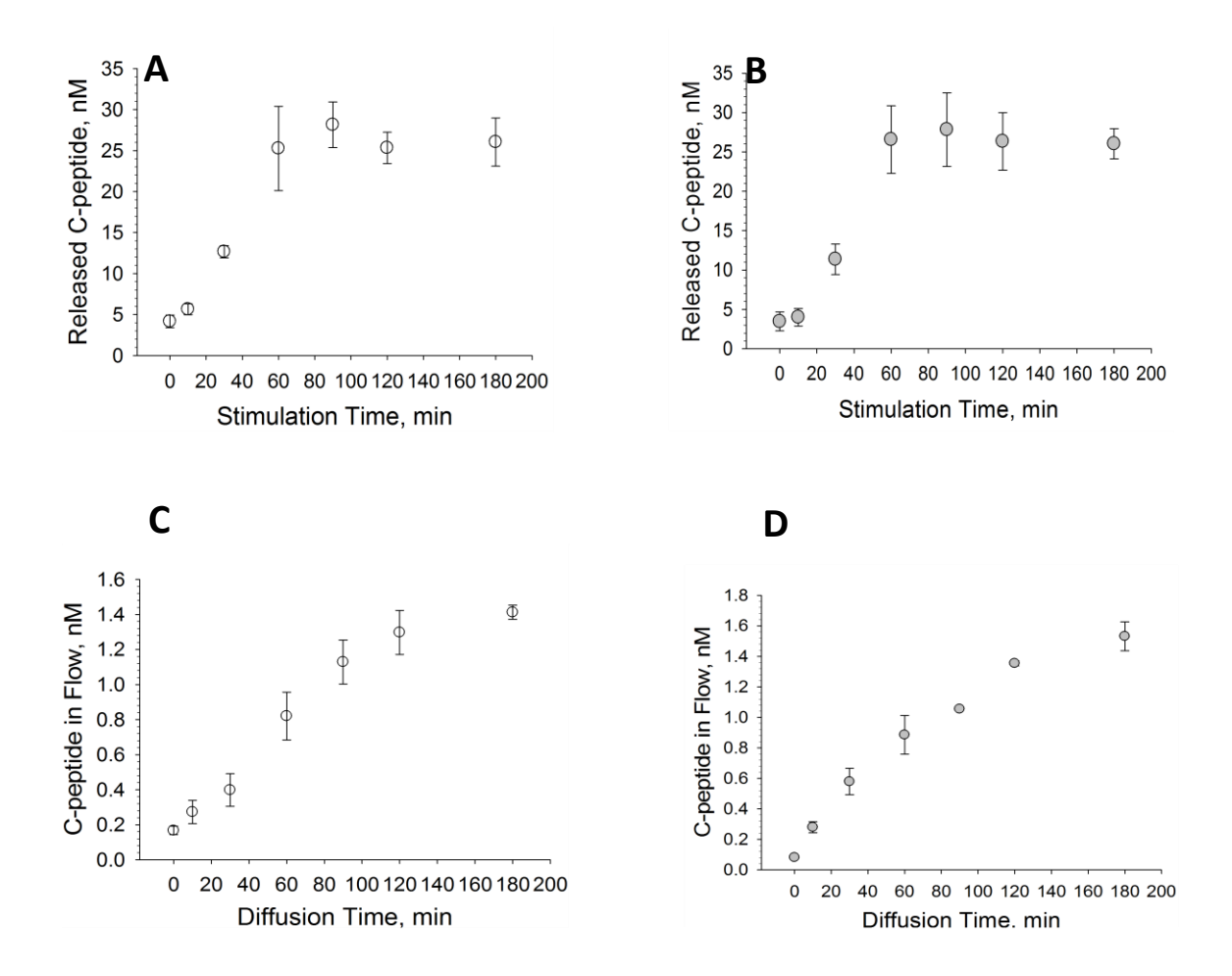


Figure 3.4. (A), INS-1 cell secretion profile in albumin-containing stimulation buffer. (B), INS-1 cell secretion profile in albumin-free stimulation solution. (C), the amount of C-peptide diffused to the following solution underneath flowing on the device, with albumin presented in the system. (D), without albumin in the system, the amount of C-peptide diffused to flowing.

### 3.3.3 Cell-cell Interaction Studies

After the establishment of the multi-Organs-on-a-Chip model, the interactions between INS-1 cells, ERYs, and endothelial cells was studied. Shown in Figure 3.5(A) is the top-down view of the strategy employed to study the interaction between the three cell types, while Figure 3.5 (B) is a side-view of the system, showing ERYs circulating underneath the various inserts. Once a 7% solution of ERYs was circulating through the system, C-peptide and Zn<sup>2+</sup> secreted from the INS-1 cells (located in the top insert, represented by the blue ovals) diffuse through the membrane and into the channel. ERYs were pumped through the channels in albumin-containing PSS, except for channel 2, which was albumin-free. After 2 hours of circulating the ERYs through the system, measurements of ATP in the middle inserts (orange circles) and NO in the bottom inserts (green circles) were performed by placing the fluidic device in a plate reader. The data in Figure 3.6 clearly show ATP levels are only increased when stimulated INS-1 cells are present in the ERYs flowing that contains albumin (channel 1). We presume that this increase in ATP release from the ERYs is due to the INS-1 secretion of C-peptide and Zn<sup>2+</sup>, which are subsequently carried to the ERYs by albumin. Note in Figure 3.6 that the absence of albumin in the stream of ERYs (channel 2) results in no significant increase in ATP release. There is also no increase in ATP release in the absence of INS-1 cells in the first well (clear oval in channel 3). In channel 4, the system contained INS-1 cells and albumin while the third well containing endothelial cells that were incubated with PPADs, a P2y purinergic receptor inhibitor. This antagonist was added to block ATP binding to the endothelial cells for inhibition

of NO production; therefore, it has no effect on ATP release. Figure 3.7 shows similar trends for measurement of ERY-derived ATP, although these measurements represent the amount of ATP determined in the channels underlying the membrane-based inserts.

Figure 3.8 contains results from measurements of NO from the bottom wells on each channel. These wells contained endothelial cells which, upon stimulation with ATP, will produce NO. As expected, based on data in Figure 3.6, the most NO production is measured when glucose is used to stimulate INS-1 cells in the presence of an albumin-containing buffered stream of ERYs (channel 1). In the absence of albumin (channel 2), there is reduced ATP release that results in decreased amounts of NO produced. Reduced levels of NO were also measured when there were no INS-1 cells in the first well (channel 3); again, reduced ATP in channel 3 (both insert and channel) suggests that reduced levels of NO would be measured in this channel, and this is confirmed in Figure 3.8. Finally, the last bar in Figure 3.8 shows that the addition of the ATP receptor blocker, PPADS, blocks ATP released by the ERY from binding to the endothelial cells, thus inhibiting NO production.

To exclude the possibility that INS-1 cells, rather than ERYs, can release large amounts of ATP diffusing to the ERY streams, after INS-1 inserts were integrated, PSS without ERYs was flowed in the channels, and ATP was measured as described above. It was found that the ATP amount from INS-1 cells was below the detection limit of the device, which is negligible compared to the ATP amount measured in Figure 3.7.

The possibility that INS-1 cells may directly stimulate endothelial cell derived NO production was also excluded.

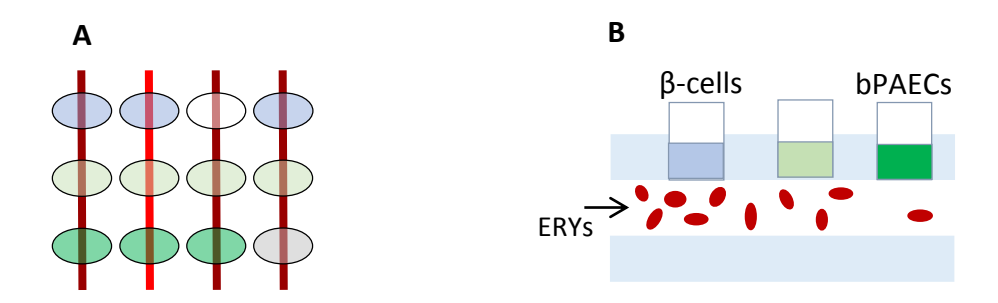


Figure 3.5. (A), the top view of the four channels with different treatments. Channel 1 contains INS-1 cells, bPAECs cultured in the membrane inserts, and ERYs flowing in PSS; channel 2 contains all three cells, but all buffers are albumin-free; channel 3 does not contain INS-1 cells, with the rest identical as channel 1; channel 4 is almost identical to channel 1, except the endothelial cells were pretreated with PPADS, a P2y receptor inhibitor. B), a side schematic view of channel 1.

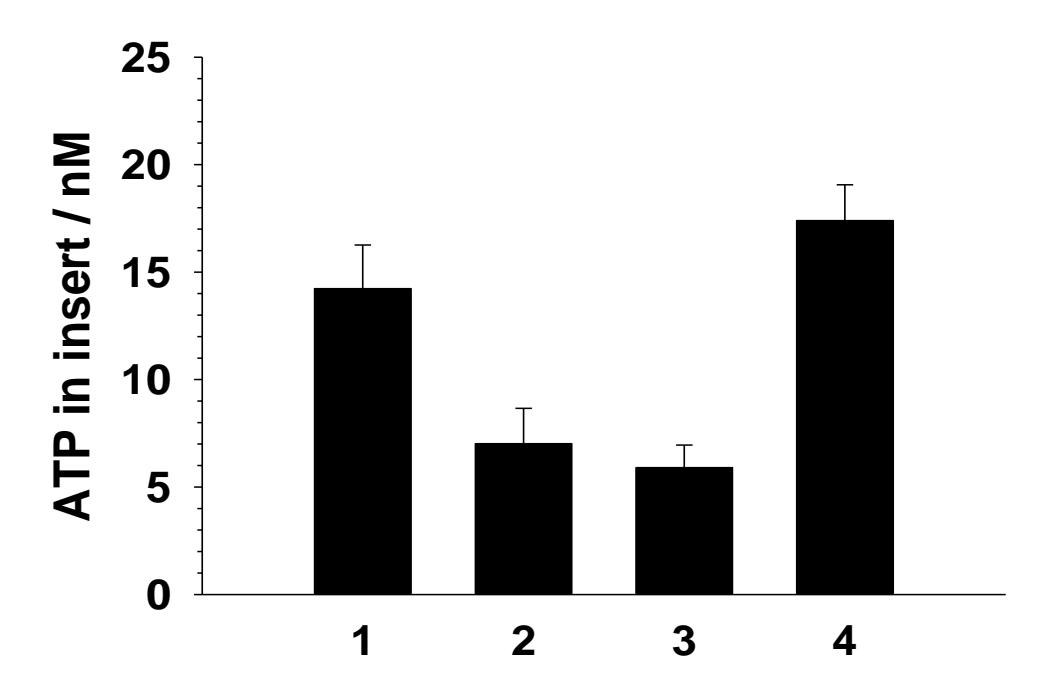


Figure 3.6. The amount of ATP collected in the insert above each channel, which is proportional to the ATP amount in corresponding flowing. Comparing channels 1 and 3, INS-1 cell stimulated ATP release from ERYs, as is shown by increased ATP amount in the collecting well. Without albumin (channel 2), however, INS-1 cells failed to stimulate ATP release from ERYs, which proved the indispensable role of albumin in this process. Channel 4 is identical to channel 1, except the endothelial cells were inhibited, which did not affect the ATP released.

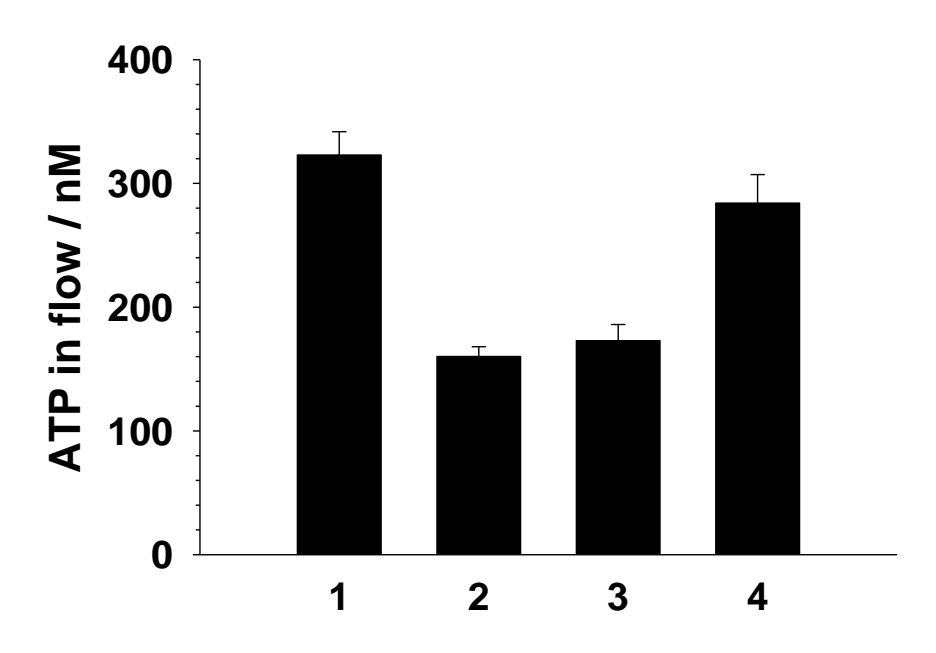


Figure 3.7. The amount of ATP in ERYs streams in the four channels, showing the same trend as in Figure 3.6.

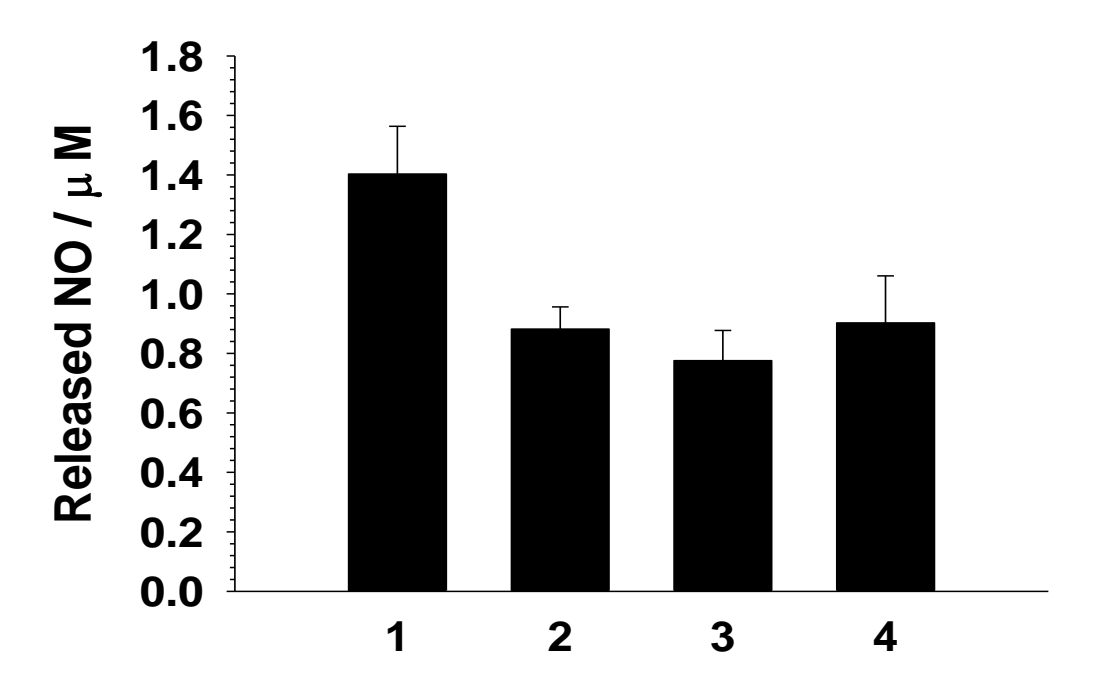


Figure 3.8. The released NO from endothelial cells culture in the last insert above each channel. The data from channels 1 to 3 are consistent with the ATP observation, which is with more ATP released, more NO will be produced in endothelial cells. In channel 4, however, though there was a higher ATP release from ERYs, the endothelial cells were pretreated with PPADs, a P2y receptor (ATP receptor in endothelial cells) inhibitor, and thus NO was not increased.

### 3.4 Discussion

Organs-on-a-Chip has become a promising tool for in vitro physiological and pharmaceutical studies, as a powerful alternative to existing 2D and 3D cell culture models<sup>2</sup>. Although many Organs-on-a-Chip platforms have been developed by researchers, these models are mainly single organ models that cannot meet the requirements of research that needs to systematically study the interactions between different tissues/cells<sup>5</sup>. Also, most of the currently developed models are not easy to use (with complicated fabrication processes), not reproducible (because the microfluidic devices are basically single use), and lab-dependent (with poor inter-lab reproducibility). One important reason for this impasse lies in the fabrication of microfluidic devices, which serve as the basis for an Organs-on-a-Chip model. As discussed in chapter 1, despite the desirable properties of PDMS, the most common material in microfluidic systems, PDMS has poor mechanical properties and the soft lithography process cannot integrate complicated features in a PDMS device. In this work, however, a 3D-printed fluidic device was applied to build an Organs-on-a-Chip model, which showed great integration and robustness. This model contains three types of cells—INS-1 cells, ERYs, and endothelial cells, as a mimic of on-chip endocrine tissue, blood flow, and blood vessel barrier, respectively. When an ERY stream flows through the endocrine mimic, the secreted molecules enter the blood stream mimic, where downstream physiological responses will be elicited and observed.

From an engineering perspective, this 3D-printed multi-Organs-on-a-Chip model avoids several problems that can occur when using PDMS based platforms. First of all,

the INS-1 cells and endothelial cells were cultured on commercial membrane inserts that can be integrated on the fluidic device, instead of being cultured directly on the device. This process allows for cell culture examination and optimization before taking a measurement. For example, if the morphology of cells in an insert tends to be abnormal, the insert can be discarded and a new one will be examined and implemented. If the cells are cultured directly on the device, it will be hard to examine the cells if the device has complicated features. Even though the cells can be examined, once a researcher finds abnormality of the cells, the whole device will likely have to be discarded. Also, this philosophy of cell culture and integration can be easily adopted for investigating other cells. Any cell that can be cultured in a membrane insert can be integrated on the fluidic device for cell-cell interaction studies.

Another important feature of the Organs-on-a-Chip platform is the realization of simultaneous on-chip detection. As discussed in chapter 2, the fluidic device was modeled following the dimensions of a standard 96-well plate, with all the wells aligned with the detectors in a plate reader. After running an experiment, the whole device can be directly placed in a plate reader to detect the optical signals above multiple wells almost simultaneously. More importantly, static wells (without a channel beneath) were also included in the device, for on-chip calibration purpose. In this study, ATP and NO standards were added in two columns of static wells to calibrate the amount of ATP and NO in dynamic wells (Figure 3.2, column 8 and 10), which not only made the measurements more efficient, but also enhanced the reliability of the results. Some other advantageous features of 3D-printed fluidic

devices, such as reusability and ruggedness also facilitate the buildup of the Organson-a-Chip platform.

From a biological perspective, this Organs-on-a-Chip platform mimics the physiological process of  $\beta$ -cell secretion entering a blood stream. Data in Figure 3.4 shows that during the experimental period (2 hours), single digit nanomolar C-peptide was secreted into the blood stream mimic, which represents the physiological concentration in a blood stream. Moreover, the secretion from  $\beta$ -cells significantly increases ATP release from ERYs, which is consistent with the discovery in chapter 2 that C-peptide/Zn<sup>2+</sup> can stimulate ERYs to release ATP. Though the  $\beta$ -cells also secrete other molecules such as insulin, it can still be initially concluded it is the C-peptide and Zn<sup>2+</sup> that increase ATP release from ERYs, because a previous study reported that insulin does not stimulate ATP release from ERYs<sup>77</sup>. However, to consolidate this theory, more research regarding on-chip separation needs to be conducted, as will be discussed in Chapter 5.

The role of albumin was also examined on the Organs-on-a-Chip platform. As shown in Figure 3.6 and 3.7, without albumin in the system, the  $\beta$ -cells failed to stimulate ATP release from ERYs, which confirmed the discovery in a more physiologically relevant way, that albumin delivers C-peptide and Zn<sup>2+</sup> to ERYs, thus playing a role in ATP release. To verify that the increased ATP was from ERYs, instead of from the INS-1 cells (which may contain ATP in cytoplasm), PSS without ERYs was

flowing under INS-1 cell inserts and the ATP amount in the flowing was quantified. The amount of ATP released under such conditions is not detectable.

Endothelial cells were integrated on the platform to mimic a blood vessel barrier. The endothelial production of NO, which is a well-recognized vessel dilator, was measured and evaluated. The interactions between  $\beta$ -cells and endothelial cells was first investigated. It was found that without ERYs flowing, the β-cells cannot stimulate NO production from the endothelial cells, which indicated there is not a direct interaction between the molecules secreted fromβ-cells and endothelial cells, in terms of NO production. However, with ERYs in the flowing channels, a higher ATP release can always elicit a higher NO production. As a control, different concentrations of ATP standards were circulated under endothelial cell inserts, showing that higher ATP levels in the flow lead to more NO production from endothelial cells. These results reveal that secreted molecules from the integrated  $\beta$ -cells can increase ATP release form ERYs, which in turn, exerts a downstream effect on endothelial cells. To prove that NO production occurs after ATP binding to endothelial cells, PPADS, an inhibitor of P2y receptor on endothelial cells was used to treat endothelial cells on channel 4 (Figure 3.5 A). Even though the ATP level in this channel is high (statistically the same as channel 1), NO production did not increase (Figure 3.8). This further proves that ATP binds onto endothelial cells via the P2y receptors, which then elicits NO synthesis in the cells.

The interaction between ERYs and endothelial cells also enlightens some possibilities for drug discovery and development. For example, for drug development to enhance endothelial cell NO production, ERYs can serve as an alternative target to endothelial cells. By increasing ERY-released ATP with a certain drug, endothelium derived NO can also be indirectly enhanced.

Keenan has reported that diabetic patients who still retain detectable C-peptide in their blood stream exhibited a lower level of diabetic complications<sup>78</sup>. The results presented in this chapter can potentially explain this clinical observation in a scenario that C-peptide secreted from pancreatic β-cells enters the blood stream and interacts with ERYs in the presence of albumin and Zn<sup>2+</sup>, subsequently increasing ERY-derived ATP that in turn, exerts a downstream effect on endothelial cells by increasing endothelium-derived NO, which promotes vasodilation and thus ameliorates diabetic complications resulting from restricted blood flow. This conclusion can also be supported by the observations of Wahren, Sjoberg, Johansson and other researchers that C-peptide reduces diabetes complications. All the evidence indicates that Cpeptide can potentially be a missing link in diabetes treatment<sup>79-84</sup>. The results from Chapter 2 and this chapter proved the indispensable role of albumin and Zn<sup>2+</sup> in the process that C-peptide affects ERYs, which represents a step forward of the development of C-peptide therapy, but also evokes further questions including the binding structure of the three molecules, the binding site of C-peptide on ERYs, and the pathway by which ATP release is stimulated. Such basic research work needs to be performed before turning C-peptide into a therapeutics for diabetes.

### 3.5 Conclusion

In this chapter, a multi-Organs-on-a-Chip model was established on a 3D-printed fluidic device, to study claimed interactions between endocrine β-cells, ERYs, and endothelial cells, in a physiological manner. This is the first Organs-on-a-Chip model that contains three interactive cell types. The philosophy of culturing cells in membrane inserts that will be plugged in the 3D-printed fluidic device guarantees the quality (morphology, confluence etc.) of the cells to be studied. It also provides a universal way to study other cells/tissue as long as the cells can be cultured in an insert. The 3D-printed fluidic device is amenable to a plate reader for simultaneous and efficient optical measurements. Also the static wells on the device enable simultaneous on-chip calibration for ATP and NO, which can enhance the reliability of detected results. The secretion profiles of the β-cells mimic the physiological secretion process well. It was found that the secretions from β-cells do not affect the endothelial cells, but increase ATP release from ERYs, which in turn, plays a downstream role on endothelial cells, stimulating NO production. Also, albumin is indispensable in these processes, without which, none of the above response could be observed. Although more on-chip separation work needs to be performed to eventually conclude which molecule(s) from the  $\beta$ -cell secretion exert the observed effects, it can be initially concluded that C-peptide and Zn<sup>2+</sup> are required. These results further confirmed the efficacy of C-peptide/Zn<sup>2+</sup> on vessel dilation, and the indispensable role of albumin, in a more physiologically relevant way. The philosophy applied in establishing the multiOrgans-on-a-Chip platform can also be used for other studies involving cell interactions and drug discovery.

**REFERENCES** 

#### **REFERENCES**

- 1. Brandenburg, D. History and Diagnostic Significance of C-Peptide. *Exp Diabetes Res* (2008).
- 2. Huh, D., Hamilton, G.A. & Ingber, D.E. From 3D cell culture to organs-on-chips. *Trends Cell Biol* **21**, 745-754 (2011).
- 3. van der Meer, A.D. & van den Berg, A. Organs-on-chips: breaking the in vitro impasse. *Integr Biol-Uk* **4**, 461-470 (2012).
- 4. Beebe, D.J., Ingber, D.E. & den Toonder, J. Organs on Chips 2013. *Lab Chip* **13**, 3447-3448 (2013).
- 5. Luni, C., Serena, E. & Elvassore, N. Human-on-chip for therapy development and fundamental science. *Curr Opin Biotech* **25**, 45-50 (2014).
- 6. Ghaemmaghami, A.M., Hancock, M.J., Harrington, H., Kaji, H. & Khademhosseini, A. Biomimetic tissues on a chip for drug discovery. *Drug Discov Today* **17**, 173-181 (2012).
- 7. Sung, J.H. et al. Microfabricated mammalian organ systems and their integration into models of whole animals and humans. *Lab Chip* **13**, 1201-1212 (2013).
- 8. Williamson, A., Singh, S., Fernekorn, U. & Schober, A. The future of the patient-specific Body-on-a-chip. *Lab Chip* **13**, 3471-3480 (2013).
- 9. Yi, L. et al. Integrated perfusion and separation systems for entrainment of insulin secretion from islets of Langerhans. *Lab Chip* **15**, 823-832 (2015).
- 10. Mohammed, J.S., Wang, Y., Harvat, T.A., Oberholzer, J. & Eddington, D.T. Microfluidic device for multimodal characterization of pancreatic islets. *Lab Chip* **9**, 97-106 (2009).
- 11. Cheah, L.T. et al. Microfluidic perfusion system for maintaining viable heart tissue with real-time electrochemical monitoring of reactive oxygen species. *Lab Chip* **10**, 2720-2726 (2010).
- 12. Huang, Y., Williams, J.C. & Johnson, S.M. Brain slice on a chip: opportunities and challenges of applying microfluidic technology to intact tissues. *Lab Chip* **12**, 2103-2117 (2012).

- 13. Mauleon, G., Fall, C.P. & Eddington, D.T. Precise spatial and temporal control of oygen within in vitro brain slices via microfluidic gas channels. *Plos One* **7** (2012).
- 14. Scott, A. et al. A microfluidic microelectrode array for simultaneous electrophysiology, chemical stimulation, and imaging of brain slices. *Lab Chip* **13**, 527-535 (2013).
- 15. Wang, Y. et al. Application of microfluidic technology to pancreatic islet research: first decade of endeavor. *Bioanalysis* **2**, 1729-1744 (2010).
- 16. Dishinger, J.F., Reid, K.R. & Kennedy, R.T. Quantitative Monitoring of Insulin Secretion from Single Islets of Langerhans in Parallel on a Microfluidic Chip. *Anal Chem* **81**, 3119-3127 (2009).
- 17. Jang, K.J. et al. Human kidney proximal tubule-on-a-chip for drug transport and nephrotoxicity assessment. *Integr Biol-Uk* **5**, 1119-1129 (2013).
- 18. Achyuta, A.K.H. et al. A modular approach to create a neurovascular unit-on-a-chip. *Lab Chip* **13**, 542-553 (2013).
- 19. van der Meer, A.D., Orlova, V.V., ten Dijke, P., van den Berg, A. & Mummery, C.L. Three-dimensional co-cultures of human endothelial cells and embryonic stem cell-derived pericytes inside a microfluidic device. *Lab Chip* **13**, 3562-3568 (2013).
- 20. Giobbe, G.G. et al. Human pluripotent stem cell derived hepatocyte-like cells integrated in microfluidic platform for drug screening applications. *Hepatology* **60**, 1187a-1188a (2014).
- 21. Lee, S.A. et al. Spheroid-based three-dimensional liver-on-a-chip to investigate hepatocyte-hepatic stellate cell interactions and flow effects. *Lab Chip* **13**, 3529-3537 (2013).
- 22. Wong, K.H.K., Chan, J.M., Kamm, R.D. & Tien, J. Microfluidic Models of Vascular Functions. *Annu Rev Biomed Eng* **14**, 205-230 (2012).
- 23. Truskey, G.A. Endothelial vascular smooth muscle cell coculture assay for high throughput screening assays to identify antiangiogenic and othe therapeutic molecules. *International Journal of High Throughput Screening* **99**, 171-181 (2010).

- 24. Tibbitt, M.W. & Anseth, K.S. Hydrogels as Extracellular Matrix Mimics for 3D Cell Culture. *Biotechnol Bioeng* **103**, 655-663 (2009).
- 25. Figallo, E. et al. Micro-bioreactor array for controlling cellular microenvironments. *Lab Chip* **7**, 710-719 (2007).
- 26. Lee, J.M., Kim, J.E., Kang, E., Lee, S.H. & Chung, B.G. An integrated microfluidic culture device to regulate endothelial cell differentiation from embryonic stem cells. *Electrophoresis* **32**, 3133-3137 (2011).
- 27. Fung, W.T., Beyzavi, A., Abgrall, P., Nguyen, N.T. & Li, H.Y. Microfluidic platform for controlling the differentiation of embryoid bodies. *Lab Chip* **9**, 2591-2595 (2009).
- 28. Kawada, J., Kimura, H., Akutsu, H., Sakai, Y. & Fujii, T. Spatiotemporally controlled delivery of soluble factors for stem cell differentiation. *Lab Chip* **12**, 4508-4515 (2012).
- 29. El-Ali, J., Sorger, P.K. & Jensen, K.F. Cells on chips. *Nature* **442**, 403-411 (2006).
- 30. Wan, C.R., Chung, S. & Kamm, R.D. Differentiation of Embryonic Stem Cells into Cardiomyocytes in a Compliant Microfluidic System. *Ann Biomed Eng* **39**, 1840-1847 (2011).
- 31. Jang, K.J. & Suh, K.Y. A multi-layer microfluidic device for efficient culture and analysis of renal tubular cells. *Lab Chip* **10**, 36-42 (2010).
- 32. Zheng, W.F. et al. A microfluidic flow-stretch chip for investigating blood vessel biomechanics. *Lab Chip* **12**, 3441-3450 (2012).
- 33. Huh, D. et al. Reconstituting Organ-Level Lung Functions on a Chip. *Science* **328**, 1662-1668 (2010).
- 34. Weibel, E.R. Morphological Basis of Alveolar-Capillary Gas-Exchange. *Physiol Rev* **53**, 419-495 (1973).
- 35. Sankar, K.S. et al. Culturing Pancreatic Islets in Microfluidic Flow Enhances Morphology of the Associated Endothelial Cells. *Plos One* **6** (2011).
- 36. Goral, V.N. & Yuen, P.K. Microfluidic Platforms for Hepatocyte Cell Culture: New Technologies and Applications. *Ann Biomed Eng* **40**, 1244-1254 (2012).

- 37. Chung, B.G. et al. Human neural stem cell growth and differentiation in a gradient-generating microfluidic device. *Lab Chip* **5**, 401-406 (2005).
- 38. Torisawa, Y.S. et al. Microfluidic platform for chemotaxis in gradients formed by CXCL12 source-sink cells. *Integr Biol-Uk* **2**, 680-686 (2010).
- 39. Kim, J.H., Kang, T.J. & Yu, W.R. Mechanical modeling of self-expandable stent fabricated using braiding technology. *J Biomech* **41**, 3202-3212 (2008).
- 40. Alford, P.W., Feinberg, A.W., Sheehy, S.P. & Parker, K.K. Biohybrid thin films for measuring contractility in engineered cardiovascular muscle. *Biomaterials* **31**, 3613-3621 (2010).
- 41. Gunther, A. et al. A microfluidic platform for probing small artery structure and function. *Lab Chip* **10**, 2341-2349 (2010).
- 42. Franco, C. & Gerhardt, H. TISSUE ENGINEERING Blood vessels on a chip. *Nature* **488**, 465-466 (2012).
- 43. Kim, Y. et al. Probing nanoparticle translocation across the permeable endothelium in experimental atherosclerosis. *P Natl Acad Sci USA* **111**, 1078-1083 (2014).
- 44. Liu, Y.L., Chen, C.P., Summers, S., Medawala, W. & Spence, D.M. C-peptide and zinc delivery to erythrocytes requires the presence of albumin: implications in diabetes explored with a 3D-printed fluidic device. *Integr Biol-Uk* **7**, 534-543 (2015).
- 45. Park, J., Koito, H., Li, J.R. & Han, A. Microfluidic compartmentalized co-culture platform for CNS axon myelination research. *Biomed Microdevices* **11**, 1145-1153 (2009).
- 46. Chung, S. et al. Cell migration into scaffolds under co-culture conditions in a microfluidic platform. *Lab Chip* **9**, 269-275 (2009).
- 47. Das, M., Rumsey, J.W., Bhargava, N., Stancescu, M. & Hickman, J.J. A defined long-term in vitro tissue engineered model of neuromuscular junctions. *Biomaterials* **31**, 4880-4888 (2010).
- 48. Hawkins, B.T. & Davis, T.P. The blood-brain barrier/neurovascular unit in health and disease. *Pharmacol Rev* **57**, 173-185 (2005).
- 49. You, L.D. et al. Osteocytes as mechanosensors in the inhibition of bone resorption due to mechanical loading. *Bone* **42**, 172-179 (2008).

- 50. Nagamine, K. et al. Spatiotemporally controlled contraction of micropatterned skeletal muscle cells on a hydrogel sheet. *Lab Chip* **11**, 513-517 (2011).
- 51. Nedachi, T., Fujita, H. & Kanzaki, M. Contractile C2C12 myotube model for studying exercise-inducible responses in skeletal muscle. *Am J Physiol-Endoc M* **295**, E1191-E1204 (2008).
- 52. Kimura, H., Yamamoto, T., Sakai, H., Sakai, Y. & Fujii, T. An integrated microfluidic system for long-term perfusion culture and on-line monitoring of intestinal tissue models. *Lab Chip* **8**, 741-746 (2008).
- 53. Mahler, G.J., Esch, M.B., Glahn, R.P. & Shuler, M.L. Characterization of a Gastrointestinal Tract Microscale Cell Culture Analog Used to Predict Drug Toxicity. *Biotechnol Bioeng* **104**, 193-205 (2009).
- 54. Imura, Y., Sato, K. & Yoshimura, E. Micro Total Bioassay System for Ingested Substances: Assessment of Intestinal Absorption, Hepatic Metabolism, and Bioactivity. *Anal Chem* **82**, 9983-9988 (2010).
- 55. Domansky, K. et al. Perfused multiwell plate for 3D liver tissue engineering. *Lab Chip* **10**, 51-58 (2010).
- 56. Lee, P.J., Hung, P.J. & Lee, L.P. An artificial liver sinusoid with a microfluidic endothelial-like barrier for primary hepatocyte culture. *Biotechnol Bioeng* **97**, 1340-1346 (2007).
- 57. Carraro, A. et al. In vitro analysis of a hepatic device with intrinsic microvascular-based channels. *Biomed Microdevices* **10**, 795-805 (2008).
- 58. Kane, B.J., Zinner, M.J., Yarmush, M.L. & Toner, M. Liver-specific functional studies in a microfluidic array of primary mammalian hepatocytes. *Anal Chem* **78**, 4291-4298 (2006).
- 59. Nakao, Y., Kimura, H., Sakai, Y. & Fujii, T. Bile canaliculi formation by aligning rat primary hepatocytes in a microfluidic device. *Biomicrofluidics* **5** (2011).
- 60. Sudo, R. et al. Transport-mediated angiogenesis in 3D epithelial coculture. *Faseb J* **23**, 2155-2164 (2009).
- 61. van Midwoud, P.M., Verpoorte, E. & Groothuis, G.M.M. Microfluidic devices for in vitro studies on liver drug metabolism and toxicity. *Integr Biol-Uk* **3**, 509-521 (2011).

- 62. van Midwoud, P.M., Merema, M.T., Verpoorte, E. & Groothuis, G.M.M. A microfluidic approach for in vitro assessment of interorgan interactions in drug metabolism using intestinal and liver slices. *Lab Chip* **10**, 2778-2786 (2010).
- 63. Khetani, S.R. & Bhatia, S.N. Microscale culture of human liver cells for drug development. *Nat Biotechnol* **26**, 120-126 (2008).
- 64. Baker, M. A Living System on a Chip. *Nature* **471**, 661-665 (2011).
- 65. Wong, K.H.K., Truslow, J.G., Khankhel, A.H., Chan, K.L.S. & Tien, J. Artificial lymphatic drainage systems for vascularized microfluidic scaffolds. *J Biomed Mater Res A* **101**, 2181-2190 (2013).
- 66. Sung, K.E. et al. Transition to invasion in breast cancer: a microfluidic in vitro model enables examination of spatial and temporal effects. *Integr Biol-Uk* **3**, 439-450 (2011).
- 67. Song, J.W. et al. Microfluidic Endothelium for Studying the Intravascular Adhesion of Metastatic Breast Cancer Cells. *Plos One* **4** (2009).
- 68. Elliott, N.T. & Yuan, F. A Review of Three-Dimensional In Vitro Tissue Models for Drug Discovery and Transport Studies. *J Pharm Sci-Us* **100**, 59-74 (2011).
- 69. Wlodkowic, D. & Cooper, J.M. Tumors on chips: oncology meets microfluidics. *Curr Opin Chem Biol* **14**, 556-567 (2010).
- 70. Wang, S.Y. et al. Application of microfluidic gradient chip in the analysis of lung cancer chemotherapy resistance. *J Pharmaceut Biomed* **49**, 806-810 (2009).
- 71. Jedrych, E., Pawlicka, Z., Chudy, M., Dybko, A. & Brzozka, Z. Evaluation of photodynamic therapy (PDT) procedures using microfluidic system. *Anal Chim Acta* **683**, 149-155 (2011).
- 72. Huh, D., Torisawa, Y.S., Hamilton, G.A., Kim, H.J. & Ingber, D.E. Microengineered physiological biomimicry: Organs-on-Chips. *Lab Chip* **12**, 2156-2164 (2012).
- 73. Vogel, P.A., Halpin, S.T., Martin, R.S. & Spence, D.M. Microfluidic Transendothelial Electrical Resistance Measurement Device that Enables Blood Flow and Postgrowth Experiments. *Anal Chem* **83**, 4296-4301 (2011).

- 74. Skelin, M., Rupnik, M. & Cencic, A. Pancreatic Beta Cell Lines and their Applications in Diabetes Mellitus Research. *Altex-Altern Anim Ex* **27**, 105-113 (2010).
- 75. Merglen, A. et al. Glucose sensitivity and metabolism-secretion coupling studied during two-year continuous culture in INS-1E insulinoma cells. *Endocrinology* **145**, 667-678 (2004).
- 76. Asfari, M. et al. Establishment of 2-Mercaptoethanol-Dependent Differentiated Insulin-Secreting Cell-Lines. *Endocrinology* **130**, 167-178 (1992).
- 77. Giebink, A.W., Vogel, P.A., Medawala, W. & Spence, D.M. C-peptide-stimulated nitric oxide production in a cultured pulmonary artery endothelium is erythrocyte mediated and requires Zn2+. *Diabetes-Metab Res* **29**, 44-52 (2013).
- 78. Keenan, H.A. et al. Residual Insulin Production and Pancreatic beta-Cell Turnover After 50 Years of Diabetes: Joslin Medalist Study. *Diabetes* **59**, 2846-2853 (2010).
- 79. Wahren, J. & Larsson, C. C-peptide: New findings and therapeutic possibilities. *Diabetes Res Clin Pr* **107**, 309-319 (2015).
- 80. Wahren, J., Johansson, B.L. & Wallberghenriksson, H. Does C-Peptide Have a Physiological-Role. *Diabetologia* **37**, S99-S107 (1994).
- 81. Sjoberg, S. et al. Residual Insulin Production, Glycemic Control and Prevalence of Microvascular Lesions and Polyneuropathy in Long-Term Type-1 (Insulin-Dependent) Diabetes-Mellitus. *Diabetologia* **30**, 208-213 (1987).
- 82. Johansson, B.L., Sjoberg, S. & Wahren, J. The Influence of Human C-Peptide on Renal-Function and Glucose-Utilization in Type-1 (Insulin-Dependent) Diabetic-Patients. *Diabetologia* **35**, 121-128 (1992).
- 83. Johansson, B.L., Kernell, A., Sjoberg, S. & Wahren, J. Influence of Combined C-Peptide and Insulin Administration on Renal-Function and Metabolic Control in Diabetes Type-1. *J Clin Endocr Metab* **77**, 976-981 (1993).
- 84. Johansson, B.L. et al. Beneficial effects of C-peptide on incipient nephropathy and neuropathy in patients with Type 1 diabetes mellitus. *Diabetic Med* 17, 181-189 (2000).

Chapter 4 - Evaluating Stored Erythrocytes Used in Transfusion Medicine using 3D-Printed Analytical Devices

# 4.1 Background

# 4.1.1 Blood Banking

Blood component transfusion has become a critical part of modern healthcare. In 2011, approximately 15.7 million units of whole blood were collected and 87% of them were transfused in the United States alone<sup>1, 2</sup>. The history of blood banking dates back to 1915, when Rous and Turner invented a mixed solution containing citrate and glucose for blood storage<sup>3</sup>. This idea was further developed by Robertson who applied citrate as an anticoagulant and, using glucose as an erythrocyte (ERY) preservative, subsequently became the basis for modern blood banking protocols<sup>4</sup>.

Currently, the FDA approved blood banking protocol consists of two steps: collection of blood in a solutions known as CPD (Citrate-Phosphate-Dextrose), and storage in a preservative "additive solution" (AS)<sup>5-7</sup>. As shown in Table 4.1, there are two types of CPD and three variants of AS solutions that are widely used for ERY storage<sup>7-10</sup>. CPD is usually used with AS-1, while CP2D, which contains double the amount of dextrose (glucose) as CPD is mainly combined with AS-3 or AS-5.

A typical ERY collection procedure involves 450 mL of whole blood drawn into a primary bag made of polyvinyl chloride (PVC) that contains 63 mL of the anticoagulant solution, CPD. After centrifugation, ERYs (~ 220 mL, containing ~ 40 mL of CPD/plasma) are sedimented and separated from the buffy coat (which contains platelets and

leukocytes) and plasma. With a semiautomated extractor, plasma is then exported out of the top port, and the ERYs are exported out of the bottom port into a satellite bag containing 100 mL of AS-1. This procedure results in a final, stored ERY solution at a 55% - 60% hematocrit<sup>11, 12</sup>. Based on the ingredient information from Table 4.1, the final concentration of dextrose (glucose) in a storage bag will be ~ 40 mM, which is much higher than the physiological level of 5.5 mM<sup>13</sup>.

#### 4.1.2 Transfusion Related Complications

Although blood transfusion has proven successful in the care of critically ill patients to replace lost hemoglobin and maintain normal oxygen delivery, transfusion related complications still exist<sup>14</sup>. Survival of patients should be the first priority in all medical treatments. Unfortunately, studies have also demonstrated that ERY transfusion is associated with increased mortality, in comparison to those patients who did not receive a transfusion<sup>15-18</sup>. An increased risk of complications such as pneumonia<sup>19, 20</sup>, infections<sup>21</sup>, and multi-organ failure<sup>18, 22</sup> (e.g., renal failure) has also been reported. Interestingly, some of these reports have indicated that the aging of stored ERYs may be significantly associated with the clinical consequences. For example, Koch reported that patients who received ERYs stored more than two weeks had higher rates of in-hospital mortality, complications, and even a higher mortality rate one year after a transfusion<sup>23</sup>. Zallen and colleagues found that blood units stored longer than 14 days increased the risk of multiple organ failure and serious infections<sup>22</sup>.

The adverse clinical consequences that occur after a transfusion potentially result from physiological alterations of ERYs, known as storage lesions, during storage in an

environment that is dramatically different from *in vivo* conditions<sup>24, 25</sup>. The hallmark feature of storage conditions is hyperglycemia, which may adversely affect the physiology of stored ERYs, especially when considering the fact that in diabetic patients, 7-9 mM blood glucose already results in noticeable ERY lesions, including impaired ATP release<sup>26</sup>. The extremely high glucose level in ERY storage solutions may be a key factor related to the ERY storage lesions.

Table 4.1. Constituents of CPD and AS Used for Blood Banking

Constituents (mM)	CPD	AS-1	CP2D	AS-3	AS-5
Sodium citrate	101.9	-	101.9	23	-
Monobasic sodium phosphate	16.1	-	16.1	23	-
Citric acid	15.6	-	15.6	2	-
Dextrose	129	111	258	55	45
Sodium chloride	-	154	-	70	150
Adenine	-	2	-	2	2.2
Mannitol	-	41	-	45.5	-

In addition to oxygen delivery, ERYs also participate in regulating blood flow by releasing ATP into the blood stream. ATP binds to endothelial cells on the inner side of vessel walls, leading to endothelium NO synthesis. As discussed previously, NO

participates in the relaxation of smooth muscle cells surrounding vessel walls, enabling vessel dilation and increased blood flow<sup>27</sup>. Interestingly, some reports show that people who received a transfusion suffer from insufficient nitric oxide bioavailability (INOBA)<sup>28, 29</sup>. In relation to decreased NO availability, Tsai and colleagues reported a 63% decrease in microvascular flow after transfusion with stored ERYs<sup>30</sup>.

Inspired by these results, the Spence group has studied the effects of hyperglycemia on stored ERYs, discovering that high glucose level leads to diminished ERY release of ATP, and thus decreases downstream endothelium derived NO. Furthermore, an alternative storage solution AS-1N (normoglycemic version of AS-1) was proposed to be beneficial to maintain a relatively normal ATP level from stored ERYs<sup>31</sup>.

#### 4.1.3 Chapter Motivation and Overview

Previous research has shown that hyperglycemic storage conditions can diminish ATP release from stored ERYs<sup>31</sup>, which may lead to insufficient NO bioavailability after a transfusion, and eventually cause severe complications. However, the performance of stored ERYs and their overall condition after being transfused into the normoglycemic blood stream of a patient remained unknown. For example, can the hyperglycemia stored ERYs reverse their function of releasing normal amount of ATP? Therefore, the reversibility of ATP release from stored ERYs will be first studied in this chapter. Also, the mechanism by which hyperglycemia decreases ATP release will be explored in this work.

As discussed in chapter 3, healthy ERYs respond to pancreatic  $\beta$ -cells by releasing ATP that can stimulate NO production from endothelial cells. The results from Chapter 3 provided motivation to examine the responsiveness of stored ERYs to  $\beta$ -cell secretion, especially C-peptide. Here, a 3D-printed intravenous (i.v.) injection device will be described that mimics an *in vitro* transfusion process, with  $\beta$ -cells integrated to examine how stored ERYs respond to a mimic of normal endocrine function.

#### 4.2 Methods

#### 4.2.1 ERY Collection and Storage

The collection process consists of preparing 6 non-siliconized and untreated (i.e., no heparin or other anticoagulant) 10 mL glass Vacutainer tubes (BD, Franklin Lakes NJ); 1 mL of CPD was injected into 3 of the tubes using a syringe, while the other 3 contained 1 mL of CPD-N. Next, approximately 7 mL of whole blood were collected into each tube, resulting in a total volume of 8 mL. The blood remained in the collection solutions for at least 30 minutes, but not more than 2 hours at room temperature ( $\sim 20^{\circ}$ C) prior to processing. Tubes were centrifuged at 2000 g for 10 minutes followed by aspiration of the plasma and buffy coat layers. Importantly, an additional 2-mm layer off the top of the packed ERYs was also removed to minimize leukocyte presence during subsequent storage in the AS-1 or AS-1N solutions. The purified ERYs from the 3 tubes containing CPD were then combined into a single 15 mL tube, followed by the addition of AS-1 such that the ratio of packed ERYs to AS-1 was 2:1. The same protocol was followed for ERYs collected in CPD-N and stored in AS-1N. Finally, 2 mL of the ERYs (stored in the AS-1 or AS-1N) were added to PVC bags

and stored at 4°C. Prior to use, the PVC bags were sterilized under UV light overnight. The PVC bags were prepared in-house using rolled PVC (ULINE, Pleasant Prairie WI) and a heat sealer. All blood collection and storage processes were performed under sterile conditions. All blood collection procedures from informed and consented donors were approved by the Biomedical and Health Institutional Review Board at Michigan State University. The ingredients of CPD, AS-1 are listed in Table 4.1. The glucose concentration is 5.5 mM in CPD-N and AS-1N, with other constituents identical to CPD and AS-1.

The ERYs stored in the normoglycemic AS-1N solution required periodic glucose feeding to provide enough nutrients for extended storage. These cells were "fed" every week by opening the PVC storage bag and adding 20 µL of 400 mM glucose in saline to the ERYs, and then re-sealing the bag in a sterile environment. The glucose saline was prepared by dissolving 0.72 g of dextrose in 10 mL of saline (a solution of 0.90% (weight/volume) of sodium chloride (NaCl)), in order to prevent cell lysis. This helped to maintain the glucose concentrations in the stored cells at around 5 mM, while maintaining a constant volume into which the cells were stored.

#### 4.2.2 Sample Preparation

The hematocrit of stored ERYs was first determined for quantitative re-suspension by collecting ERYs in a microcapillary tube, spinning in a microhematocrit centrifuge (CritSpin M960-22, Statspin, Westwood, MA) and visually quantifying the percentage of packed cells using a microcapillary reader (Statspin, Westwood, MA). The glucose

levels in corresponding storage solutions were also monitored by a portable Accu-Chek Aviva glucose meter (Indianapolis, IN). Buffered physiological salt solution (PSS, contains 4.7 mM KCl, 2.0 mM CaCl<sub>2</sub>, 1.2 mM MgSO<sub>4</sub>, 140.5 mM NaCl, 21.0 mM trishydroxymethyl aminomethane, 5.5 mM glucose, and 5% bovine serum albumin at pH = 7.4) was prepared to re-suspend the ERYs. A high glucose version of PSS (referred to as PSSH) was also prepared as a control, whose glucose concentration equals the extracellular glucose level of ERYs to be suspended.

Three samples were prepared for a single experiment. AS-1N-PSSN cells refer to those stored in normoglycemic AS-1N and transfused into normoglycemic PSS; AS-1-PSSH refers to cells stored in hyperglycemic AS-1 and transfused to hyperglycemic PSS; and the AS-1-PSSN cells were those stored in hyperglycemic AS-1 but transfused to normoglycemic PSS. The final hematocrit of ERYs in all three samples was 5 % in corresponding PSS, which was preheated to 37 °C before mixing with ERYs.

# 4.2.3 Determination of ATP Release Reversibility

The 3D-printed fluidic device that mimics the *in vitro* circulation, as described in the previous chapter, was applied to measure ATP release from stored ERYs after resuspension in PSS. Briefly, the device consists of two parts, channels that allow samples to flow through, and wells above the channels where membrane inserts can be plugged in to form a membrane barrier between the flow and the well. The three ERY samples were pumped to fill all six channels on the device in duplicate, after which each channel and corresponding tubing were closed to form a loop of 450  $\mu$ L. The

circulation in the loops was driven by a peristaltic pump (IDEX Health & Science LLC, Oak Harbor, WA) at a flow rate of 200 µL/min. An aliquot of 50 µL PSS was then loaded in wells in Row E above each channel to collect ATP from the flowing ERY samples via diffusion. The entire setup of the pump, the device and closed loops with circulating samples was then placed in an incubator at 37 °C for 20 min to better mimic circulation conditions, after which, the bulk device was detached from tubing and placed in the sample holder of a plate reader (SpectraMax 4, Molecular Devices, Sunnyvale, CA). The well-established luciferase/luciferin chemiluminescence assay was used to detect ATP in the wells. Specifically, 10µL of L/L assay (dissolving 2.0 mg of D-luciferin in 5 mL of DDW, and adding 100 mg of firefly extract) were added into the wells simultaneously by a multichannel pipet. After 15 s, the chemiluminescence intensity above all six wells was detected by the plate reader, simultaneously. To confirm that the increase of released ATP was not due to cell lysis, an absorbance measurement was performed to evaluate if free hemoglobin was detected in the supernatant after flow was concluded. If hemoglobin was detected, that particular sample would be discarded due to indication of lysis. In the studies reported here, there were no samples discarded due to lysis.

A calibration curve was obtained for quantification purpose by circulating five ATP standards prepared in PSS (concentrations of 0, 100, 200, 300 and 400 nM) in five randomly chosen channels with identical subsequent detection processes as described above.

## 4.2.4 Study of Reversibility of ERY Deformability by a 3D-printed Cell Filter

Deformability of stored ERYs was detected by forcing the cells through a piece of porous membrane in a filter. The number of cells that passed through the filter, relative to the number that were pumped to the filter, were counted on a hemacytometer (Reichert, Buffalo, NY), as a measurement of deformability.

The filter was fabricated by 3D-printing on the Objet Connex 350 printer (Stratasys Ltd, Eden Prairie, MN) with XY resolution of 100 µm and Z of 16 µm, housed in the Engineering Department of Michigan State University. As shown in Figure 4.1, the main parts of the filter are two flange-shaped slabs that were printed by VeroClear material (Stratasys Ltd, Eden Prairie, MN) whose exact composition is proprietary, but approximately contains isobornyl acrylate (15-30%), acrylic monomer (15-30%), urethane acrylate (10-30%), acrylic monomer (5-10; 10-15%), epoxy acrylate (5-10; 10-15%), acrylate oligomer (5-10; 10-15%), and a photoinitiator (0.1-1;1-2%). A sample inlet was fabricated on the top slab, which was a female fitting with printed screw threads on the inside. The two slabs can be clamped together with a piece of semipermeable membrane in between to construct the filter, and the simultaneously printed O rings by rubber-like TangoBlack material (Stratasys Ltd, Eden Prairie, MN, approximately contains 30-60% urethane acrylate oligomer, 1-20% exo-1,7,7trimethylbicyclo[2.2.1]hept-2-yl acrylate, 1-20% methacrylate oligomer, 1-20% resin, polyurethane, and 0.1-1% photoinitiator) on the binding sides of both slabs ensured tight holding of the membrane without liquid leaking. Figure 4.2 shows the engineering sketch of the filtration device, with detailed dimensions.

A piece of polycarbonate membrane with a pore size of 5  $\mu$ m, which is smaller than the mean diameter (6-8  $\mu$ m) of ERYs, was used in the filter. After the slab-membrane-slab device was constructed by binding the two slabs with binder clips, a section of tubing for sample introduction was connected to the top slab by screwing the male finger tight adapter at the end of the tubing into the female inlet. The tubing was forced by a peristaltic pump (IDEX Health & Science LLC, Oak Harbor, WA) to drive samples into the filter, with a driving pressure of 12 cm  $H_2O$  column (0.17 psi). All three samples of AS-1N-PSSN, AS-1-PSSH and AS-1-PSSN were measured through the device in a random order. The effluent was collected for 10 min, after which, the number of cells in the effluent was counted on the hemacytometer. Cell lysis in the effluent was also checked and in the studies reported here, no filtration induced lysis was observed.

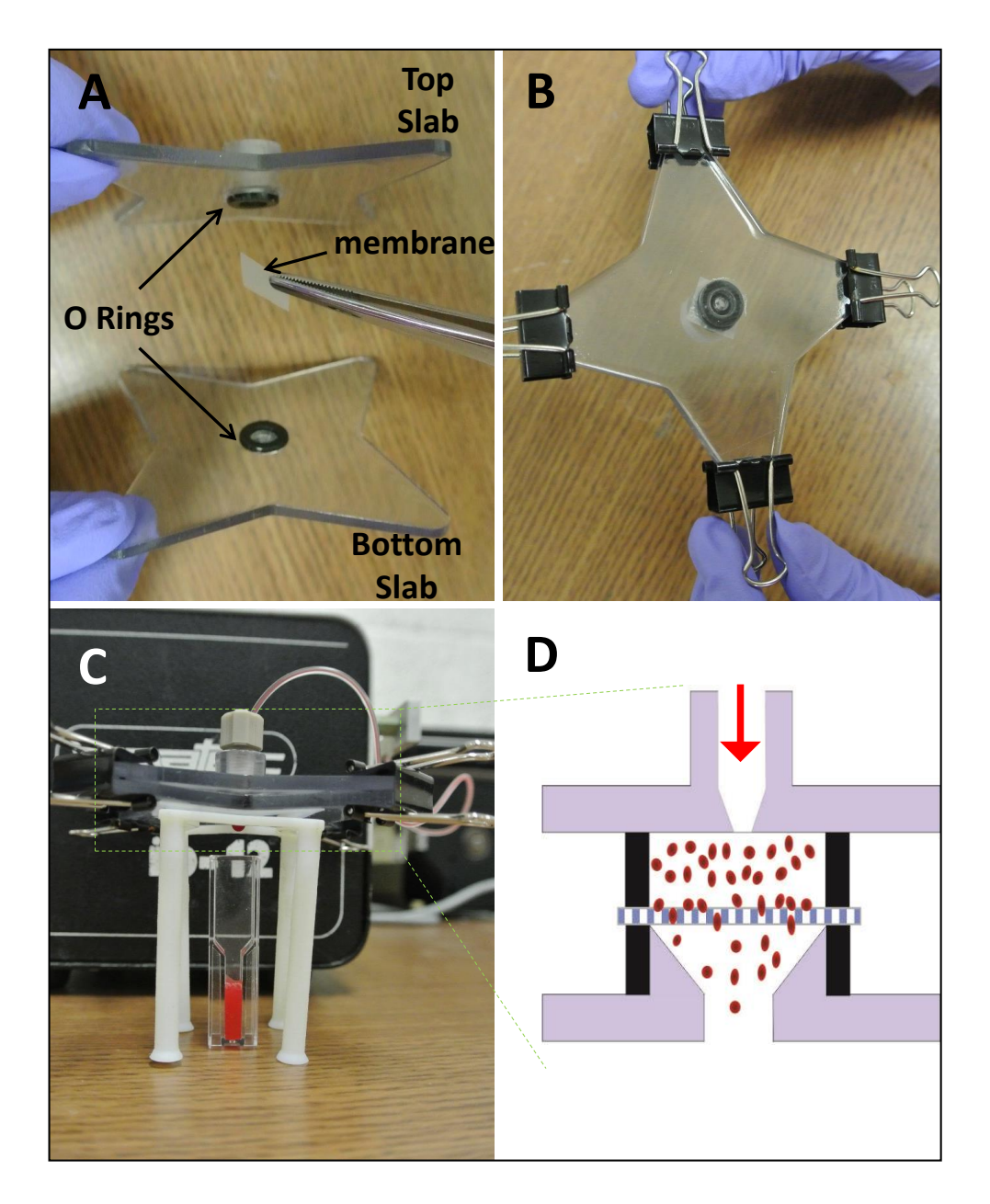


Figure 4.1. The 3D-printed cell filter for ERY deformability measurements. (A): the two slabs with O rings on the binding sides. A piece of semipermeable membrane is the key part of the filter device, which was 5 µm pore size polycarbonate membrane. (B): A view of the assembled device, with the membrane between the slabs. The assembling was achieved by simply binding the two slabs on the four wings with binder clips. (C): The view of a real filtration experiment. A sample was introduced by a pump into the top slab, which would be forced to go through the membrane and was then collected for subsequent cell counting. (D): The schematic cross view of a filtration process. A pressure was applied to push cells to deform to pass through the membrane between the O rings. However, only cells with sufficient deformability can go through, otherwise they will be blocked by the membrane.

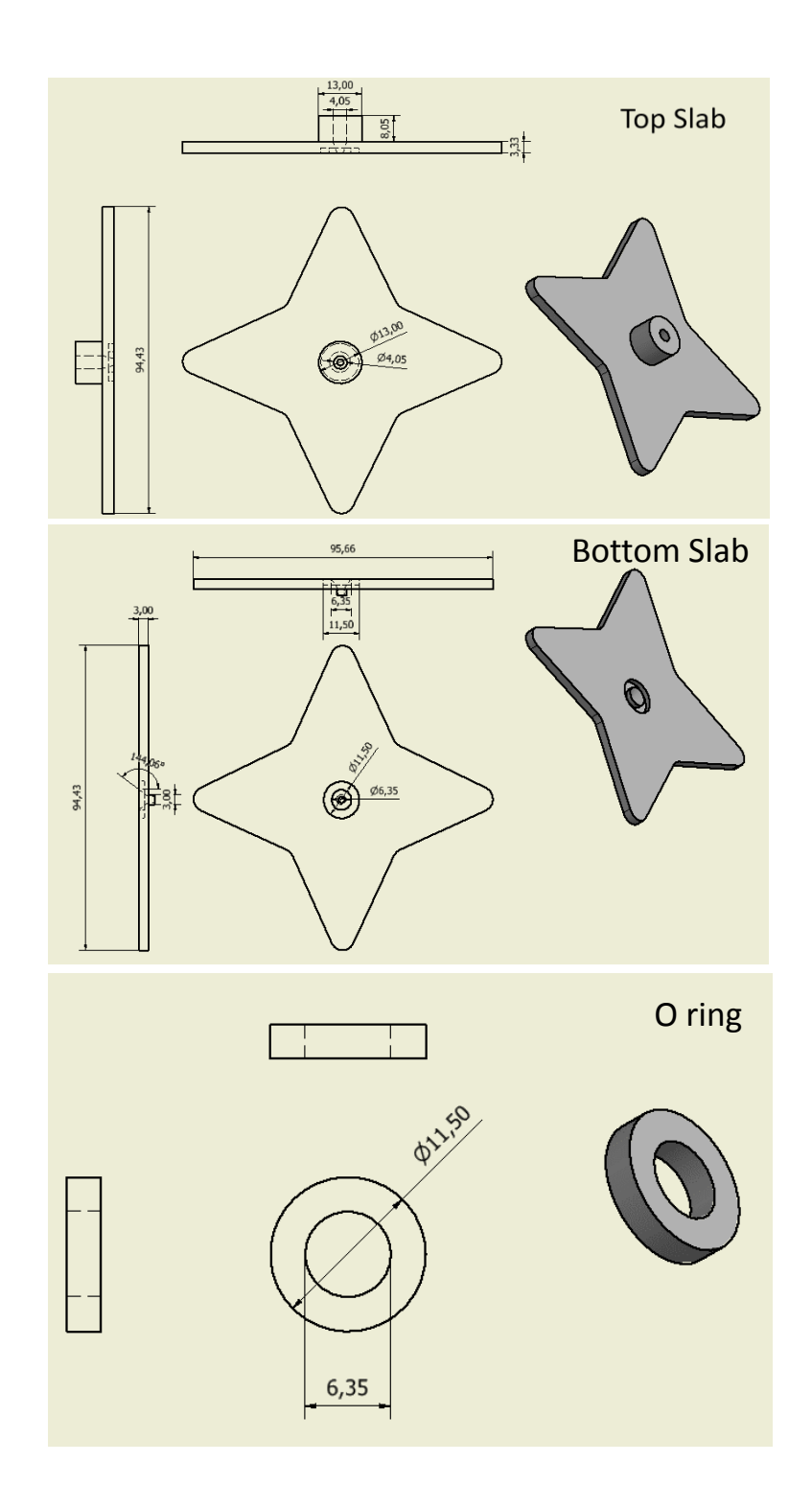
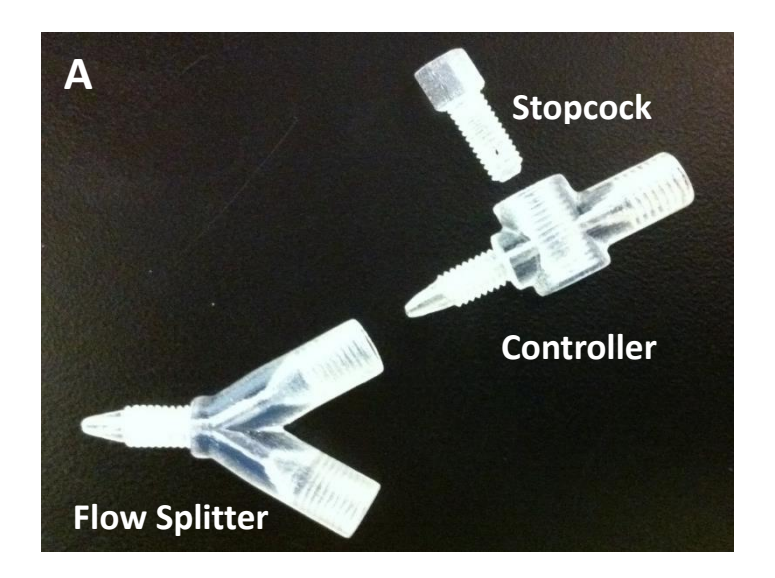


Figure 4.2. The technical drawings of the top slab, bottom slab and O rings of the filtration device, achieved by the autodesk inventor software. Before sending the files into the printer, the O rings were assembled to both slabs in the software so that they can be printed simultaneously. The unit for all the dimensions is mm.

## 4.2.5 Design and Fabrication of an i.v. Injection Device

A Y shaped adapter was designed and 3D-printed by the same printer as mentioned above, to mimic an in vitro i.v. injection process. As shown in Figure 4.3A, this adapter consists of three parts: a flow splitter, a controller and a stopcock. Screw threads were printed on the parts for easy connection. Just prior to use, the three parts were assembled and then the Y shaped flow splitter was connected to a channel on the fluidic device. The low branch of the flow splitter is connected with the other end of the channel by soft tubing, which goes around the rollers of a peristaltic pump to drive the flow. The top branch and the flow controller were connected to a syringe via a male finger tight adapter. Figure 4.3B displays the injection of fluorescein by the syringe into a water circulation. Upon injection, the stopcock is adjusted to make the hole (through the stopcock) align with the channel so that liquid can be injected through. When an injection was finished, the stopcock was rotated 90° to stop further injection. Teflon tape may be needed for better sealing between the stopcock and the controller in some cases. The top branch and the controller need to be prefilled with the liquid to be injected at the beginning of an experiment. Otherwise, some trapped air in this part will be injected into the circulation and thus the injection amount cannot be easily quantified.



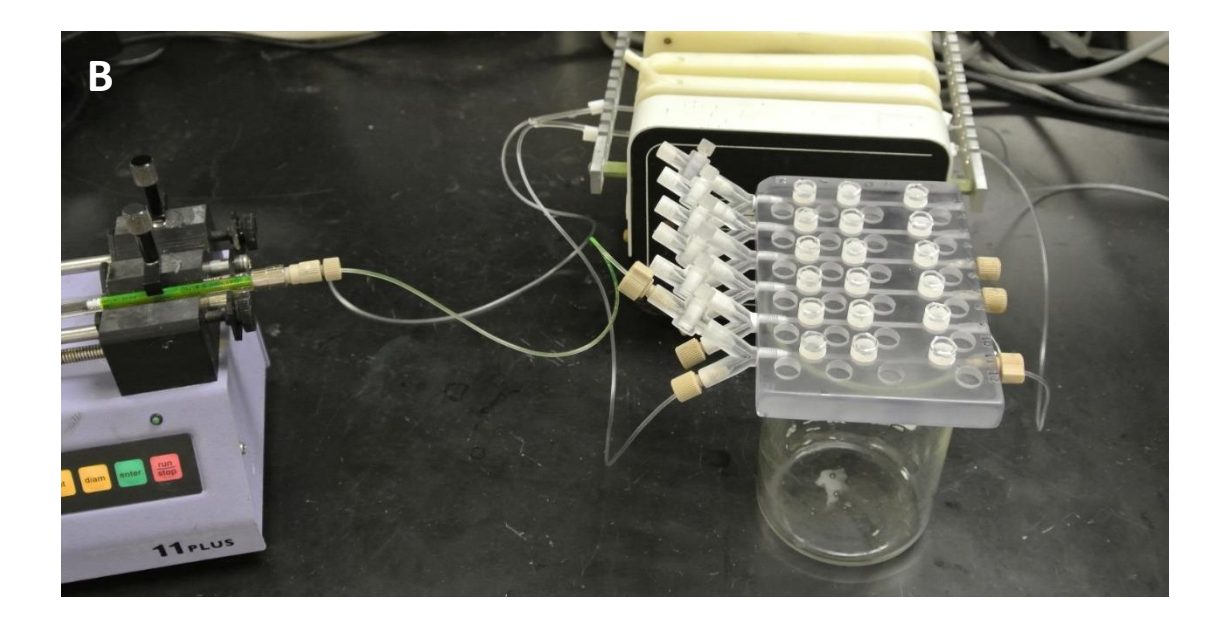


Figure 4.3. The 3D-printed i.v. injection device. (A): the device comprises three parts: a flow splitter, a flow controller, and a stop cock. Screw threads were printed on each part for easy but tight connection. When the hole that goes through the stopcock was adjusted along the channel in the flow controller, liquid can be injected through. Otherwise, the flow will be stopped. (B): Injection of fluorescein into a water circulation. Water was circulating in the loop that connects the low branch of the splitter and the other end of a channel, while fluorescein was injected in by a syringe pump.

## 4.2.6 Characterization of the i.v. Injection Device

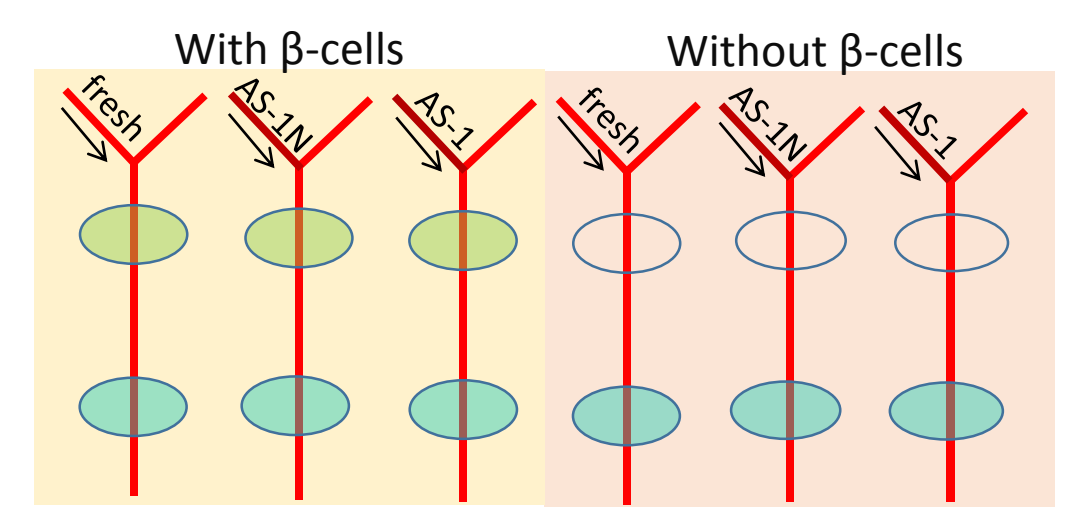
This device will be eventually used to study i.v. injection (transfusion) of stored ERYs, and quantitative injection will be required to acquire reliable experimental results. Therefore, the injection accuracy was first characterized. Fluorescein injection was conducted to investigate the injection accuracy of small molecules, and for ease of detection. An aliquot of 50 μL of fluorescein (300 μM) was injected to a loop of water with a volume of 450 μL. The injection was performed at 100 μL/min for 30 s by a syringe pump. The liquid was allowed to circulate for another 2 min after the injection, after which, the liquid in the loop (tubing and channel) was collected and the fluorescein concentration was quantified on a plate reader (ex. 494 nm; em. 521 nm). Based on the injection ratio (1 to 9), the concentration of fluorescein in a loop was expected to be 30 μM. The detected fluorescein concentration was compared with this calculated number, the difference between which, can indicate injection accuracy. The possibility that the the fluidic device material may absorb fluorescein molecules was examined by detecting the loss of fluorescence signal intensity of a fluorescein solution after being circulated in a channel for hours.

The injection accuracy of ERYs was also measured. A 5% ERY sample suspended in PSS was circulating in a loop, while 50  $\mu$ L of 50 % ERYs were injected at 100  $\mu$ L/min for 30 s. The calculated hematocrit of ERYs in the loop after an injection was expected to be 10%. By comparing the detected hematocrit and the calculated value of 10%, injection accuracy of ERYs can be determined. In these experiments, counting of ERYs on a hemacytomer was performed for accurate hematocrit measurements.

The distribution of injected fluorescein molecules and ERYs in the circulating loops was also characterized. After fluorescein was injected, 2 min of circulation were allowed, after which, the liquid in the loop was divided into three random sections that were collected in three vials, respectively. If the fluorescein molecules distribute evenly in the loop after an injection, the concentrations in the three parts were expected to be the same. The distribution of ERYs after an injection was characterized with the same method, except 5 min of circulating time were applied before measuring the hematocrit in the three sections of tubing.

#### 4.2.6 Study of Responsiveness of Stored ERYs to Pancreatic $\beta$ -cells

INS-1 cells were integrated on the fluidic device, with 5 % fresh ERYs circulating in the channels. As shown in Figure 4.4, INS-1 cells cultured in membrane inserts were integrated on the left three channels of the fluidic device, while the other three did not contain the endocrine-like cells (empty ovals). Fresh, AS-1 and AS-1N stored ERYs (hematocrit 50 %) from the same donor were injected via the i.v. injection device into the fresh ERY streams. After the ERYs were injected by the procedures discussed previously, the entire setup was placed in a 37 °C incubator for 2 hours, with moisture napkins covering the wells to minimize evaporation of buffers, after which, the ATP amount in each channel was quantified on a plate reader, with the method introduced in Chapter 2.



5 % fresh ERYs are flowing in the channels

Figure 4.4. The strategy to study the responsiveness of stored ERYs to  $\beta$ -cells. Fresh ERYs with a hematocrit of 5% were circulating in the six channels of the fluidic device, while fresh, AS-1N stored, and AS-1 stored ERYs were injected into the circulations via the i.v. injection device. INS-1 cells were included on the left three channels (green ovals). A 2-hour incubation at 37 °C was applied after the injection, after which, ATP amount in each channel was quantified by the luciferase/luciferin assay in the blue ovals.

#### 4.3 Results

# 4.3.1 ERY Collection and Storage, Sample Preparation

Two blood storage solutions, one hyperglycemic (AS-1, currently FDA approved) and one normoglycemic (AS-1N, Spence modified), were used to study the effect of glucose on stored ERYs. Although the normoglycemic storage solution AS-1N was reported beneficial to stored ERYs, it is not conducive for a storage period over 1 week due to the exhaustion of glucose by cell metabolism. Therefore, the ERYs stored in AS-1N were fed with a 20 μL of 200 mM glucose saline solution every week to maintain the glucose level at around 5.5 mM. Before ATP and deformability of the ERY samples were characterized, glucose levels in corresponding storage solutions were first monitored. Figure 4.5 shows that the glucose level in AS-1 stays at an extremely high level around 40 mM for the whole storage period of 36 days, while in AS-1N, the glucose concentration maintains at around 5 mM with periodic feeding of glucose, which falls into the healthy physiological range.

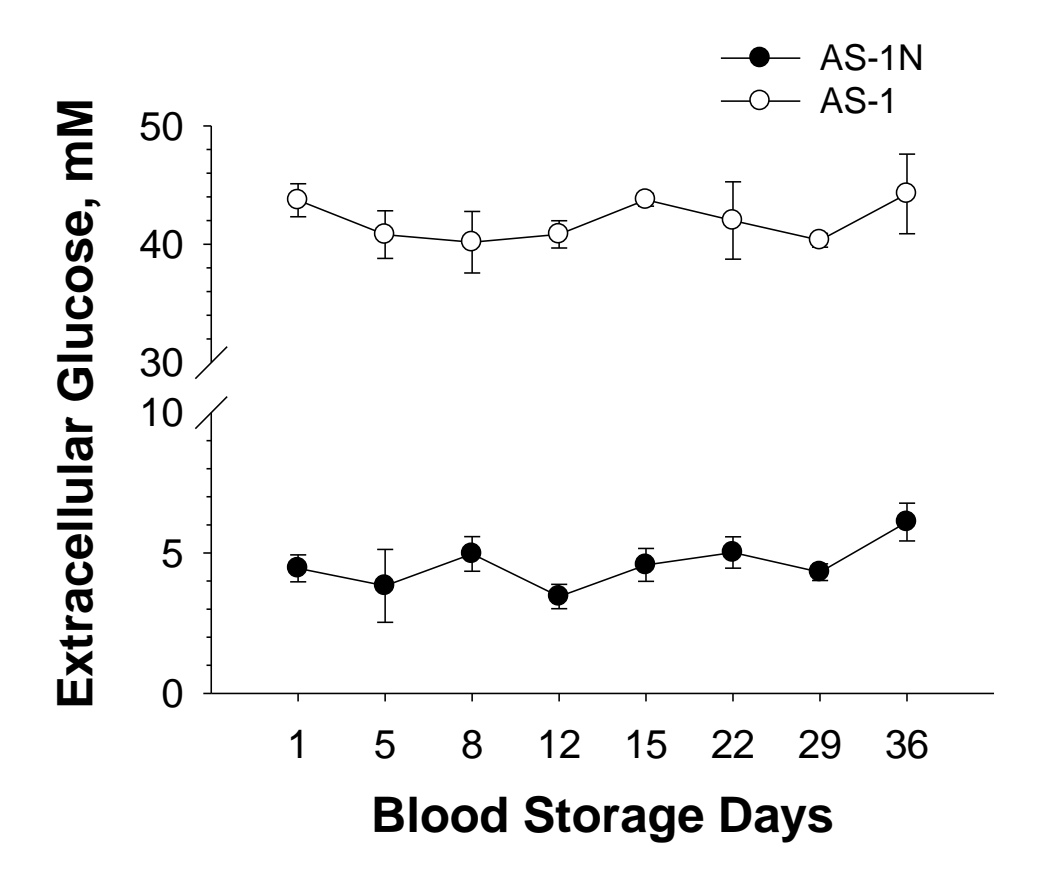


Figure 4.5. Extracellular glucose levels in AS-1 and AS-1N storage solutions. Throughout the whole 36-day storage, glucose in AS-1 solutions (open circles) stayed at an extremely high level around 40 mM, while AS-1N solutions (filled circles) showed physiological glucose levels around 5 mM. Data present the mean of 7 trials  $\pm$  S. E. M.

## 4.3.2 Study of Reversibility of ATP Release on the 3D-Printed Fluidic Device

ATP is an important molecule in the blood stream because of its participation in regulating blood flow. It was previously reported that ERYs stored in hyperglycemic AS-1 solution released significantly less ATP than those stored in AS-1N<sup>31</sup>. However, the performance of hyperglycemia stored ERYs transfused into a normoglycemic environment, remains unknown. Therefore, three experimental trials were designed and conducted to determine if the ATP release capability of hyperglycemia stored ERYs is reversible. A physiological salt solution (PSS) was used as the transfusion media, into which the stored ERYs would be transfused. The AS-1N-PSSN trial was to transfuse AS-1N stored ERYs to normoglycemic PSS (glucose 5.5 mM), the AS-1-PSSH was to transfuse AS-1 stored ERYs to hyperglycemic PSS (glucose concentration was equal to that in AS-1) and the AS-1-PSSN trial was to transfuse AS-1 stored ERYs to normoglycemic PSS to investigate the reversibility of ATP release. To better mimic a real transfusion process, the stored ERYs were transfused into corresponding PSS by a 1:10 v/v ratio (with a final hematocrit of 5%), and the blood samples were then introduced into the six channels, in duplicate, on the 3D-printed fluidic device that allows the blood samples to circulate for 20 min at 37 °C. ATP in each flowing stream was collected from loaded buffer in wells E above the channels for subsequent quantification on a plate reader.

As shown in Figure 4.6, ATP release from AS-1N-PSSN cells maintains constant at around 200 nM for the whole storage period, while AS-1-PSSH released ATP stays at a much lower level and the AS-1-PSSN released ATP keeps decreasing with time.

Comparably speaking, on Day 1, or after several hours of storage, ATP released from the AS-1-PSSH cells is already 40% less than AS-1N-PSSN cells, while the AS-1-PSSN cells release even a little more ATP than AS-1N-PSSN, though the difference between the latter two strategies is not significant. However, on Day 5, AS-1-PSSN released ATP begins to decrease and on Day 8, it is significantly lower than AS-1N-PSSN, yet still higher than AS-1-PSSH. The same trend is observed until Day 15, when the ATP release from AS-1-PSSN have decreased to an extent that is not significantly different from AS-1-PSSH. After Day 15, ATP release from both AS-1-PSSH and AS-1-PSSN are statistically the same (p>0.5), but are dramatically lower than AS-1N-PSSN. These results confirmed our previous results that the high glucose levels in the storage solutions impair ATP release from ERYs. Furthermore, Figure 4.6 clearly indicates that ATP release from hyperglycemia stored ERYs is conditionally reversible after ERYs are transfused back to a normoglycemic environment. After 8 days of storage, the ATP release reversibility is partially impaired and after Day 15, the reversibility is no longer observed, suggesting permanent adverse alteration has occurred on these cells after 15 days of storage in hyperglycemic environments.

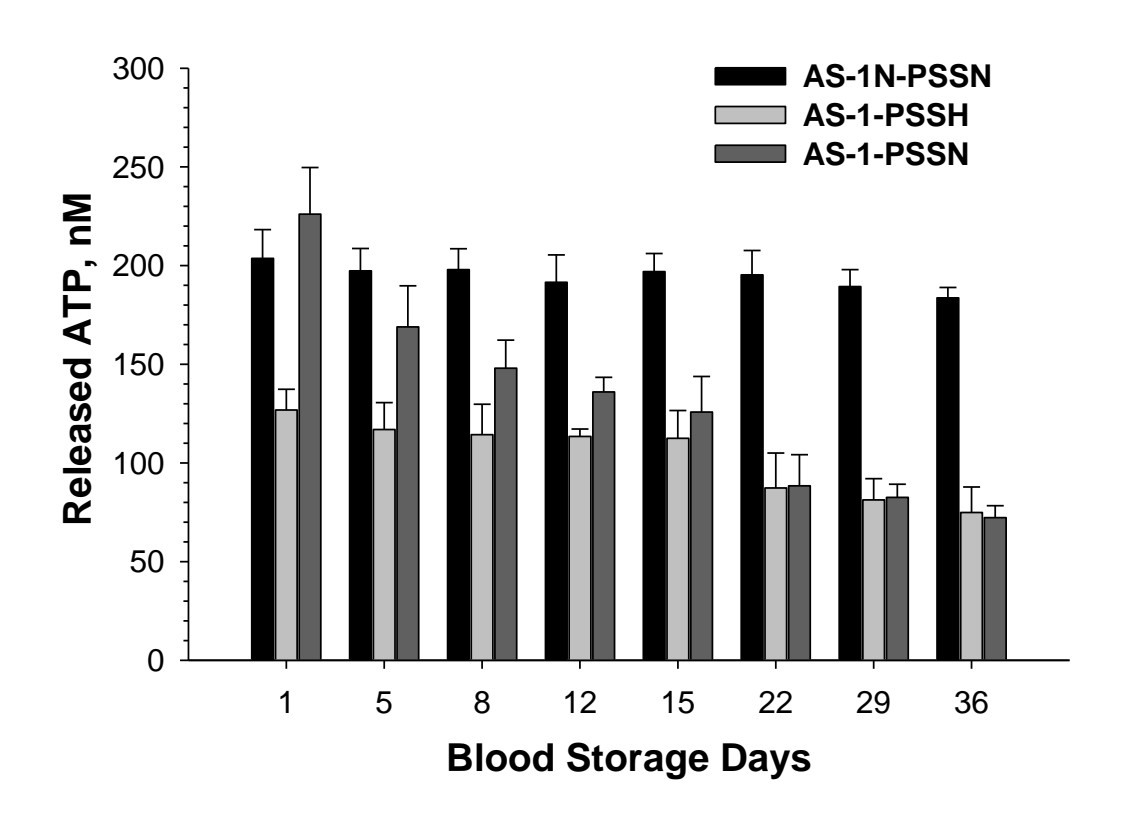


Figure 4.6. ATP release reversibility data at different storage days. AS-1N-PSSN trial referred to ERYs stored in AS-1N (normoglycemic) transfused into normoglycemic PSS; AS-1-PSSH trial represented ERYs stored in AS-1 (hyperglycemic) transfused into hyperglycemic PSS; AS-1-PSSN trial was ERYs stored in AS-1 but transfused into normoglycemic PSS. During the 36 storage days, AS-1N-PSSN ERYs released higher ATP at a constant level, while AS-1-PSSH ERYs released less ATP. The AS-1-PSSN ERYs, however, could reverse the ATP release before 15 days (complete reverse before Day 5 and partial reverse on Day 8 and 12). Seven biological replica were analyzed and the data represent mean ± S.E.M.

## 4.3.3 Study of Reversibility of ERY Deformability

The reversibility of stored ERY deformability was also studied due to the causal relationship between deformability and ATP release<sup>32</sup>. A deformability investigation was completed by a filtration test that has been widely used to study ERY deformability due to its low instrument requirements and high reproducibility<sup>33, 34</sup>. Because commercial devices were not found proper for this application, 3D-printing, which can model objects with high resolution based on the users' own demands, was used to fabricate a filtration device that minimizes dead volumes, saves the usage of filtering membranes and simplifies experimental operation. As shown in Panel A in Figure 4.1, the device is comprised of two slabs, with simultaneously 3D-printed O rings to seal a piece of semipermeable membrane in between for cell filtration. Due to the small sizes of the O rings, the dead volume of the filter is minimized to about 55 µL. Panel B shows the device assembly, which was constructed by clamping the slabs with four binder clips on the wings. Panel C demonstrates a real ERY filtration experiment on the device. ERY samples were pumped into the inlet on the top slab, and were forced to go through the membrane into the cone shaped chamber in the bottom slab, and were collected for cell counting. Cells that had sufficient deformability would deform to pass through the filter, whose pore size (5 µm) was smaller than the cell's diameter (6-8 µm), while less deformable cells would not be able to go through (Panel D).

Resuspended 5% AS-1N-PSSN, AS-1-PSSH and AS-1-PSSN cells were evaluated with this method. For a clearer data presentation, the cell number in the filter effluent

of AS-1N-PSSN trial on Day 1 was set to 100%, and all other collected data were normalized to this 100% value. As shown in Figure 4.7, the deformability of AS-1N-PSSN ERYs maintains constant at around 100% during the whole 36 days storage, while AS-1-PSSN trial keeps decreasing from 100% on Day 1 to 60% on Day 36. The deformability of AS-1-PSSH ERYs also maintains constant, but at a significantly lower level than AS-1N-PSSN. Comparably speaking, on Day 1, AS-1-PSSH cells lose much deformability (about 25%) compared with AS-1N-PSSN, while AS-1-PSSN cells completely reverse their deformability after being transfused to the normoglycemic PSS. The trend continues until Day 8, when deformability of AS-1-PSSN trial drops to AS-1-PSSH level. After Day 8, however, the deformability of AS-1-PSSN cells keeps decreasing, though at a slow rate, without any observed reversibility.

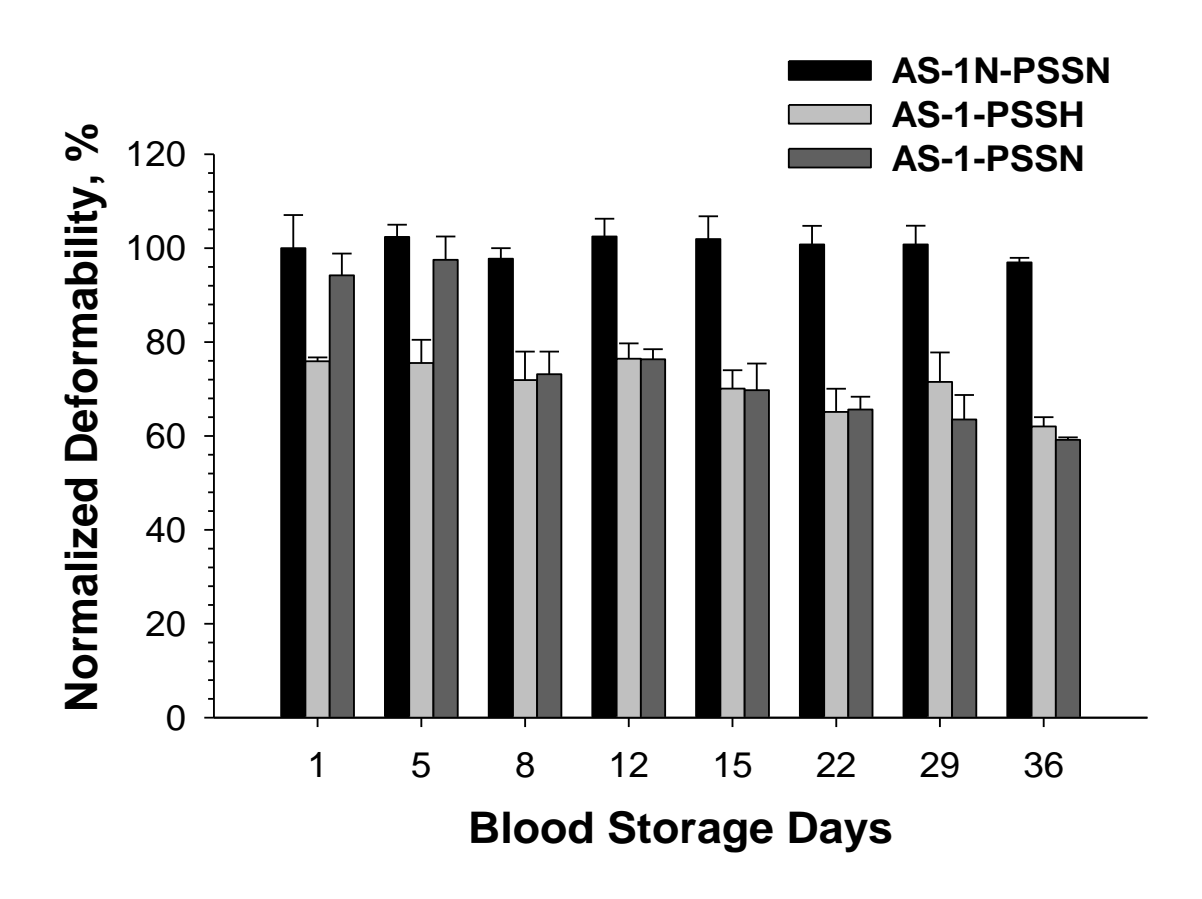


Figure 4.7. Deformability reversibility data at different storage days. Black bars were constant around 100% during 36 days storage, which indicate normoglycemia stored ERYs did not lose deformability after being transfused to normoglycemic PSS. The AS-1-PSSH cells, however, lost their deformability even on the first storage day. The hyperglycemia stored ERYs could reverse their deformability after being transfused into normoglycemic PSS for the first five days of storage. From Day8, these cells also lost the ability to reverse their deformability. Data represent mean values of 4 biological replica ± S.E.M.

## 4.3.4 Characterization of the i.v. Injection Device

After 50  $\mu$ L of 300  $\mu$ M fluorescein were injected into a water circulation of 450  $\mu$ L, the expected concentration of fluorescein in the loop is 30  $\mu$ M. As shown in Table 4.2, the measured fluorescein concentrations in the six loops of the fluidic device after an injection were around 30  $\mu$ M, suggesting the injection of small molecules such as fluorescein via the 3D-printed i.v. injection device can be very accurate. On the other hand, the detected fluorescein concentrations do no show significant difference between loops, which indicates the reproducibility between different injection devices is high. Although an extra fluorescein aliquot (50  $\mu$ L) was injected into a loop, due to the elasticity of the tubing, no leakage or burst was observed due to the additional fluorescein added.

To examine if the injected fluorescein molecules mixed well in a flowing stream, the liquid in a loop was divided into three parts randomly, and each of them was collected in a separate vial. The concentrations of fluorescein in the three parts were then quantified by a plate reader. If the molecules distribute evenly in a loop after injection, the concentrations of fluorescein in the three parts are expected to be the same. The data summarized in Table 4.3 clearly show that the concentration of fluorescein in each part of a loop is around 30  $\mu$ M, which indicates that the injected fluorescein molecules are able to distribute evenly along a whole loop after 2 min mixing after the injection.

Table 4.2. The concentration of fluorescein in each loop after an injection

	loop 1	loop 2	loop 3	loop 4	loop 5	loop 6
Fluorescein (μM)	30.3±2.4	29.3±1.1	30.7±0.9	29.2±0.8	30.5±1.2	30.0±1.0

N=5; error=stdev

Table 4.3. The concentrations of fluorescein in each part of a loop

	loop 1			loop 2			loop 3		
Fluorescein	P1	P2	Р3	P1	P2	Р3	P1	P2	Р3
(μM)	30.6±	30.5±	30.6±	29.5±	29.6±	30.1±	29.8±	30.5±	29.8±
	1.2	0.1	1.1	1.7	1.7	1.2	0.9	1.3	1.1
	loop 4			loop 5			loop 6		
Fluorescein	P1	P2	Р3	P1	P2	Р3	P1	P2	Р3
(μM)									
,	29.5±	29.5±	29.9±	29.8±	28.7±	28.3±	30.4±	30.4±	31.0±
-	1.4	1.7	1.5	0.3	0.5	0.1	0.6	0.7	1.3

N=5; error=stdev

The injection accuracy of ERYs and the distribution of injected ERYs were also characterized using a similar method as fluorescein. ERYs with a hematocrit of 50 % were injected into 5 % ERY streams, with an expected final hematocrit of 10 % in the loops. Data in Table 4.4 and Table 4.5 prove that ERYs can be injected accurately and can distribute evenly along a loop after being injected.

Table 4.4. The hematocrit of ERYs in each loop after an injection

	loop 1	loop 2	loop 3	loop 4	loop 5	loop 6
Hct, %	10.3±0.6	9.7±0.5	10.1±1.0	10.7±1.3	10.7±0.8	10.4±0.5

N=5; error=stdev

Table 4.5. The hematocrit of ERYs in each part of a loop

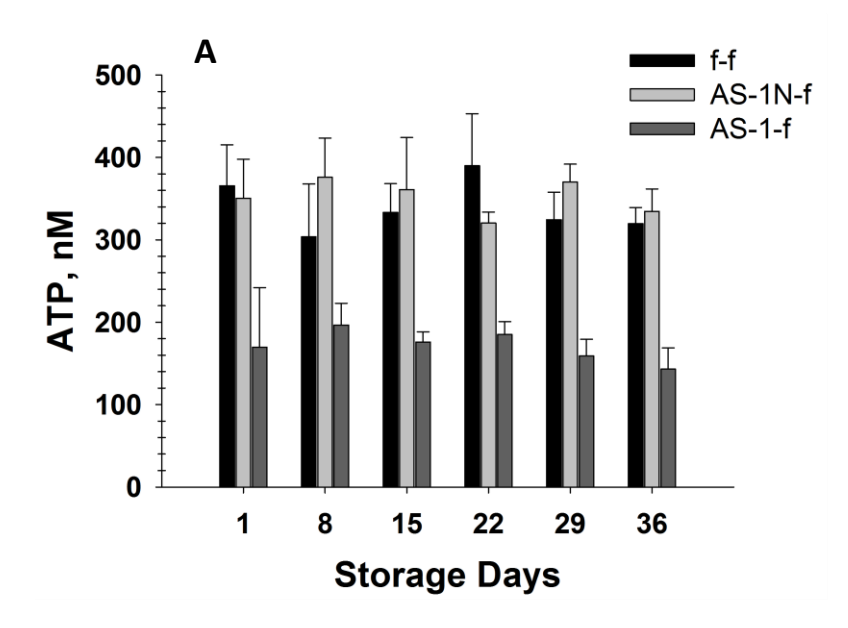
	loop 1			loop 2			loop 3		
Hct, %	P1	P2	Р3	P1	P2	Р3	P1	P2	Р3
	9.9±0.	10.2±	10.7±	10.4±	10.4±	10.2±	10.3±	10.4±	10.4±
	4	0.5	0.2	0.3	0.3	0.3	0.1	0.7	0.5
	loop 4			loop 5			loop 6		
Hct, %	P1	P2	P3	P1	P2	Р3	P1	P2	Р3
	9.9±0.	10.0±	10.3±	10.3±	10.4±	10.3±	9.7±0.	10.1±	10.3±
	1	0.3	0.3	0.3	0.1	0.5	5	0.5	0.3

N=5; error=stdev

## 4.3.5 Study of Responsiveness of Stored ERYs to Pancreatic $\beta$ -cells

The results in Tables 4.4 and 4.5 show that ERYs can be transfused quantitatively via the i.v. injection device, and the injected ERYs can mix evenly in a circulation stream. In this part, the response of the injected ERYs to pancreatic β-cells was evaluated. INS-1 cells were cultured in membrane inserts and integrated on the fluidic device. Next, a 5% hematocrit of fresh ERYs were delivered through the six channels, while three types of ERYs were injected into the circulation: fresh, AS-1 stored, and AS-1N stored ERYs. After incubation at 37 °C for 2 hours, the ATP in each channel was quantitatively determined by a plate reader measurement of luciferase/luciferin assay. In Figure 4.8, f-f refers to fresh ERYs transfused to a fresh ERY stream; AS-1N-f refers to AS-1N stored ERYs transfused to fresh ERYs; and AS-1-f refers to AS-1 stored ERYs transfused to fresh ERY streams. The f-f trial is to transfuse fresh ERYs to fresh ERYs in circulation, AS-1N-f is to transfuse AS-1N stored ERYs to fresh ERYs in circulation, and AS-1-f trial is to transfuse AS-1 stored ERYs to fresh ERY in circulation. By comparing Figure 4.8A and Figure 4.8B, it can first be concluded that with INS-1 cells, the ATP release in the trials of f-f and AS-1N-f is significantly higher (A) than those without the endocrine cells (B), suggesting that after being transfused, like fresh ERYs, AS-1N stored ERYs can respond to β-cells by releasing ATP. The AS-1 stored ERYs, however, failed to respond to the endocrine cells. Interestingly, though a loop after an injection consists of 5 % fresh ERYs and the same amount of AS-1 stored ERYs, the fresh cells did not respond to β-cells either. Though more evidence will be needed, it appears that the transfusion of AS-1 stored ERYs had an adverse effect on fresh ERYs.

Considering the reported clinical observation that patients who received transfused blood are prone to suffer from insufficient NO bioavailability, which may be a determinant in post transfusion complications, these results indicate that ERYs stored in a normoglycemic condition (AS-1N) retained their ability to respond to  $\beta$ -cells, which can potentially prevent the problems of insufficient NO bioavailability and related complications.



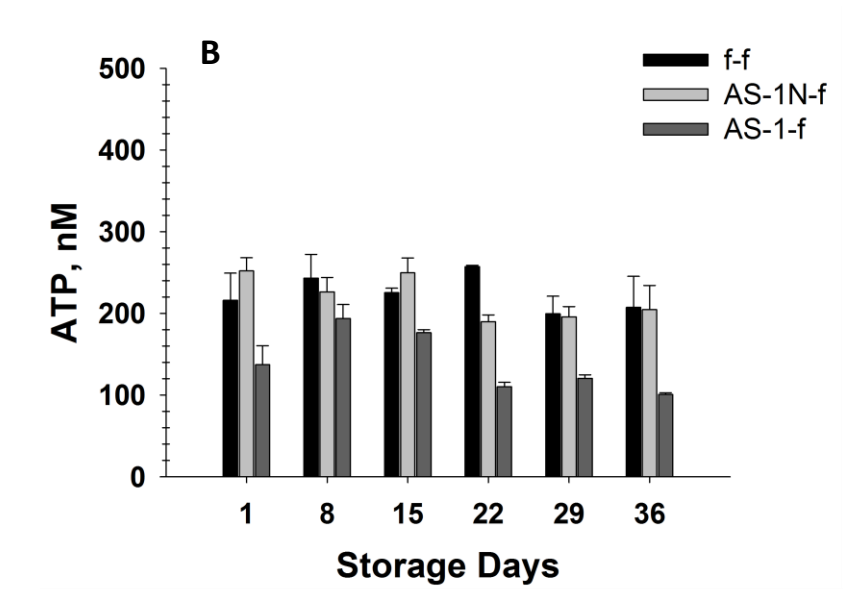


Figure 4.8. ATP release from ERYs after being transfused via the 3D-printed i.v. injection device. (A): with INS-1 cells on the channels; (B): without INS-1 cells on the channels. f-f: fresh ERYs transfused to fresh ERYs; AS-1N-f: AS-1N stored ERYs transfused to fresh ERYs; AS-1-f: AS-1 stored ERYs transfused to fresh ERYs. In these experiments, 50  $\mu$ L of f/AS-1N/AS-1 ERYs were transfused to a circulation of 450  $\mu$ L. N=4, error=S.E.M.

#### 4.4 Discussion

The Spence group has reported that the currently approved hyperglycemic ERY storage solutions impair ATP release from the cells and proposed an alternative storage solution (AS-1N) with a physiological glucose level, in which the ERYs have proven to release significantly more ATP. This study continues to investigate the adverse effects of hyperglycemia on stored ERYs by 3D-printed devices, with an emphasis on biochemical reversibility of the ERYs and the response of stored ERYs to endocrine  $\beta$ -cells.

The reversibility of ATP release from stored ERYs was studied by applying the 3D-printed fluidic device as discussed in Chapter 2. This device can better mimic the real conditions of ERYs by circulating samples at 37°C. Furthermore, it allows for simultaneous measurements of all three samples under a plate reader in a high throughput fashion. All these features make it an ideal platform for flow induced ATP measurements from stored ERYs. Data shown in Figure 4.6 reaffirmed our previous findings that high glucose in storage solutions reduced ERY ATP release, and extended that observation to demonstrate how reversible these ERYs are, in terms of ATP release, during the storage period. Day 15 was observed as a turning point, before which, the hyperglycemia stored ERYs are able to reverse (completely or at least partially) the ATP release ability, but after which the reversibility cannot be observed.

ERYs participate in regulating blood flow through releasing ATP that has proven to be able to stimulate endothelium-derived NO production, a well-established vessel

dilator. Numerous studies and surveys have demonstrated the existence of adverse complications after transfusion and the 15 storage day as a turning point of the quality of stored ERYs. It is not to be assumed that the failed ATP release reversibility after 15 days storage in hyperglycemia is the root cause of the clinical consequences. However, the ATP reversibility trend against storage time was consistent with the clinical observations, both showed an adverse alteration after two weeks. And given the important role of ERY released ATP in a blood stream, though more direct evidence will be required, it is rational to hypothesize a link between irreversible ATP release and the post transfusion health problems in such a scenario that insufficient ATP release from long-term stored (e.g. two weeks or longer) ERYs causes insufficient NO bioavailability, which restricts blood transportation to tissues and thus adversely affects the patient's health.

However, the mechanism that describes how hyperglycemia leads to failed reversibility of ATP release still remains unknown. The mechanism would lie in one of the two possible scenarios: hyperglycemia induces less intracellular ATP production or affects the ATP release process. Wang reported that intracellular ATP in hyperglycemia stored ERYs was higher than those stored in normoglycemic solutions, and it did not significantly decrease throughout 36 days storage<sup>31</sup>, which inferred hyperglycemia may adversely alter the ATP release process, rather than reducing intracellular ATP production.

Sprague reported that sheer stress induced deformability of ERYs leads to ATP release through a CFTR involved mechanism, suggesting that ATP release is related to cell deformability<sup>32</sup>. These findings provided a clue to potentially explain the failed ATP reversibility by studying the deformability of stored ERYs.

A user-friendly 3D-printed cell filter with a small dead volume was fabricated and applied to study the deformability of stored ERYs. Since the filter membrane pore size is smaller than human ERY mean diameter, only cells with sufficient deformability can go through. Therefore, the number of cells in the filter effluent can be used as a measurement of deformability. As shown in Figure 4.7, compared with the AS-1N-PSSN cells, the AS-1-PSSN cells' deformability was not able to reverse after Day 8, and continued to decrease beyond that time point.

By combining the ATP and deformability data (Figure 4.6 and Figure 4.7), a correlation between deformability and ATP release can be preliminarily revealed. During the first five days of storage in AS-1, ERY deformability could completely reverse after being transfused into a normoglycemic condition, as did the ATP release. On Day 8 and 12, however, the deformability of ERYs could not reverse, and the ATP release could only partially reverse, which was significantly lower than AS-1N-PSSN cells. After 15 Days storage, a permanent alteration of cell deformability had occurred, as did the ATP release. This correlation suggests that hyperglycemia may permanently and adversely alter the deformability of ERYs via a certain mechanism, which eventually leads to decreased ATP release.

Although the results discussed above suggest ERYs stored in hyperglycemic conditions can reverse their deformability and ATP release in the first a few days of storage, ERYs stored in normoglycemic condition never lost their deformability or ATP release during the whole 36-day storage, which reinforced our hypothesis that an alternative normoglycemic solution should be considered for ERY storage used in transfusion medicine.

To better study a transfusion process in vitro, a 3D-printed i.v. injection device was invented, which consists of a flow splitter, a controller and a stopcock. 3D-printing enables the fabrication of threads on the device and precisely controlled dimensions, which contribute to the high inter-device reproducibility. The characterization experiments of the device showed that it enables quantitative injection of solutions and ERY suspensions without leakage, and the injected parts can be mixed evenly in a circulation in a short time after an injection. Pancreatic  $\beta$ -cells (INS-1 cells) were integrated on the platform for investigation of the responsiveness of stored ERYs to these endocrine cells. It was found that AS-1N stored ERYs respond as fresh ERYs to the  $\beta$ -cells by releasing significantly more ATP than those without the  $\beta$ -cells. However, after the AS-1 stored ERYs were transfused to a stream of fresh ERYs, no response to the β-cells was observed. It appears that even the preexisting fresh ERYs in the flowing stream did not respond to the endocrine cells, which indicated that transfusion of hyperglycemia (AS-1) stored ERYs may adversely affect the original fresh ERYs in a patient. More evidence will be needed to confirm this hypothesis, which will be

discussed in Chapter 5. All these results suggest that AS-1N stored ERYs can potentially be healthier than those stored in currently approved AS-1.

#### 4.5 Conclusion

In this study, the reversibility of ATP release and deformability of hyperglycemia stored ERYs was studied with 3D-printed devices. Measurements on a 3D-printed circulation mimic device showed that hyperglycemia-stored ERYs cannot reverse or restore ATP release to normal levels after 15 days of storage, while normoglycemiastored ERYs are robust to release ATP throughout the whole storage period. Deformability reversibility of stored ERYs was also examined by a 3D-printed cell filter, which indicated hyperglycemia induces a permanent deformability alteration on stored ERYs after 1 to 2 weeks storage, which may explain the failure of ATP release reversibility. An i.v. injection device was designed and 3D-printed to investigate the responsiveness of stored ERYs to pancreatic β-cells, in a more clinically relevant manner. The results suggest that AS-1N stored ERYs can respond to β-cells like fresh ERYs, by releasing increased ATP. The AS-1 stored ERYs, however, failed to respond to the β-cells even after only 1 day storage, indicating some lesions has occurred on the stored cells by hyperglycemia. More importantly, after being mixed with AS-1 stored ERYs, original fresh ERYs cannot respond to the β-cells either, which initially suggests that AS-1 stored ERYs may adversely affect the original ERYs of a patient by a certain mechanism. All these results, combined with the previous reports involving ERY storage and post transfusion complications, strongly suggest that normoglycemic

storage conditions for ERYs may help maintain normal properties of the cells and potentially reduce the risk of post-transfusion complications.

- 1. Witaker, B.I. 2011 National Blood Collection and Utilization Survey. *American Association of Blood Banks* (2011).
- 2. Rubin, O., Crettaz, D., Tissot, J.D. & Lion, N. Pre-analytical and methodological challenges in red blood cell microparticle proteomics. *Talanta* **82**, 1-8 (2010).
- 3. Rous, P. & Turner, J.R. The preservation of living red blood cells in vitro. I. Methods of preservation. *J Exp Med* **23**, 219-237 (1916).
- 4. Robertson, O.H. & Rous, P. Autohemagglutination experimentally induced by the repeated withdrawal of blood. *J Exp Med* **27**, 563-U566 (1918).
- 5. Mollison, P.L. The introduction of citrate as an anticoagulant for transfusion and of glucose as a red cell preservative. *Brit J Haematol* **108**, 13-18 (2000).
- 6. Hogman, C.F., Hedlund, K. & Sahlestrom, Y. Red-Cell Preservation in Protein-Poor Media .3. Protection against Invitro Hemolysis. *Vox Sang* **41**, 274-281 (1981).
- 7. Hogman, C.F., Hedlund, K., Akerblom, O. & Venge, P. Red Blood-Cell Preservation in Protein-Poor Media .1. Leukocyte Enzymes as a Cause of Hemolysis. *Transfusion* **18**, 233-241 (1978).
- 8. Moore, G.L., Ledford, M.E. & Brooks, D.E. Distribution and Utilization of Adenine in Red Blood-Cells during 42 Days of 4c Storage. *Transfusion* **18**, 538-545 (1978).
- 9. Moore, G.L., Ledford, M.E. & Peck, C.C. The Invitro Evaluation of Modifications in Cpd-Adenine Anti-Coagulated-Preserved Blood at Various Hematocrits. *Transfusion* **20**, 419-426 (1980).
- 10. Moore, G.L. Additive Solutions for Better Blood Preservation. *Crit Rev Cl Lab Sci* **25**, 211-229 (1987).
- 11. Hogman, C.F., Eriksson, L., Hedlund, K. & Wallvik, J. The Bottom and Top System a New Technique for Blood Component Preparation and Storage. *Vox Sang* **55**, 211-217 (1988).

- 12. Hill, H.R., Oliver, C.K., Lippert, L.E., Greenwalt, T.J. & Hess, J.R. The effects of polyvinyl chloride and polyolefin blood bags on red blood cells stored in a new additive solution. *Vox Sang* **81**, 161-166 (2001).
- 13. Said, O. et al. Maintaining A Physiological Blood Glucose Level with Glucolevel, A Combination of Four Anti-Diabetes Plants Used in the Traditional Arab Herbal Medicine. *Evid-Based Compl Alt* **5**, 421-428 (2008).
- 14. Tinmouth, A., Fergusson, D., Yee, I.C., Hebert, P.C. & Investigators, A. Clinical consequences of red cell storage in the critically ill. *Transfusion* **46**, 2014-2027 (2006).
- 15. Fratantoni, J.C. Points to Consider in the Safety Evaluation of Hemoglobin-Based Oxygen Carriers. *Transfusion* **31**, 369-371 (1991).
- 16. Purdy, F.R., Tweeddale, M.G. & Merrick, P.M. Association of mortality with age of blood transfused in septic ICU patients. *Can J Anaesth* **44**, 1256-1261 (1997).
- 17. Basran, S. et al. The association between duration of storage of transfused red blood cells and morbidity and mortality after reoperative cardiac surgery. (vol 103, pg 15, 2006). *Anesth Analg* **108**, 1953-1953 (2009).
- 18. Basran, S. et al. The association between duration of storage of transfused red blood cells and morbidity and mortality after reoperative cardiac surgery. *Anesth Analg* **103**, 15-20 (2006).
- 19. Hoyt, D. et al. A 12-year prospective study of postinjury multiple organ failure Has anything changed? Discussion. *Arch Surg-Chicago* **140**, 439-440 (2005).
- 20. Ciesla, D.J. et al. A 12-year prospective study of postinjury multiple organ failure Has anything changed? *Arch Surg-Chicago* **140**, 432-439 (2005).
- 21. Offner, P.J., Moore, E.E., Biffl, W.L., Johnson, J.L. & Silliman, C.C. Increased rate of infection associated with transfusion of old blood after severe injury. *Arch Surg-Chicago* **137**, 711-716 (2002).
- 22. Zallen, G. et al. Age of transfused blood is an independent risk factor for postinjury multiple organ failure. *Am J Surg* **178**, 570-572 (1999).
- 23. Koch, C.G. et al. Duration of red-cell storage and complications after cardiac surgery. *New Engl J Med* **358**, 1229-1239 (2008).
- Szymanski, I.O. & Odgren, P.R. Studies on the Preservation of Red Blood-Cells
   Attachment of the 3rd Component of Human-Complement to Erythrocytes during Storage at 4-Degrees-C. Vox Sang 36, 213-224 (1979).

- 25. Valtis, D.J. & Kennedy, A.C. Defective Gas-Transport Function of Stored Red Blood-Cells. *Lancet* **1**, 119-125 (1954).
- 26. Carroll, J. et al. An altered oxidant defense system in red blood cells affects their ability to release nitric oxide-stimulating ATP. *Mol Biosyst* **2**, 305-311 (2006).
- 27. Sprague, R.S., Ellsworth, M.L., Stephenson, A.H. & Lonigro, A.J. ATP: The red blood cell link to NO and local control of the pulmonary circulation. *Am J Physiol-Heart C* **271**, H2717-H2722 (1996).
- 28. Roback, J.D., Neuman, R.B., Quyyumi, A. & Sutliff, R. Insufficient nitric oxide bioavailability: a hypothesis to explain adverse effects of red blood cell transfusion. *Transfusion* **51**, 859-866 (2011).
- 29. Allen, B.W. & Piantadosi, C.A. How do red blood cells cause hypoxic vasodilation? The SNO-hemoglobin paradigm. *Am J Physiol-Heart C* **291**, H1507-H1512 (2006).
- 30. Tsai, A.G., Hofmann, A., Cabrales, P. & Intaglietta, M. Perfusion vs. oxygen delivery in transfusion with "fresh" and "old" red blood cells: The experimental evidence. *Transfus Apher Sci* **43**, 69-78 (2010).
- 31. Wang, Y.M., Giebink, A. & Spence, D.M. Microfluidic evaluation of red cells collected and stored in modified processing solutions used in blood banking. *Integr Biol-Uk* **6**, 65-75 (2014).
- 32. Sprague, R.S., Ellsworth, M.L., Stephenson, A.H., Kleinhenz, M.E. & Lonigro, A.J. Deformation-induced ATP release from red blood cells requires CFTR activity. *Am J Physiol-Heart C* **275**, H1726-H1732 (1998).
- 33. Juhan, I. et al. Abnormalities of Erythrocyte Deformability and Platelet-Aggregation in Insulin-Dependent Diabetics Corrected by Insulin Invivo and Invitro. *Lancet* **1**, 535-537 (1982).
- 34. Srour, M.A., Bilto, Y.Y., Juma, M. & Irhimeh, M.R. Exposure of human erythrocytes to oxygen radicals causes loss of deformability, increased osmotic fragility, lipid peroxidation and protein degradation. *Clin Hemorheol Micro* **23**, 13-21 (2000).

# Chapter 5 – Conclusions and Future Directions

# 5.1 Conclusions

5.1.1. C-peptide Stimulated ATP Release from Erythrocytes on a 3D-printed Circulation-mimic Fluidic Device

Microfluidics technologies have become a powerful tool in the field of bioanalytical chemistry because of their ability to control flow and reduce the consumption of reagents and samples<sup>1</sup>. Most microfluidic devices are fabricated in PDMS, a nontoxic and transparent elastomer<sup>2, 3</sup>. However, despite the advantages of this polymer, it possesses some drawbacks that prevent microfluidics from becoming a common tool in the laboratory. For example, PDMS devices are not rigid, which may cause flow problems such as leakage and uneven pressure distribution<sup>4</sup>. These devices are single use, which not only increases research cost (time and money), but also compromises the reproducibility of results. Although previous research has successfully integrated multiple functional units, such as on-chip mixers and detectors on PDMS microfluidic devices, the fabrication is lab-dependent, with poor inter-lab reproducibility<sup>5</sup>. Finally, although there has been a large number of publications involving microfluidic development since the 1990's, these studies did not elicit many commercialized products<sup>6, 7</sup>. The lack of standardization and ruggedness of PMDSbased devices are probably partially responsible for this impasse<sup>8</sup>.

In this work, 3D-printing was employed to fabricate a more standard and rugged microfluidic device. 3D-printing is a novel rapid prototyping technique using an

additive process to build a 3D object<sup>9</sup>. Instead of the multiple soft lithography steps and binding multiple layers of PDMS slabs, 3D-printing can fabricate a microfluidic device in one step, with precisely controlled shapes, features and dimensions <sup>10-12</sup>. The device developed in this study is based on the dimensions of a standard 96-well plate, thereby enabling convenient and high content readout by a plate reader. Moreover, the ruggedness of the device allows for long term experiments (*e.g.*, >2 hours circulation of ERYs), which cannot be easily achieved on soft PDMS devices. The reusability of the device also enhances the precision of the results. Some unique features are also implemented on the device. For example, threads are printed on the ends of each channel to connect a tubing via standard male finger tight adapters. The design of static wells enables on-chip simultaneous calibration. All these results suggest that with 3D-printing, a microfluidic device can be fabricated in a more standard and simple way, with integration of complicated features.

This 3D-printed device facilitates the study of the effect of C-peptide on circulating ERYs. First of all, our previous conclusion that C-peptide and Zn<sup>2+</sup> can stimulate ATP release from ERYs was confirmed on the device. More importantly, this result has further advanced by discovering the indispensable role of albumin in this process. Without albumin, C-peptide and Zn<sup>2+</sup> cannot exert their effect on ERYs, suggesting that albumin may be the molecule that delivers C-peptide and Zn<sup>2+</sup> to the ERY. Without albumin in the solutions, C-peptide cannot be delivered onto ERYs<sup>13</sup>. These results support our previous theory involving C-peptide and Zn<sup>2+</sup> and provide further evidence that this effect requires an ensemble of albumin, C-peptide, and Zn<sup>2+</sup>.

5.1.2 An Organs-on-a-Chip platform to Study the Interactions between Pancreatic  $\beta$ -cells and Blood Components

The 3D-printed fluidic device described in this dissertation also shows its versatility in an Organs-on-a-Chip platform. To study the effect of endogenous Cpeptide on ERYs in a more physiologically relevant manner, this platform contains a βcell line, INS-1 cells, to secret C-peptide gradually into an ERY circulation. The β-cells and endothelial cells were successfully integrated on the device by using membrane inserts. The application of membrane inserts presents a novel philosophy of Organson-a-Chip construction. Any cells that can be cultured in a membrane insert can be directly plugged into a fluidic device, before which the cell properties can be thoroughly examined. The secretion profiles of the β-cells on the platform resemble a real C-peptide secretion process, by producing C-peptide at the same levels as those believed to occur *in vivo*. Interactions between the β-cells, ERYs, and endothelial cells were studied. It was found that the β-cells do not have any effect on the endothelial cells, in terms of NO production. However, ERYs are affected by the endocrine cell secretion, the result of which is an increase of ERY-derived ATP. The ERY released ATP will then exert a downstream effect on the endothelial cells by stimulating NO production and release. By using PPADS, a P2y receptor on endothelial cells that ATP binds, it is confirmed that ATP acts as an indirect vasodilator by stimulating endothelium-derived NO, which is consistent with Sprague's theory that ERYs need to be present for shear stress to enhance NO production from endothelial cells<sup>14</sup>.

5.1.3 Evaluating Stored Erythrocytes used in Transfusion Medicine by 3D-Printed Analytical Devices

Stored ERYs suffer from adverse physiological alterations, or storage lesions that can lead to serious complications for transfusion patients, including increased morbidity<sup>15-17</sup>. Previous studies show that the hyperglycemia (40 mM) in a storage bag can diminish ERYs released ATP, which is an important molecule in regulating blood flow. However, in a common transfusion process, about 1/10 ERYs of the whole volume of blood (400 mL v.s. 5 L) are transfused to a normoglycemic circulation. The performance of the stored ERYs after being transfused back to a normoglycemic environment remains unknown. Therefore, a primary focus of this work is to determine if hyperglycemia-stored ERYs can restore or reverse their capability to release ATP after suspension in a normoglycemic environment. PSS was used as the transfusion media, into which stored ERYs were transfused at a 1:10 ratio. After this in vitro transfusion, the samples were allowed to circulate in the 3D-printed fluidic device followed by on-chip ATP determination. The results show that after about 5 days storage in hyperglycemic AS-1, the ability of the ERYs to release ATP can recover back to normal levels. However, after about 1 week, the ATP release can only partially reverse, and after about 2 weeks, the reversibility cannot be observed anymore, suggesting a permanent adverse alteration has occurred on the ERYs after 2 weeks of storage.

Patients who receive stored ERYs older than two weeks are more likely to suffer the complications<sup>18, 19</sup>, which is consistent with our observation that the

hyperglycemic solutions impair the ATP release of ERYs after 15 days storage. A reduction in ATP release correlates with impaired vessel dilation and restricted blood flow<sup>20</sup>. Though more direct evidence will be needed, given the important role of ATP in the blood stream, and the 15 day clinical observations, it is rational to hypothesize a correlation between impaired ATP release reversibility and post-transfusion complications.

To better mimic a real transfusion process *in vitro*, an i.v. injection device was developed and fabricated using 3D-printing. Initial characterization shows that this device enables quantitative injection of solutions and ERY suspensions. The injected parts can distribute evenly along a loop in a short time after an injection. The INS-cells were integrated on the i.v. injection platform to study the response of stored ERYs to the endocrine cells. AS-1N stored ERYs can respond to the  $\beta$ -cells by releasing ATP, as fresh ERYs do. AS-1-stored ERYs, however, cannot respond to the  $\beta$ -cell secretions as wells as ERYs in normoglycemic environments. Moreover, after the AS-1-stored ERYs were transfused to preexisting fresh ERYs, the original ERYs cannot respond to the endocrine cells either, indicating that the transfused ERYs may affect those fresh ERYs in an unknown mechanism. More evidence will be needed to confirm this.

A possible mechanism by which hyperglycemia impairs ATP release from ERYs was also investigated. It has been shown that there exists a causal relationship between ERY deformability and ATP release<sup>21</sup>. Therefore the effect of hyperglycemia on ERY deformability was investigated using an in-house prepared 3D-printed cell filter.

Because 3D-printing enables the fabrication of desired features for a user, this 3D-printed cell filter has a minimized dead volume of 55  $\mu$ L. Moreover, this device does not require complicated instruments and its use is very straightforward. The deformability data show that hyperglycemia can permanently stiffen stored ERYs after 5 days of storage, which is consistent with the ATP reversibility observation. Based on these results, it can be initially concluded that hyperglycemia impairs ERY deformability, which leads to a diminished ATP release.

#### 5.1.4 Summarized Conclusion

In this dissertation, several 3D-printed devices were invented to study the role of ERYs in a variety of biological fields. From an engineering perspective, 3D-printing can fabricate functional, reusable, and reproducible microfluidic devices used for bioanalysis, and provides superior advantages over PDMS-based microfluidics. Also, with 3D-printing, analytical devices can be invented and fabricated based on the users' specific demands. From a physiological perspective, the results acquired on these 3D-printed device revealed new information towards our ultimate goal of developing an additional replacement therapy for people with type 1 diabetes. The adverse effects of currently approved ERY storage solutions on ERYs were also evaluated and verified.

# 5.2 Future Directions

5.2.1 C-peptide-Stimulated ATP Release from Erythrocytes on a 3D-printed Circulation-mimic Fluidic Device

The main problem of the 3D-printed fluidic device is the dimensions (mm) of the channels. It appears to be a common problem that the resolution of current 3D-printers needs to be improved. Taking the Connex 350 that was used in this study for example, the best resolution on the XY plane is 100 µm. The relatively poor (compared with soft lithography) resolution can also cause high surface roughness that will lead to resistive flow and cell adhesion. The further development of 3D-printing technology can naturally solve these problems in the future. However, for now, other strategies may be used to avoid these problems. For example: PDMS coating on 3D-printed fluidic devices can effectively reduce the dimensions of channels and smooth the surfaces<sup>22</sup>. The shape of channels on the device can also be optimized to better mimic blood circulation. For example, bifurcations can be applied to study the physiology of ERYs under different flow conditions (bifurcated smaller channels will increase shear stress for ERYs).

The results shown in this work reveal the important role of albumin in delivering C-peptide and Zn<sup>2+</sup> to ERYs. However, the binding structure of the three molecule ensemble remains unknown. Crystallography combined with X-ray diffraction, or NMR spectroscopy can be applied to further study the binding structure. Also, the ERY receptors for C-peptide and Zn<sup>2+</sup> are not understood.

5.2.2 An Organs-on-a-Chip platform to Study the Interactions between Pancreatic  $\beta$ -cells and Blood Components

This Organs-on-a-Chip platform that integrates pancreatic  $\beta$ -cells, ERYs, and endothelial cells enables studies of interactions between cell types. However, future research may make it a better physiological mimic. First, the culture of the INS-1 cells can be improved. These cells were cultured in a planar way along the membrane in this study. Though the INS-1 cells are prone to aggregate to form pseudo islets, this culture cannot completely mimic *in vivo*  $\beta$ -cells, which are aggregated in an islet. The technique of 3D cell culture can be applied to culture a spheroid of the  $\beta$ -cells, which can then be placed in a membrane insert on the fluidic device. The tumor cell property of the INS-1 cells increases the feasibility of culturing an islet *in vitro*. In such a manner, the secretion profiles of the cells need to be re-measured because the interactions between the INS-cells in a spheroid may change the secretion patterns.

Another study that needs to be conducted is on-chip separation. The results presented in this work can only directly prove that the secretions of INS-1 cells stimulate ATP release from ERYs. However, in addition to C-peptide, these endocrine cells also secrete other molecules, such as insulin and amylin. Though previous results in our group show that insulin does not stimulate ERY-derived ATP, our results will be more conclusive if a separation process can be applied before the secretions entering an ERY circulation.

Chelates and affinity reagents immobilized on a piece of porous membrane have become a commonly used technique for membrane based separations<sup>23</sup>. Here, results will be improved if on the membrane where INS-1 cells are cultured, an anti-C-peptide antibody can be immobilized to prevent the secreted C-peptide from entering ERY streams. If no increased ATP release is observed after this, it can be concluded that it is C-peptide that plays the important role (as opposed to, say, insulin). In a similar way, the role of  $Zn^{2+}$ , which is also secreted from the  $\beta$ -cells, insulin and amylin can be examined.

5.2.3 Evaluating Stored Erythrocytes used in Transfusion Medicine by 3D-Printed Analytical Devices

The results in this work proved the irreversibility of hyperglycemia stored ERYs after 15 days of storage, which is potentially caused by the alteration of cell deformability during storage. However, the mechanism by which hyperglycemia impairs ERY deformability remains unknown. ERY deformability is mainly regulated by structural proteins such as actin and spectrin on the inside of the cell membrane<sup>24</sup>. We suspect that hyperglycemic storage changed the configuration of the binding pattern between the proteins. A characterization method that can detect these proteins needs to be developed to study how hyperglycemia affects these structures.

It is also possible that the hyperglycemia causes glycation of certain proteins in ERYs. There are reports showing that the oxygen delivery of stored ERYs is compromised during storage<sup>25, 26</sup>, which indicates that the hemoglobin may have been

affected by the high glucose levels. Some research focusing on this part can help to understand the lesions of stored ERYs from a broader perspective. The response of stored ERYs to  $\beta$ -cells needs to be further explored too, especially the effect of transfused ERYs on original ERYs. Results have shown that hyperglycemia stored ERYs may foul preexisting fresh ERYs. If this is true, the mechanism behind it should be elucidated, which can potentially change the game rules of the field of blood banking in a profound way.

The i.v. injection device was used to inject stored ERYs into fresh ERYs in this study. However, this device can also be used for other applications such as drug administration and drug dosing. For example, diabetic ERYs, which release less ATP than ERYs from healthy people<sup>27</sup>, can be circulating in the fluidic device, while a drug candidate, such as the ensemble of albumin, C-peptide, and Zn<sup>2+</sup> can be injected via the side branch, to study the effect of the drug candidate.

- 1. Whitesides, G.M. The origins and the future of microfluidics. *Nature* **442**, 368-373 (2006).
- 2. McDonald, J.C. et al. Fabrication of microfluidic systems in poly(dimethylsiloxane). *Electrophoresis* **21**, 27-40 (2000).
- 3. McDonald, J.C. & Whitesides, G.M. Poly(dimethylsiloxane) as a material for fabricating microfluidic devices. *Accounts Chem Res* **35**, 491-499 (2002).
- 4. Chen, C.P., Wang, Y.M., Lockwood, S.Y. & Spence, D.M. 3D-printed fluidic devices enable quantitative evaluation of blood components in modified storage solutions for use in transfusion medicine. *Analyst* **139**, 3219-3226 (2014).
- 5. Mukhopadhyay, R. Hard-soft microfluidic device bypasses drawbacks of PDMS. *Anal Chem* **81**, 5108-5108 (2009).
- 6. Volpatti, L.R. & Yetisen, A.K. Commercialization of microfluidic devices. *Trends Biotechnol* **32**, 347-350 (2014).
- 7. Chin, C.D., Linder, V. & Sia, S.K. Commercialization of microfluidic point-of-care diagnostic devices. *Lab Chip* **12**, 2118-2134 (2012).
- 8. Coltro, W.K.T., Lunte, S.M. & Carrilho, E. Comparison of the analytical performance of electrophoresis microchannels fabricated in PDMS, glass, and polyester-toner. *Electrophoresis* **29**, 4928-4937 (2008).
- 9. Gross, B.C., Erkal, J.L., Lockwood, S.Y., Chen, C.P. & Spence, D.M. Evaluation of 3D Printing and Its Potential Impact on Biotechnology and the Chemical Sciences. *Anal Chem* **86**, 3240-3253 (2014).
- 10. Waldbaur, A., Rapp, H., Lange, K. & Rapp, B.E. Let there be chip-towards rapid prototyping of microfluidic devices: one-step manufacturing processes. *Anal Methods-Uk* **3**, 2681-2716 (2011).

- 11. Lee, K.G. et al. 3D printed modules for integrated microfluidic devices. *Rsc Adv* **4**, 32876-32880 (2014).
- 12. Kitson, P.J., Rosnes, M.H., Sans, V., Dragone, V. & Cronin, L. Configurable 3D-Printed millifluidic and microfluidic 'lab on a chip' reactionware devices. *Lab Chip* 12, 3267-3271 (2012).
- 13. Liu, Y.L., Chen, C.P., Summers, S., Medawala, W. & Spence, D.M. C-peptide and zinc delivery to erythrocytes requires the presence of albumin: implications in diabetes explored with a 3D-printed fluidic device. *Integr Biol-Uk* **7**, 534-543 (2015).
- 14. Dietrich, H.H., Ellsworth, M.L., Sprague, R.S. & Dacey, R.G. Red blood cell regulation of microvascular tone through adenosine triphosphate. *Am J Physiol-Heart C* **278**, H1294-H1298 (2000).
- 15. Zallen, G. et al. Age of transfused blood is an independent risk factor for postinjury multiple organ failure. *Am J Surg* **178**, 570-572 (1999).
- 16. Purdy, F.R., Tweeddale, M.G. & Merrick, P.M. Association of mortality with age of blood transfused in septic ICU patients. *Can J Anaesth* **44**, 1256-1261 (1997).
- 17. Basran, S. et al. The association between duration of storage of transfused red blood cells and morbidity and mortality after reoperative cardiac surgery. (vol 103, pg 15, 2006). *Anesth Analg* **108**, 1953-1953 (2009).
- 18. Koch, C.G. et al. Duration of red-cell storage and complications after cardiac surgery. *New Engl J Med* **358**, 1229-1239 (2008).
- 19. Offner, P.J., Moore, E.E., Biffl, W.L., Johnson, J.L. & Silliman, C.C. Increased rate of infection associated with transfusion of old blood after severe injury. *Arch Surg-Chicago* **137**, 711-716 (2002).
- 20. Sprague, R.S., Stephenson, A.H., Bowles, E.A., Stumpf, M.S. & Lonigro, A.J. Reduced expression of G(i) in erythrocytes of humans with type 2 diabetes is associated with impairment of both cAMP generation and ATP release. *Diabetes* **55**, 3588-3593 (2006).

- 21. Sprague, R.S., Ellsworth, M.L., Stephenson, A.H., Kleinhenz, M.E. & Lonigro, A.J. Deformation-induced ATP release from red blood cells requires CFTR activity. *Am J Physiol-Heart C* **275**, H1726-H1732 (1998).
- 22. Gross, B.A., Storey, A., Orbach, D.B., Scott, R.M. & Smith, E.R. Microsurgical treatment of arteriovenous malformations in pediatric patients: the Boston Children's Hospital experience. *J Neurosurg-Pediatr* **15**, 71-77 (2015).
- 23. Ning, W.J., Wijeratne, S., Dong, J.L. & Bruening, M.L. Immobilization of Carboxymethylated Polyethylenimine-Metal-Ion Complexes in Porous Membranes to Selectively Capture His-Tagged Protein. *Acs Appl Mater Inter* **7**, 2575-2584 (2015).
- 24. Gokhin, D.S. et al. Dynamic actin filaments control the mechanical behavior of the human red blood cell membrane. *Mol Biol Cell* **25** (2014).
- 25. Chaplin, H., Beutler, E., Collins, J.A., Giblett, E.R. & Polesky, H.F. Current Status of Red-Cell Preservation and Availability in Relation to Developing National Blood Policy. *New Engl J Med* **291**, 68-74 (1974).
- 26. Dawson, R.B. Hemoglobin Function in Stored-Blood .19. Inosine Maintenance of 2,3-Dpg for 35 Days in a Cpd-Adenine Preservative. *Transfusion* **17**, 525-528 (1977).
- 27. Carroll, J. et al. An altered oxidant defense system in red blood cells affects their ability to release nitric oxide-stimulating ATP. *Mol Biosyst* **2**, 305-311 (2006).